8-2015

ASSESSMENT OF UNCERTAINTY IN PLANNING AND DOSE DELIVERY OF PROTON THERAPY IN AN IROC- HOUSTON QA PHANTOM DUE TO VARIABLE CT TECHNIQUE AND PROTON ENERGY

Mattie M. McInnis

ASSESSMENT OF UNCERTAINTY IN PLANNING AND DOSE DELIVERY OF PROTON THERAPY IN AN IROC-HOUSTON QA PHANTOM DUE TO VARIABLE CT TECHNIQUE AND PROTON ENERGY

by

Mattie Margaret McInnis, B.S.

APPROVED:

_____

David Followill, Ph.D.
Advisory Professor

_____

Laurence Court, Ph.D.

_____

Michele Guindani, Ph.D.

_____

Falk Poenisch, Ph.D.

_____

Paige Taylor, M.S.

APPROVED:

_____

Dean, The University of Texas
Graduate School of Biomedical Sciences at Houston

ASSESSMENT OF UNCERTAINTY IN PLANNING AND DOSE DELIVERY OF PROTON THERAPY IN IROC- HOUSTON QA PHANTOM DUE TO VARIABLE CT TECHNIQUE AND PROTON ENERGY

A

THESIS

Presented to the Faculty of
The University of Texas
Health Science Center at Houston
and
The University of Texas
M. D. Anderson Cancer Center
Graduate School of Biomedical Sciences
in Partial Fulfillment
of the Requirements
for the Degree of

MASTER OF SCIENCE

By

Mattie Margaret McInnis, B.S.
Houston, Texas

August 2015

Dedication

I would like to dedicate this work to my family and to Josh

Acknowledgements

I would like to thank and acknowledge my Advisory Committee: Chair David Followill, Ph.D., Paige Taylor, MS, Falk Poenisch, Ph.D., Laurence Court, Ph.D., and Michele Guindani, Ph.D., for their support and insight throughout this project.

I would like to thank Michael Gillin, Ph.D., and Falk Poenisch, Ph.D., for their help with proton beam delivery, John Costales for his help with phantom materials, Kit Ciura for her assistance with dosimetry and treatment planning, Ryan Grant and Mitchell Carroll for their help with CERR, Tyler Keith for his help with IROC-H phantoms, and Shane and Marcy, PTC-H CT techs, for their help and cooperation with CT simulations.

Finally I would like to thank my family and friends whose encouragement and support made this project possible.

ASSESSMENT OF UNCERTAINTY IN PLANNING AND DOSE DELIVERY OF PROTON THERAPY IN IROC- HOUSTON QA PHANTOM DUE TO VARIABLE CT TECHNIQUE AND PROTON ENERGY

Publication No. _____

Mattie M. McInnis, B.S.

Advisory Committee Chair: David S. Followill, Ph.D.

Abstract

As proton therapy increases in popularity, so does the need for effective quality assurance. Proton therapy institutions participating in NCI funded clinical trials rely heavily on the credentialing and auditing services of IROC-H and therefore the process must be well understood. The purpose of this project is to understand the uncertainties in proton therapy treatment planning for the IROC-H proton phantom QA program due to variations in CT technique and proton energy. It was hypothesized that variations in CT technique and proton energy will alter the delivered dose distributions of typical proton treatments by reducing the percent of passing pixels by 10% using a gamma analysis criteria of ±3%/5mm as measured using a heterogeneous proton QA phantom. A CT phantom used by IROC-H during therapy site visits was scanned using three CT techniques (80, 120, 140kV) with a CT scanner used for proton therapy simulations and irradiated with a passively scattered beam at three energies (140, 200, 250 MeV) to measure, respectively, HU and Relative Linear Stopping Power (RLSP) in order to create HU to RLSP calibration curves for comparison with reference curves as defined by this study. The phantom has proton equivalent materials with a wide variety of HU and RLSPs to allow for the creation of a calibration curve for common tissue equivalent materials. Treatment plans were created for an anthropomorphic proton lung phantom using the various CT technique/ beam energy calibration curves to determine the differences in the dose distributions by performing a gamma analysis. The 3D gamma analysis resulted in a pass rate of 100% for all plans and the 2D gamma analysis resulted in a pass rate above 99%. This result implied the varying treatment plans did not substantially affect the outcome of the dose comparison and therefore rejects the stated hypothesis and further work is needed to investigate the uncertainty present in this QA process.

Table of Contents

Table of Illustrations

List of Tables

List of Abbreviations

1D: One Dimensional

2D: Two Dimensional

3D: Three Dimensional

ACB: Ambulatory Clinical Building

CERR: Computational Environment for Radiotherapy Research

CGE: Cobalt Gray Equivalent

CSDA: Continuous Slowing Down Approximation

CT: Computed Tomography

DECT: Dual Energy Computed Tomography

DTA: Distance to Agreement

DVH: Dose Volume Histogram

E2E: End to End

HU: Hounsfield Unit

IROC-H: Imaging and Radiation Oncology Core- Houston

MDACC: M.D. Anderson Cancer Center

MLIC: Multi-Layer Ion Chamber

NCI: National Cancer Institute

NCTN: National Clinical Trials Network

PTC-H: Proton Therapy Center- Houston

QA: Quality Assurance

RBE: Relative Biological Effectiveness

RLSP: Relative Linear Stopping Power

ROI: Region of Interest

RPC: Radiological Physics Center

SBRT: Stereotactic Body Radiation Therapy

SOBP: Spread Out Bragg Peak

TLD: Thermoluminescent Dosimeter

Chapter 1

1 Introduction and Background

1.1 Statement of Problem

1.1.1 General Problem Area

Proton and radiation therapy is continuing to grow as a radiation oncology treatment modality, being adopted by an increasing number of institutions in the United States and around the world. There are currently 17 clinically active proton centers in the United States with another 14 under construction and an additional 3 centers still in the planning stages [1][2][3]. As the number of proton therapy facilities grows, so does the number of facilities seeking to participate in the National Cancer Institute's (NCI) funded proton therapy clinical trials and the number of patients impacted by these proton trials. The NCI, in 2014, implemented the National Clinical Trials Network (NCTN), a network of five clinical trial groups conducting multi-institutional phase I, II and III clinical trials with the goal of developing new protocols, conducting the trials and compiling data from many institutions in order to improve the standard of care for the treatment of cancer [4]. As a part of the NCTN, the NCI funded a central Core group to a provide quality assurance and data management service to the NCTN and their participants. This Core group is the Imaging and Radiation Oncology Core (IROC) Cooperative. IROC consists of 6 different radiotherapy and imaging QA centers located across the USA. One of the QA centers is the Imaging and Radiation Oncology Core Houston (IROC-H) QA Center, formerly known as the Radiological Physics Center (RPC). The mission of IROC-H is to ensure consistent and comparable radiation doses are delivered by the participating institutions and that the highest quality data is included in NCTN radiation therapy clinical trials. To accomplish its mission, IROC-H performs dosimetry audits of institutions participating in NCI funded clinical trials with a combination of off-site mail-in thermoluminescent dosimeter (TLD) and optically stimulated luminescent dosimeter programs, on-site dosimetry review visits, retrospective inspection of patient records, and trial credentialing activities that include end-to-end (E2E) anthropomorphic phantom irradiations [5]. These dosimetry audits are performed for both photon and proton radiotherapy facilities. Currently, IROC-H currently monitors 2040 institutions worldwide of which 17 are institutions utilizing proton therapy [5].

The anthropomorphic phantoms used by IROC-H include phantoms designed for photon and proton therapy. The phantoms cover various anatomical sites such as the head, head & neck, thorax, spine, abdomen and pelvis [5]. In 2014, 627 phantoms were shipped from IROC-H to institutions all over the world. These phantoms are used for the purpose of credentialing an institution's ability to use advanced radiotherapy technologies in the NCTN clinical trial setting. Phantoms are constructed to be anatomically similar to humans, have targets and organs at risk, have plastics that are good tissue substitutes and contain radiation dosimeters (TLD and radiochromic film). Institutions are asked to treat the phantom as if it were a patient and to complete the end-to-end treatment process from imaging, to treatment planning, to patient setup, and finally treatment delivery. The phantom is then sent back to IROC-H for the evaluation of the dosimeters.

A key component of the treatment process is the imaging phase. In both photon and proton therapy computed tomography (CT) imaging is used for simulating and planning the radiation treatment. CT enables the physician and dosimetrist to visualize targets, organs at risk and tissue heterogeneities so that a conformal treatment plan may be designed. Each treatment planning system used by an institution has a built-in calibration curve used to convert the Hounsfield units (HU) of the CT to electron density for photon treatment dose calculations or to relative linear stopping power (RLSP) for proton treatment range definition. These calibration curves are essential for accurate dose distribution calculations. Any uncertainty in the calibration curves may ultimately lead to variability in the dose delivery to a patient or one of IROC-H's QA phantoms. An example of a proton CT calibration curve can be seen in the curve used clinically at MD Anderson's PTC-H shown below in Figure 1.

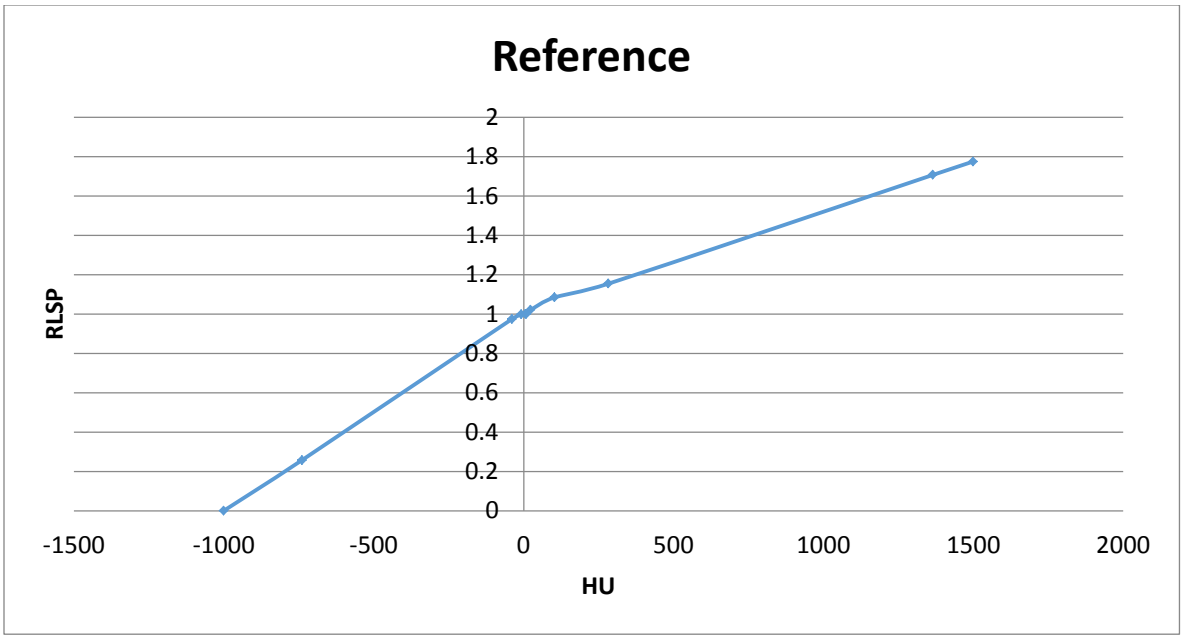

Figure 1. Proton CT Calibration curve used clinically at the PTC-H

1.1.2 Specific Problem

The use of proton therapy in NCI clinical trials requires that a proton facility first be approved by IROC-H and then it may have to complete additional credentialing requirements depending on the specific clinical trial. Both of these phases include the irradiation of IROC-H's E2E proton QA phantoms, specifically designed for use with proton therapy, to assess the facility's ability to deliver accurate doses to the desired location.

Proton E2E QA phantoms are designed with materials that have an HU value and RLSP that fall on the proton calibration curve used by proton planning systems to convert HU to RLSP. A phantom made of such materials is termed "proton equivalent." A phantom is designated as proton equivalent when it has an RLSP within five percent of the tissue-equivalent calibration curve [6]. These phantoms are designed by IROC-H and the materials are tested extensively to determine proton equivalence. It has been determined that phantom materials suitable for use in photon beams are not always suitable for use in proton beams. For this reason IROC-H has separate phantoms for use with photon and proton therapy quality assurance testing. IROC-H

currently has five E2E QA phantoms that can be used for proton therapy: head, spine, thorax, liver, and pelvis. All of these phantoms require CT imaging as a part of the E2E audit and any variation in the HU assigned to each phantom component could lead to errors in the dose calculation by the planning system due to variations in the calibration curve as a function of CT technique. Since the proton calibration curve (HU vs. RLSP) in each planning system is determined for a single proton reference energy, changes in proton energy used to deliver treatment could also result in dose delivery errors if the RLSP values for the new proton energy do not match those used for the calibration curve. Variability in CT technique and proton beam energy may play a role in the observed differences in the dose and dose distributions measured by IROC-H's QA phantoms as compared to the planning system calculations.

IROC-H monitors 17 institutions using proton therapy and has observed a lower phantom pass rate for proton institutions. This low proton pass rate has raised red flags in the proton phantom quality assurance program. The participating proton institutions receive an initial site visit by IROC-H physicists during which their calibration curve or curves are inspected. It has been discovered that most institutions use a single calibration curve with a minority using two curves, but no institutions uses more than two. IROC-H believes that a proton institutions' use of a single reference calibration curve, created with the parameters of a single CT technique used to determine HU and a single proton energy used to determine RLSP, may be a source of uncertainty in the E2E quality assurance process that contributes to institutional phantom failures. Uncertainty arises when the parameters under which the calibration curve was created are not the same parameters as those that are used to image and irradiate the phantom according to IROC-H's quality assurance protocols. Moyers' work on this subject supports the claim that changes in the calibration curve can impact dose delivery [7].

This project will focus on the uncertainty in the proton calibration curve due to CT technique and proton energy and how this uncertainty may translate to distributions in dose.

1.1.3 Importance of Topic

Clinical trials are research studies involving the direct treatment of patients to test a therapy before it becomes standard practice in the clinic. Thousands of patients are treated each year under clinical trials and provide data to determine the effectiveness of various cancer treatment approaches. New technology and methods would not be able to be utilized without first being subject to clinical trial research. In this way clinical trials are vital to moving forward in the successful detection and treatment of cancer.

In 2014, over 19,000 patients participated in NCI clinical trials conducted by 14,000 investigators at 3,100 different institutions [8]. This massive aggregate of data is only useful if the programs and protocols deliver treatment accurately and consistently. A large portion of these trials involve radiation therapy and must be monitored regularly to maintain the necessary quality of data to be used in cooperative clinical trial studies. IROC is instrumental in credentialing and monitoring these institutions and makes it possible for trials to successfully accomplish their goals.

The goal of this study is to better understand the uncertainty in the measures used by IROC-H for determining the quality of an institution's proton therapy delivery. A better understanding of this uncertainty will result in a higher level of confidence for the use of the phantom services for proton QA. This study is focusing on the uncertainty associated with the calibration curve used by the treatment planning system to convert CT number, or HU, of the images used for planning to the RLSP of protons to determine the desired energy to be deposited by the protons in a particular tissue.

As previously discussed, many proton institutions monitored by IROC are using a single calibration curve regardless of simulation and treatment parameters. The use of a single curve has the potential to cause errors in dose distribution during an IROC-H phantom irradiation if the parameters used are not those that were used to develop the calibration curve. This discrepancy could lead to a material being shifted on the calibration curve, which could cause

the treatment planning system to incorrectly calculate the range of the protons and dose to be delivered to a particular material in the phantom.

In addition to monitoring clinical trial participants and their ability to provide correct trial data, IROC-H has also been successful at detecting and preventing radiation incidents [9][10], thus playing a role in patient safety. Proton therapy utilizes the Bragg peak behavior of protons in which a very large percentage of energy is deposited at the distal end of the proton's path. Due to these high doses and steep dose gradients involved in proton therapy, accidents have the potential to cause more harm to patients than photon therapy, furthering the need for independent quality assurance checks by institutions such as IROC-H and their QA phantoms. This safety aspect enhances the incentive to reduce the uncertainty in IROC-H's proton phantom program.

1.2 Hypothesis

The hypothesis of this project is as follows:

> *Variations in CT technique and proton energy will alter the delivered dose distributions of typical proton treatments by reducing the percent of passing pixels by 10% using a gamma analysis criteria of ±3%/5 mm as measured using a heterogeneous proton QA phantom.*

The specific aims to test this hypothesis are:

1. Measure the RLSP of designated materials and create custom HU vs. proton RLSP curves for 3 commonly used CT techniques and 3 proton energies.
2. Create a treatment plan for a heterogeneous proton QA phantom with a standard treatment planning system HU vs. RLSP calibration curve. Then create nine treatment plans for the same QA phantom using the three CT image datasets.

3. Incorporate custom proton energy dependent calibration curves determined in Aim 1 into the treatment planning system and estimate the change in dose coverage due to a change in proton energy. Analyze the plan differences with a gamma analysis.

1.3 Literature Review

1.3.1 Proton background

1.3.1.1 History

The discovery of the proton is credited to Ernest Rutherford for his published experiments in 1919 in changing one element to another titled "Collision of Alpha Particles with Light Atoms" in which he identified a hydrogen nucleus [11]. Protons have since been discovered to be particles in the nucleus of every atom with a positive charge of $1.602 * 10^{-19}$ Coulombs and a mass of $1.673 * 10^{e-27}$ kg.

The use of protons for therapeutic purposes was first proposed by Robert Wilson in 1946 in his paper "Radiological Use of Fast Protons" [12]. He suggested that the new technology that allowed for the acceleration of protons to higher energies enabled charged particles to penetrate bodies for medical uses.

From the early 1950's to 1990 proton therapy began to grow as an idea for therapy and patients began to be treated at physics laboratories around the world [13]. In 1990, the nation's first hospital-based accelerator used for proton therapy opened at Loma Linda University Medical Center [14][15]. The field has continued to grow in the years since and there are now 17 proton therapy facilities in operation throughout the United States having treated over fifty thousand patients [1].

M.D. Anderson Cancer Center's (MDACC) proton therapy center - Houston (PTC-H) became clinically active in 2006 and has three rotating gantries, two providing passive scattering beams and one providing a pencil beam scanning option, and a fourth treatment room with two fixed

beamlines [16]. The center has the capability of treating patients with energies up to 250 MeV. This project was completed at the MDACC PTC-H.

1.3.1.2 Proton behavior

Protons are valuable for therapeutic use because of their unique behavior in tissue. Protons can interact via coulomb, elastic, or inelastic interactions. Protons primarily lose energy via coulomb interactions with the outer electrons of target atoms. This loss of energy is described by the continuous slowing down approximation (CSDA). As a proton interacts with particles it loses energy as a first approximation to the inverse of the proton's velocity squared. As the proton slows down more and more, this causes the majority of a proton's energy to be deposited at the distal end of its range. The mass stopping power is described by the Bethe Bloch equation which is approximated below [17].

$$\frac{S(E)}{\rho} = \frac{4\pi r_e^2 mc^2}{\beta^2}\frac{1}{u}\frac{Zz^2 L(\beta)}{A} \qquad \textit{(Equation 1)}$$

In this formula, the following variables are defined:

- S(E) Linear stopping power
- r_e Radius of an electron
- m Mass of an electron
- c Speed of light
- β Particle velocity/ speed of light
- u Atomic mass unit
- Z Atomic number
- z Charge of a proton
- L(β) Stopping power

The large characteristic deposition of energy at the end of the range of a monoenergetic proton beam is called a Bragg peak after William Henry Bragg who discovered it in 1903 [18]. Bragg peaks can be used to deposit a large dose in a tumor while sparing surrounding tissue because of the steep falloff of the dose gradient. The range of the protons and therefore the depth of energy deposition can be manipulated by changing the energy of the protons to better conform to a disease site.

Bragg peaks can be further manipulated with the use of a spread out Bragg peak (SOBP) to deliver a uniform dose over a specified distance. A range modulation wheel as pictured in Figure 2 is used to create this plateau of dose at the desired depth. A range modulation wheel is made of steps of varying absorber thickness to alter the range and intensity of protons passing through as the RMW rotates rapidly. This has the effect of creating many Bragg peaks that are superimposed to create a uniform dose across the tumor.

Figure 2. Range Modulation Wheels used at PTC-H [17]

A comparison of proton and photon depth dose profiles reveals the benefits of using protons therapeutically and can be visualized through their depth dose curves shown in Figure 3. Two apparent advantages of the proton profile are the uniform maximum dose and the steep dose falloff at the distal end of the range. While this steep gradient provides the advantage of sparing normal tissue, it also requires very precise localization of the SOBP so as to not deliver a very high dose to the normal tissue. Contrastingly, photons have a maximum dose at a shallow depth and a decreasing but relatively high distal dose.

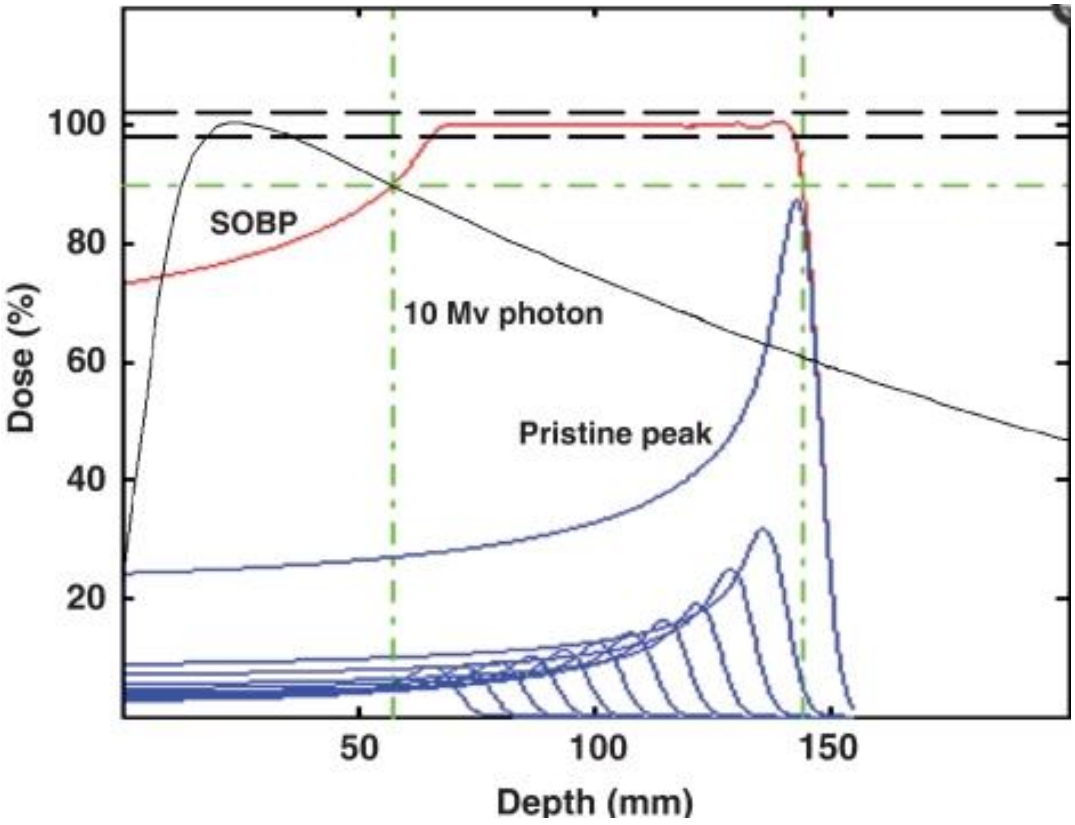

Figure 3. Depth Dose Comparison of Proton and Photon Therapy [19]

1.3.1.3 Radiobiology

Protons and other heavy ions have the advantage of having a relative biological effectiveness (RBE) greater than that for photons. RBE is defined in Equation 2.

$$RBE = \frac{Dose\ of\ referene\ radiation\ to\ produce\ an\ effect}{Dose\ of\ test\ radiation\ to\ produce\ an\ effect} \quad \textit{(Equation 2)}$$

The reference dose is generally defined to be ^{60}Co and protons are clinically defined to have an RBE of 1.1, compared to an RBE of 1.0 for photons and electrons. This implies that for the same biological effect, 10% less physical dose will be needed with protons than with photons or electrons. For this reason proton dose is often expressed in terms of Cobalt Gray Equivalent (CGE) which is defined in Equation 3.

$$CGE = Dose_{protons} * 1.1 \quad \textit{(Equation 3)}$$

In Equation 3, $Dose_{protons}$ is the physical dose of the protons.

1.3.2 Proton beam

The PTC-H has the capability of producing both passively scattered and pencil beam spot scanning proton beams. This project focuses on passive scattering. PTC-H uses the double scatter technique to create the passive scatter beam using a series of nozzle components that include a first scatterer, a RMW, a second scatterer, a range shifter, an aperture, and a compensator as shown in Figure 4. All of these components may be altered to modify the beam. The first scatterer serves to spread the beam laterally while the second scatterer serves to flatten the beam, creating a uniform energy across the entire beam [20]. A rendering of the nozzle can be seen below.

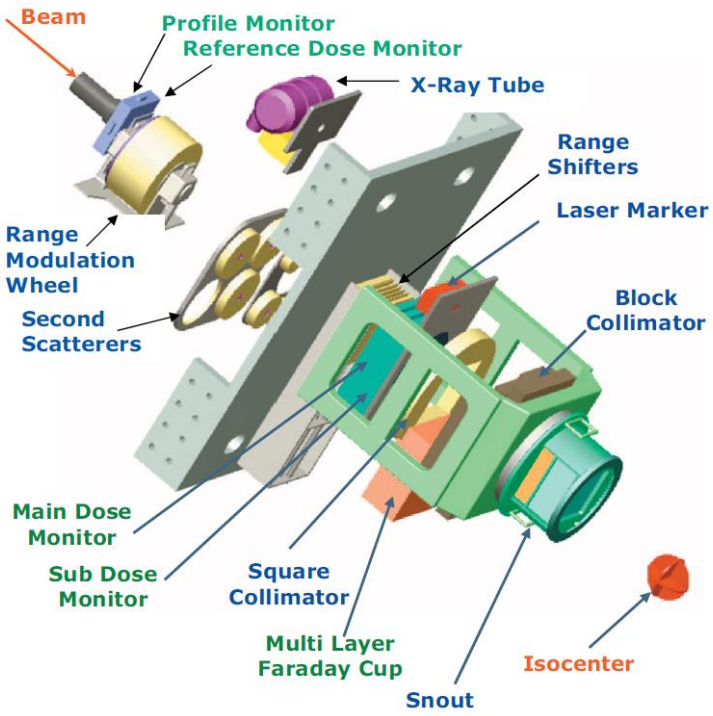

Figure 4. Passive scatter nozzle from PTC-H [16]

To be therapeutically useful, protons must be accelerated to very high energies with a cyclotron, synchrotron, or synchrocyclotron. The PTC-H uses a synchrotron system. This consists of a linac injector that generates the proton beam and accelerates it to be funneled into the synchrotron ring where it is further accelerated to the desired energy then extracted to be used in an individual gantry for a patient [16].

Pencil beam scanning, though a growing area of proton therapy, is not utilized in this project and will not be discussed here.

1.3.3 CT calibration

Proton therapy is able to effectively treat conformal tissues because of the use of computed tomography (CT) imaging. CT images serve as the input to treatment planning systems that

enable the creation of a conformal plan to treat the tumor and spare normal tissue by accounting for these heterogeneities.

The process of patient treatment of an IROC-H phantom audit begins with CT simulation in which the patient or phantom is imaged with CT to be used for planning on. These images are imported into the facility's treatment planning system at which point the system uses a predefined calibration curve to convert HU, the data from the CT image, to RLSP, the energy to be deposited by the protons. This calibration can be determined in one of two ways, with the stoichiometric method, or with the tissue substitution method.

The CT number, or HU, is defined in Equation 4.

$$HU = 1000 * \frac{\mu_{material} - \mu_{water}}{\mu_{water}} \qquad \textit{(Equation 4)}$$

In Equation 4 $\mu_{material}$ is the linear attenuation coefficient of the material being analyzed and μ_{water} is the linear attenuation coefficient of water [7]. HU is a convenient way to quantitatively describe how a material attenuates x-rays in a CT image.

The second factor used in the calibration curve is the RLSP of the protons. This is a measure of how protons deposit energy in a particular material relative to that of water.

1.3.3.1 Stoichiometric method

Although not used for this project, it is worth noting that the stoichiometric method has been shown to be more accurate than the tissue substitution method and is the method used by the PTC-H [21][22][23]. The stoichiometric method examines the problem that tissue equivalent materials are not always sufficiently close in composition to yield accurate RLSP values for patient tissues. This method seeks to correct for the differences in elemental composition

between tissue substitutes and real tissues. This is accomplished by parameterizing the HU values into a scaled HU with photoelectric, coherent scatter, and incoherent scatter components [24]. The dependence of attenuation is fit as a function of atomic number as shown in Equation 5. This can be done for any tissue substitute with a known composition and density.

$$HU_{scaled} = \rho_e(AZ^{3.62} + BZ^{1.86} + C) \qquad \textit{(Equation 5)}$$

In Equation 5 ρ_e is the electron density, Z is the atomic number, and A is a photoelectric component constant, B is a coherent scatter component constant, and C is an incoherent scatter component constant.

1.3.3.2 Tissue substitution method

The tissue substitution method is the original method of determining the calibration curve. In this method, a variety of materials determined to be tissue equivalent are scanned and irradiated to determine their HU and RLSP. This curve can then be imported into the treatment planning system to be used to correct for heterogeneities in patient plans. The RLSP is calculated using the Bethe-Bloch formula described previously. The Moyers et al. describes the creation of a calibration curve with a large number of materials and outlines a simplistic alternative for RLSP calculations. Moyers defines the RLSP in Equation 6.

$$RLSP = \frac{R_{90,water} - R_{90,material}}{t_m} \qquad \textit{(Equation 6)}$$

$R_{90,water}$ is the depth to distal 90% ionization in the water phantom by itself and $R_{90,material}$ is the depth to distal 90% ionization in the water phantom with the slab of material in front. t_m is the

thickness of the slab and must be known very precisely in this calculation to yield accurate results [7].

1.3.4 Gamma Analysis

The comparison of measured and calculated dose distributions is a critical part of commissioning and quality assurance on treatment planning systems. Daniel Low developed a technique that provides a quantitative measure of this comparison that can be displayed and analyzed where this had previously not been possible. He termed this measure the gamma index and this method was used in this study to compare dose distributions.

Low's method uses an elliptical surface to take into account both dose difference and distance to agreement (DTA) metrics when comparing distributions. Criteria for both dose difference and DTA are inputs into the calculation and determine the size and shape of the ellipsoid used. Dose difference is emphasized in regions of uniform dose while DTA is emphasized in regions of steep dose gradients. The ellipsoid is centered on a measured point to be tested and if the measured value is found on this surface the point is considered "passing" [25][26]. Figure 5 shown below was developed by Low and gives a geometrical presentation of the dose difference and DTA applications independently for both 2D and one dimensional (1D), respectively, and Figure 6 is Low's geometrical presentation of how these metrics work together, again in 2D and 1D, respectively.

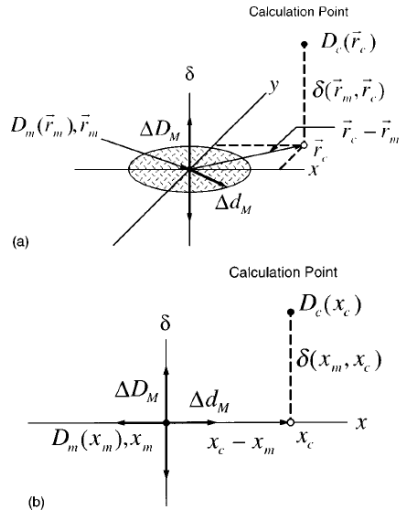

Figure 5. Geometrical representation of dose difference and DTA [20]

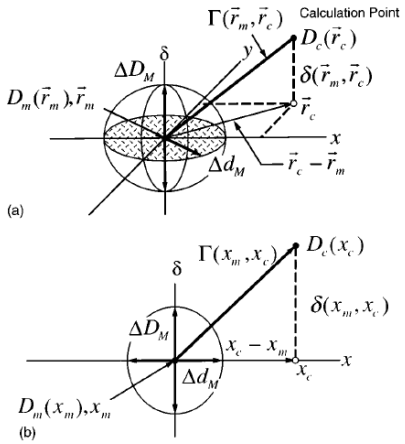

Figure 6. Geometrical representation of both dose difference and DTA [20]

In these representations, the following variables are used:

ΔD_M: Dose-difference criterion

Δd_M: DTA criterion

$D_m(r_m)$: Measured dose

$D_c(r_c)$: Calculated dose

$\delta(r_m,r_c)$: Difference between measured and calculated doses

The gamma index is quantitatively defined in Equation 7 below. A γ≤1 is considered "passing," while a γ>1 is considered "failing."

$$\gamma(r_m, r_c) = \sqrt{\frac{r^2(r_m,r_c)}{\Delta d_M^2} + \frac{\delta^2(r_m,r_c)}{\Delta D_M^2}} \qquad \textit{(Equation 7)}$$

The method described here was developed to compare two dimensional (2D) measured dose distributions to dose distributions calculated by a treatment planning system. IROC-H has a need to compare 2D dose distributions from film and three dimensional (3D) dose measurements and performs a registration and gamma analysis using an open source program called A Computational Environment for Radiotherapy Research (CERR). CERR uses the Matlab language and is widely used to share radiotherapy data results in an easily accessible format. The goal of this study is to compare 3D dose calculations against other 3D dose calculations which has recently been made possible with upgrades in the CERR software to include 3D gamma analysis.

Chapter 2

2 Materials and Methods

2.1 Phantoms

2.1.1 Proton CT Phantom

The proton CT phantom shown in Figure 7 was created by IROC-H while searching for "proton equivalent" materials to be used for QA purposes. All materials in the phantom were measured to have RLSP's within 5% of the proton CT calibration curve used clinically at the MD Anderson Proton Center. It contains inserts of materials all measured to be "proton equivalent" including water, polyethylene, balsa wood, blue water, PRESAGE®, and Techtron® HPV [6]. These materials span a wide range of HU and RLSP's on the curve and are intended to be utilized to create a reasonable fit with only a small number of materials. Currently IROC-H end-to-end audit procedures utilize anthropomorphic phantoms with materials that are not always "proton equivalent." This requires institutions to override RLSPs for certain materials, which does not allow the accurate assessment of the calibration curve and may introduce errors in the dose calculations. The proton CT phantom is currently used by IROC-H to verify consistency of calibration curves used by proton facilities participating in NCI-funded proton therapy clinical trials.

The proton CT phantom was used in this project as the standard for creating calibration curves to be used for analyzing the differences in curves with varying proton parameters.

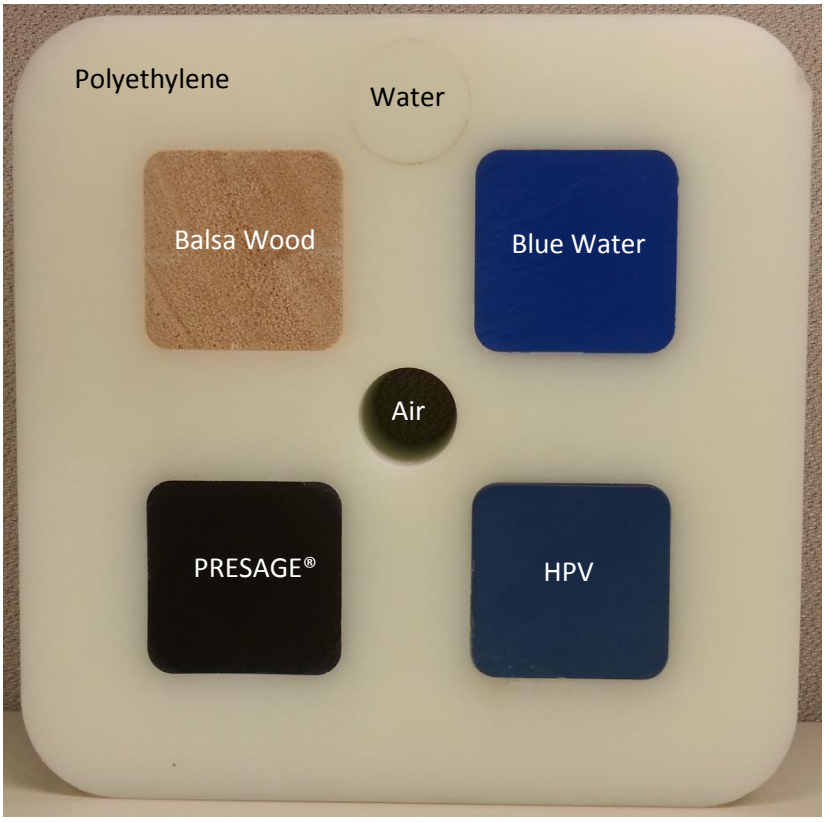

Figure 7. Proton CT Phantom

2.1.2 Proton lung phantom

In 2011 Tony Blatnica modified an existing IROC-H thorax phantom that was used for photon stereotactic body radiation therapy (SBRT) to be more "proton equivalent" so that it could be sent out to proton institutions for approval/credentialing purposes. The need for the modification stemmed from the lack of proton equivalent materials and air gaps in the existing dosimetry insert that created difficulties in characterizing the insert in a proton beam [27]. Blatnica utilized the existing base phantom and created a new dosimetry insert using balsa wood as a verified lung equivalent material to replace the cork that was previously being used. In 2013 Jim Neihart developed a new lung phantom as shown in Figure 8 that was completely proton equivalent. This new

phantom retained the insert designed by Blatnica and received a new phantom base, ribs and heart made of materials more suitable for use in a proton beam as well as the addition of an intra-fractional respiratory motion simulation capability.

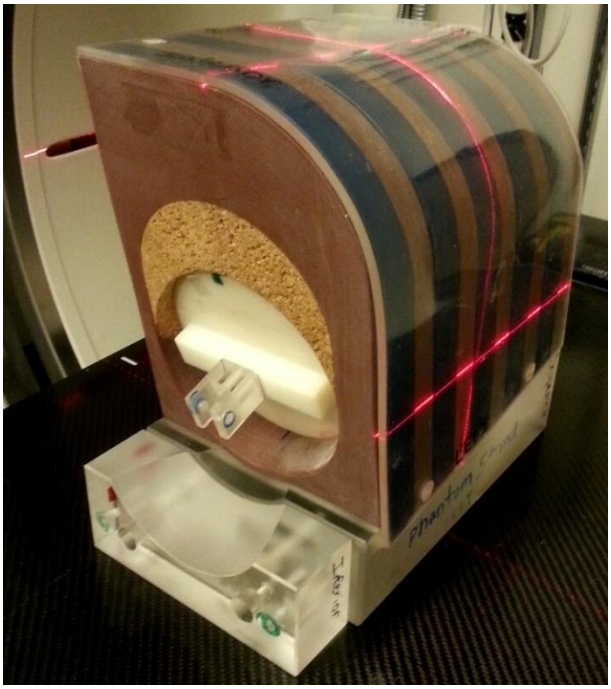

Figure 8. Proton Lung Phantom

The proton lung phantom designed by Neihart pictured above in Figure 8 is currently in use by IROC-H for proton quality assurance assessments and is the lung phantom used in this project. The phantom is designed to simulate a single lung, deemed sufficient due to the fact that most lung tumors are treated with a single lateral field and a single oblique or anterior field, thus there was no need to provide a contralateral lung. The phantom is comprised of five proton equivalent tissue simulating materials. To simulate lung, soft tissue, heart tissue, tumor, and bone, the phantom uses respectively balsa wood and cork, solid water, blue water, high impact polystyrene, and Techtron® HPV Bearing grade plastic [28]. These materials were all measured to be within IROC-H's "proton equivalent" criteria, that is to be within 5% of M.D. Anderson Cancer Center's Eclipse HU vs. RLSP CT calibration curve [6].

2.2 CT scans

2.2.1 CT Scanner Constancy

HU values of the materials in the proton CT phantom were measured on the clinical CT simulation scanners at MD Anderson's PTC-H and Ambulatory Clinical Building (ACB). To ensure the reliability of HU measurements, multiple measurements were taken at varying intervals on the scanners to confirm the constancy of the output. The CT phantom was scanned (see Figure 7) and HU was measured for five consecutive days and then on a weekly basis for five weeks. The CT scans were performed on the two CT machines with parameters shown in Table 1:

Table 1. Parameters of CT Constancy Scans

Parameter	GE Lightspeed (Located in PTC-H)	GE Lightspeed (Located in ACB)
kV	120	120
Pitch	1.375:1	1.5:1
Extent	S50mm-I50mm	S50mm-I50mm
Beam Configuration	16x0.625	4x1.25
No. of Images	41	41
Beam collimation	10 mm	5 mm
Speed	13.75 mm/rot	7.5 mm/rot
Matrix size	512	512
Reconstruction	Standard	Standard
DFOV	50 cm	50 cm
SFOV	Large	Large
Rotation speed	0.8 sec	1.0 sec

The setup for the scans is pictured in Figure 9.

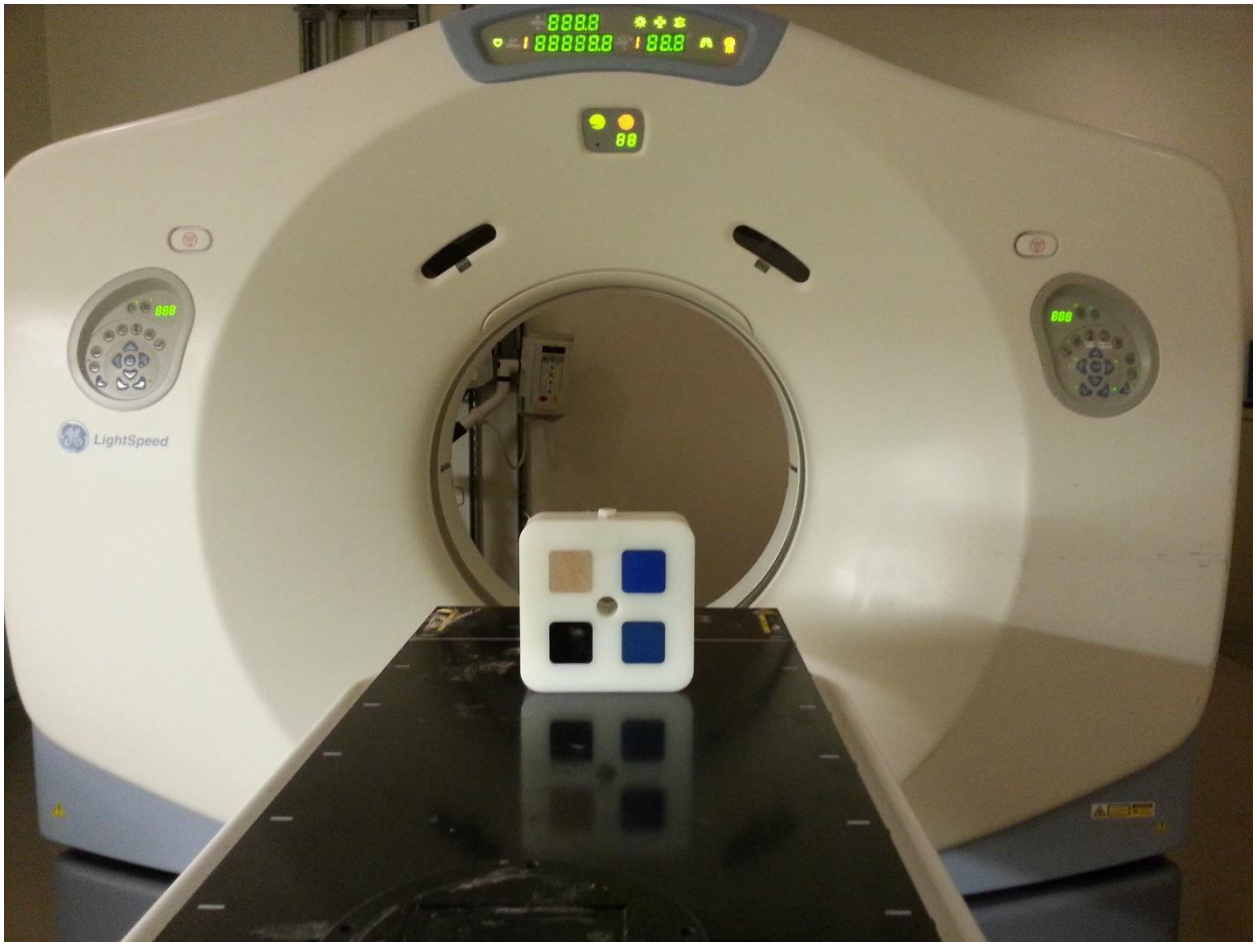

Figure 9. Setup of CT phantom in CT simulator

The resulting scans were loaded into the iSite (Philips, Amsterdam, The Netherlands) interface created by Philips where it was possible to create ROI's and measure the average HU as shown in Figure 10. Because all measurements were taken with this software, consistency between GE equipment and Philips viewing software is not of concern.

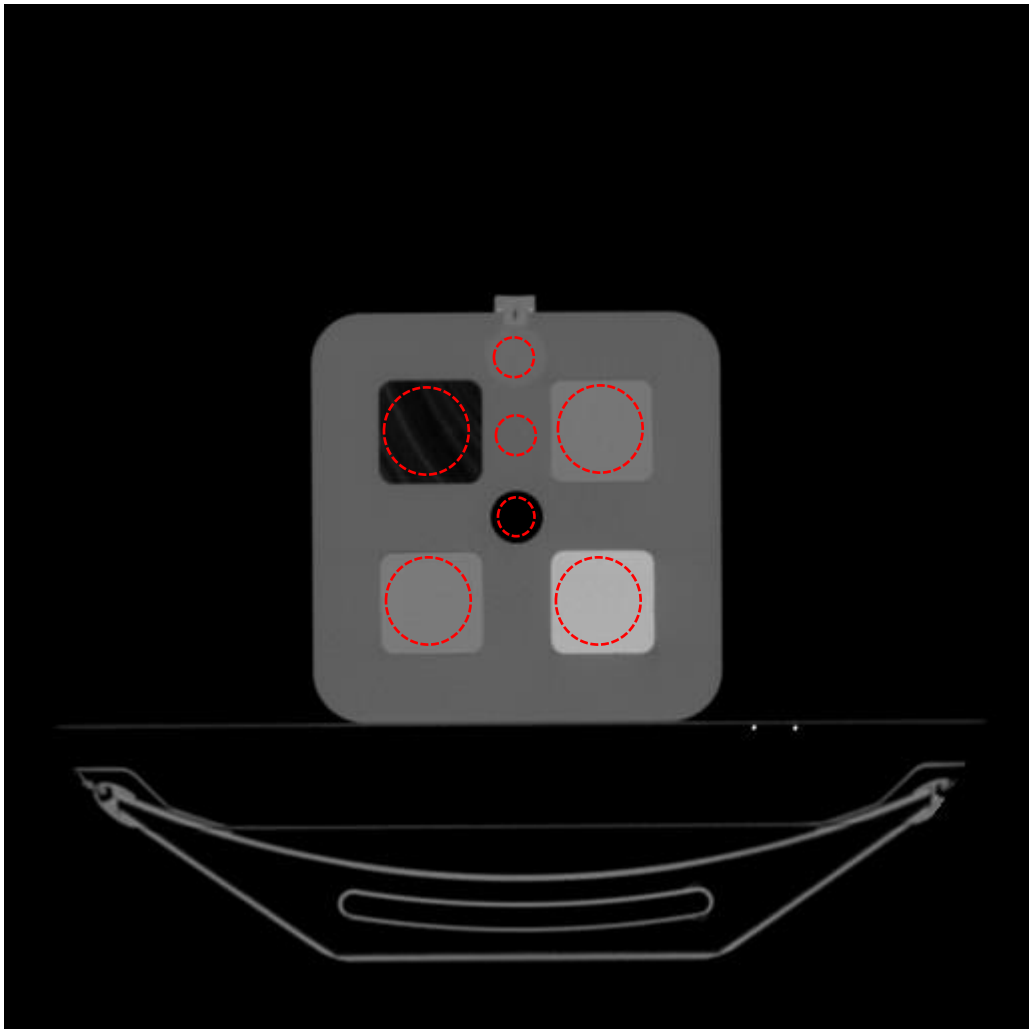

Figure 10. Measurement of HU

2.2.2 HU measurement

Institutions participating in proton audits by IROC-H at this time are using both 120 and 140 kV, with a majority using 120 kV when imaging the proton lung phantom during the CT simulation step of the audit process. These energies were therefore both included in this study, with 80 kV being included because of the possible future use of dual energy. Dual energy CT (DECT) is gaining momentum as a modality for simulations [29] and most methods of DECT use 80 kV as the lower energy used for increased contrast [30]. In the event that institutions participating in IROC-H QA begin using DECT

for simulations, it is valuable to understand how this change could affect the random uncertainty in the IROC-H QA process. It is also valuable to include this large range of CT techniques used to evaluate worst case scenarios for criteria used by institutions, in the event that an institution may be trying to simulate a special procedure involving uncommon criteria.

CT scans were taken of the proton CT phantom using 3 different CT techniques, 80 kV, 120 kV, and 140 kV to investigate changes in the proton CT calibration curve as a function of CT technique. For each CT beam quality, ten scans were taken of the proton CT phantom and the HU of each phantom material was averaged for a given energy to input into a unique proton CT calibration curve.

2.3 Determination of Proton RLSP

2.3.1 Tissue substitution method

The RLSP of each material in the proton CT phantom was determined using the tissue substitution method described by Moyers using a passive scatter proton beam on gantries 1 and 2 at the PTC-H. This method was introduced in the previous chapter.

To determine the RLSP for a material using this method, a slab of the material is placed in front of a water phantom and central axis depth dose curve measurements with the beam passing through the material are taken with an ionization chamber. A second depth dose curve in water only is measured without the material in the proton beam. RLSP is then calculated according to Equation 6 as previously defined.

An electronic caliper was used to measure the average thickness of each measureable material in the CT phantom as detailed below in Table 2.

Table 2. Thickness of CT phantom materials

Material	**Average Thickness [cm]**
Polyethylene	7.0167 ± 0.0099
Balsa wood	7.0037 ± 0.0018
Blue water	7.0087 ± 0.0008
HPV	6.9690 ± 0.0080

Presage®	6.9200 ± 0.0066

Instead of using a water phantom and ionization chamber as Moyers suggested, this project used a Zebra multi-layer ion chamber (MLIC) (IBA, Bartlett, USA) designed to simulate a water phantom to determine proton depth dose curves. The Zebra is an MLIC produced by IBA for high precision particle therapy dosimetry and is shown in Figure 11.

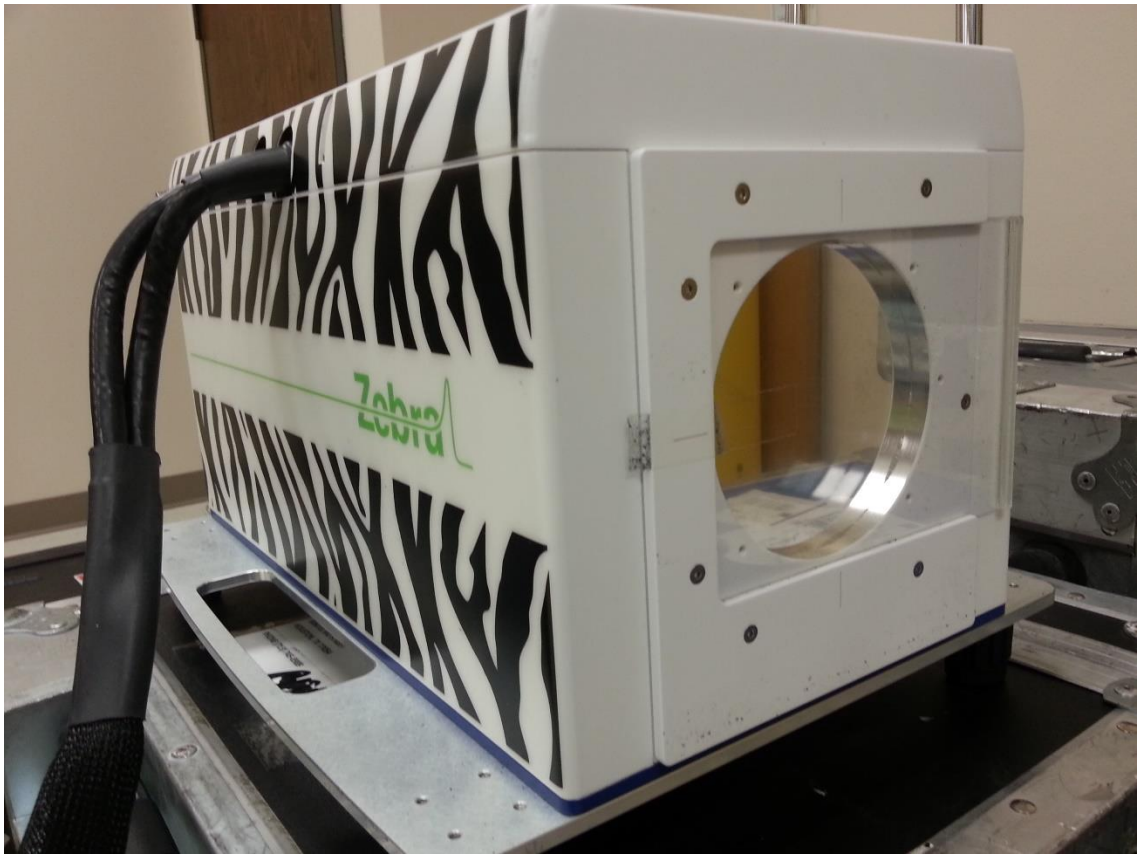

Figure 11. Zebra MLIC

It is comprised of 180 plane parallel ionization chambers spaced 2 mm apart with a removable 1 mm WET buildup block to increase the resolution of measurements [31]. The buildup screen was not used in this experiment because there was not a need for the increased precision of measurements. Each proton CT phantom material was

placed in the beam path near the front window of the Zebra to acquire the data to create the proton depth dose curves with the material in place.

The Zebra utilizes the OmniPro-Incline software, also produced by IBA, for the measurement and analysis of depth dose curves. The software allows the user to manually select the plateau region as well as manually defining the background locations on the depth dose profile in order to calculate the R_{90} that can be used in the RLSP calculation. These defined areas can be seen below in Figures 12 and 13 and the resulting compilation of depth dose profiles measured by the Zebra and reported by Incline can be seen in Figure 14.

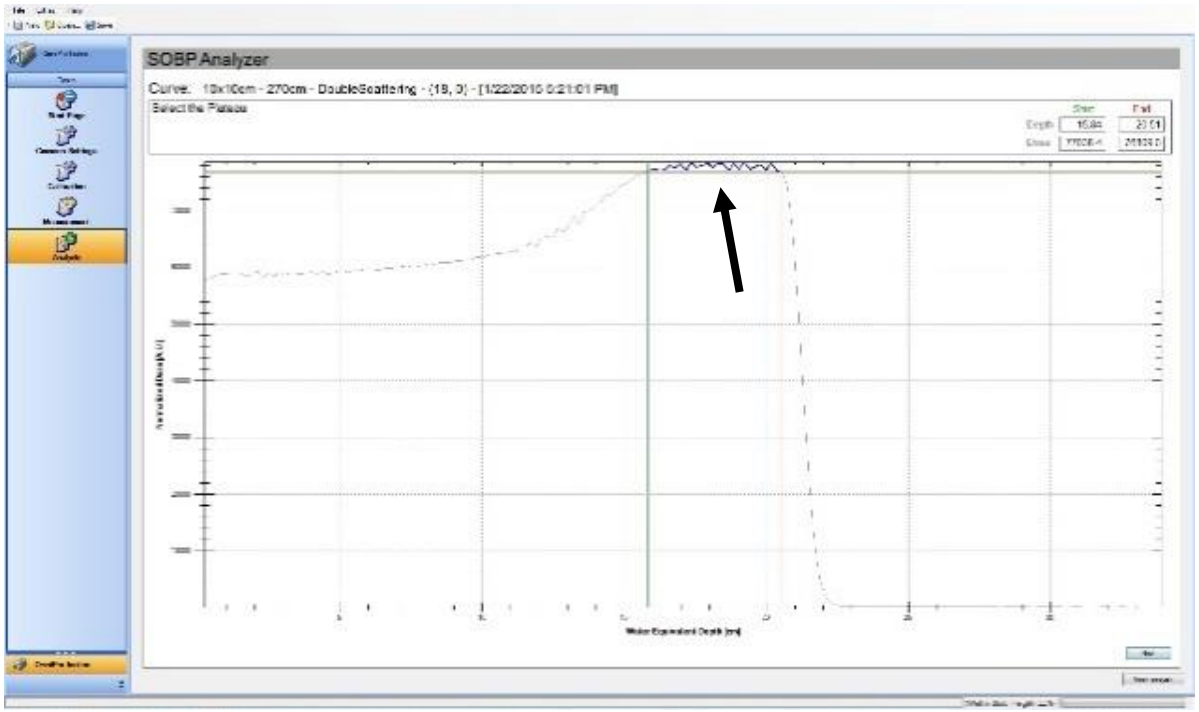

Figure 12. Selection of plateau in Incline

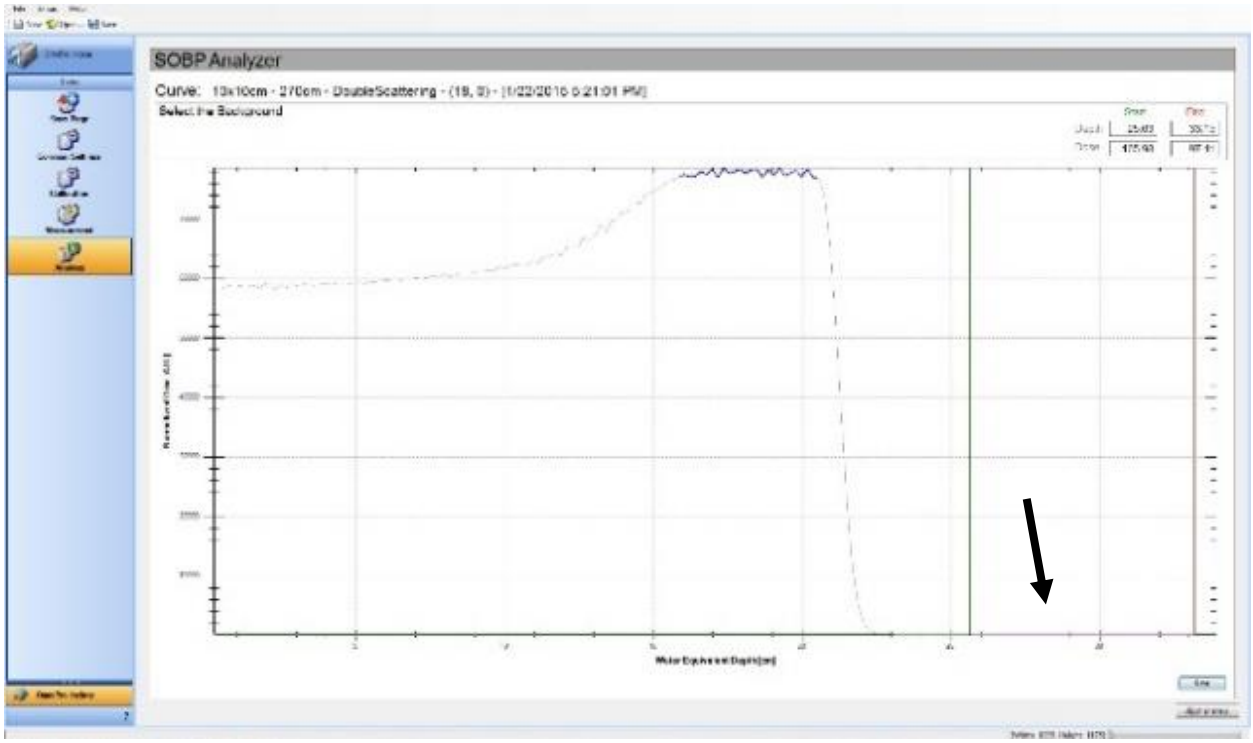

Figure 13. Selection of background in Incline

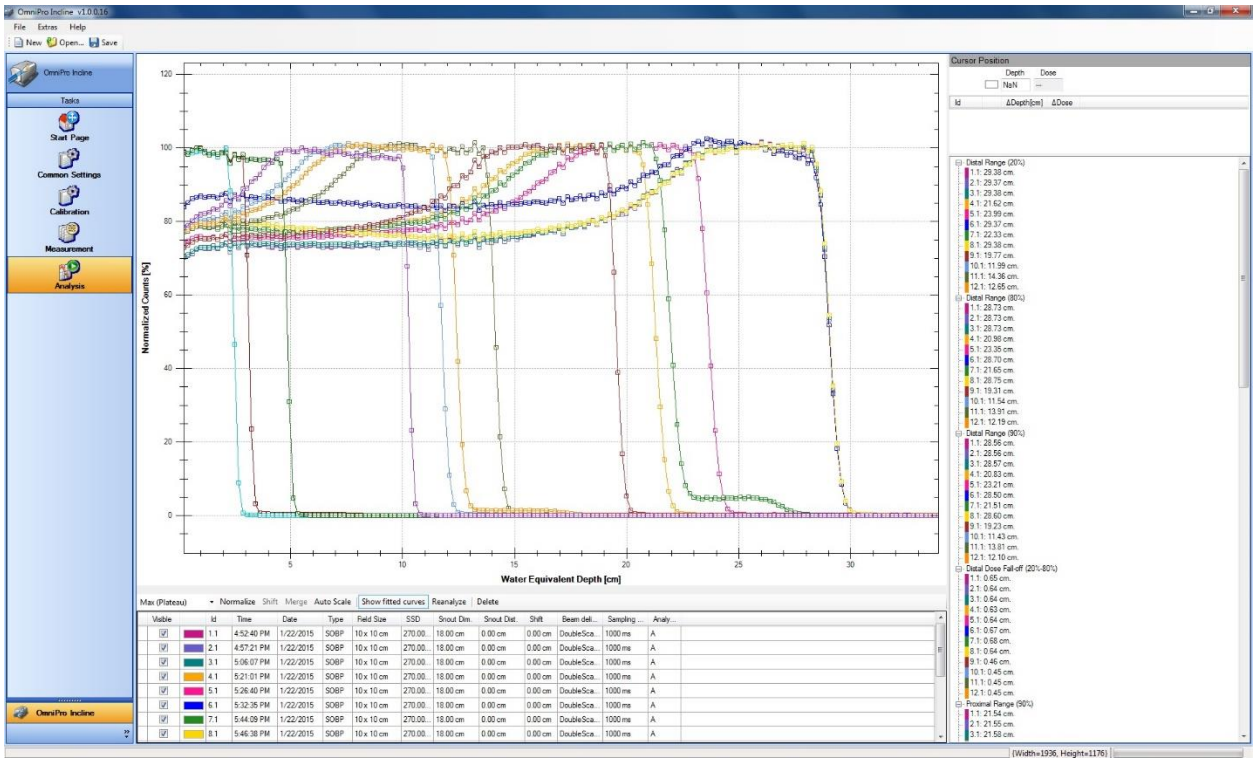

Figure 14. Depth Dose Profiles Measured by Zebra and Analyzed by Incline

At low proton energies, such as the 140 MeV beam used for this project, the SOBP is very shallow and can be only partially measured by the Zebra when the proton equivalent materials are placed in front of the Zebra. Because of this specific issue, the $R_{90,material}$ had to be manually determined from the incomplete measured SOBPs for blue water, Presage®, bone equivalent, and polyethylene to calculate the 140 MeV RLSP measurements.

Three sets of RLSPs were calculated using Equation 6 as previously defined for each material with each set corresponding to a specific proton energies, 140, 200, and 250 MeV.

2.4 Creation of custom calibration curves

Nine separate custom HU to RLSP proton CT calibration curves were created using three different CT techniques and 3 different proton energies. 7 different materials were measured for HU and corresponding RLSP under each of the 9 different sets of conditions. An example of a curve plotting HU against RLSP is shown below in Figure 15 for a single CT technique and proton energy pair, with each point representing a material from the proton CT phantom. All nine of the custom curves created can be found compiled in Chapter 3 and individually in Chapter 5.

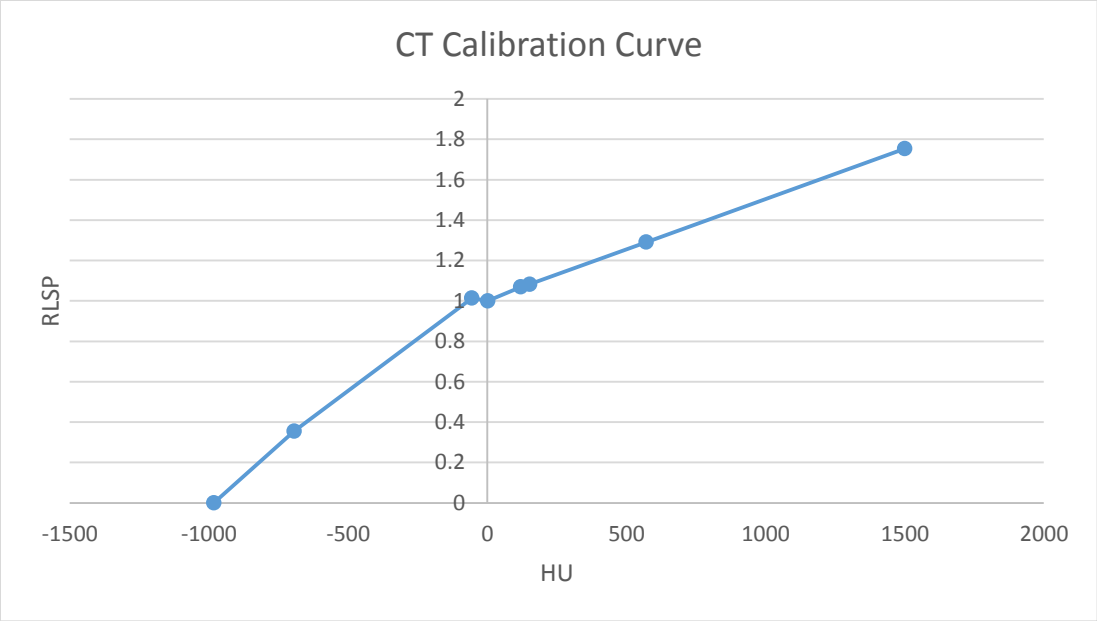

Figure 15. CT Calibration Curve for 120 kV CT technique and 140 MeV proton energy

Each generated proton CT calibration curve was imported into the Eclipse treatment planning system (Varian, Palo Alto, CA) to be used during treatment planning. The curves were imported manually, one point at a time. To be used by the treatment planning system, the curves were modified by extending to the minimum and maximum HU values in order to be read by the planning system software. It was assumed that all values above 1500 would have the same RLSP and so the curve was extended to the maximum HU, 3071, at the same RLSP to ensure the inclusion of every pixel above 1500 HU in the treatment plan. This same method was also employed at the low end of the HU spectrum. The curve was extended to the lowest possible HU value, -1024, and defined with the same RLSP as air in order to ensure the inclusion of all pixels with HU values below that measured for air.

In addition to the extension of each curve to meet Eclipse requirements, the curves were also altered to have only increasing values to meet Eclipse requirements. The curves specific to the 250 MeV proton energy already had this feature, but the curves specific to 140 and 200 MeV were altered to fit this requirement due to the RLSP of polyethylene being higher than its adjacent material, water. This was accomplished through an HU override feature

available in the Eclipse treatment planning system. This method involved defining 4 new contours for each plan that used a curve specific to 140 or 200 MeV. The region to be redefined was the area under the curve starting from the HU at which the curve first has an RLSP equal to unity up to the HU at which the curve has an RLSP equal to unity for a second time (the point defined by water). This region was divided into 4 sub-regions based on the maximum RLSP and half of the maximum RLSP. A thresholding tool was used to define four contours (labeled Override1 through Override4) that encompassed all of the pixels with HU defined in these sub-regions.

The average RLSP of each of the four regions was determined and the corresponding HU for the region of the curve in which HU > 0 was used to override the originally assigned HU value. In this manner the RLSP on the calibration curve in the entire region being redefined could be set as unity to satisfy the requirement of Eclipse because all HU values in this region have been redefined as described for the purposes of dose calculations. An example of these Override contours for the plan utilizing the 120 kV, 140 MeV calibration curve is shown below in Figures 16-18.

In reality, Eclipse will not allow any points on the CT calibration curve to have the same RLSP or HU, so 0.001 was added or subtracted from RLSP values as necessary to fulfill this requirement. This was determined to not be a significant source of uncertainty in the results of this project.

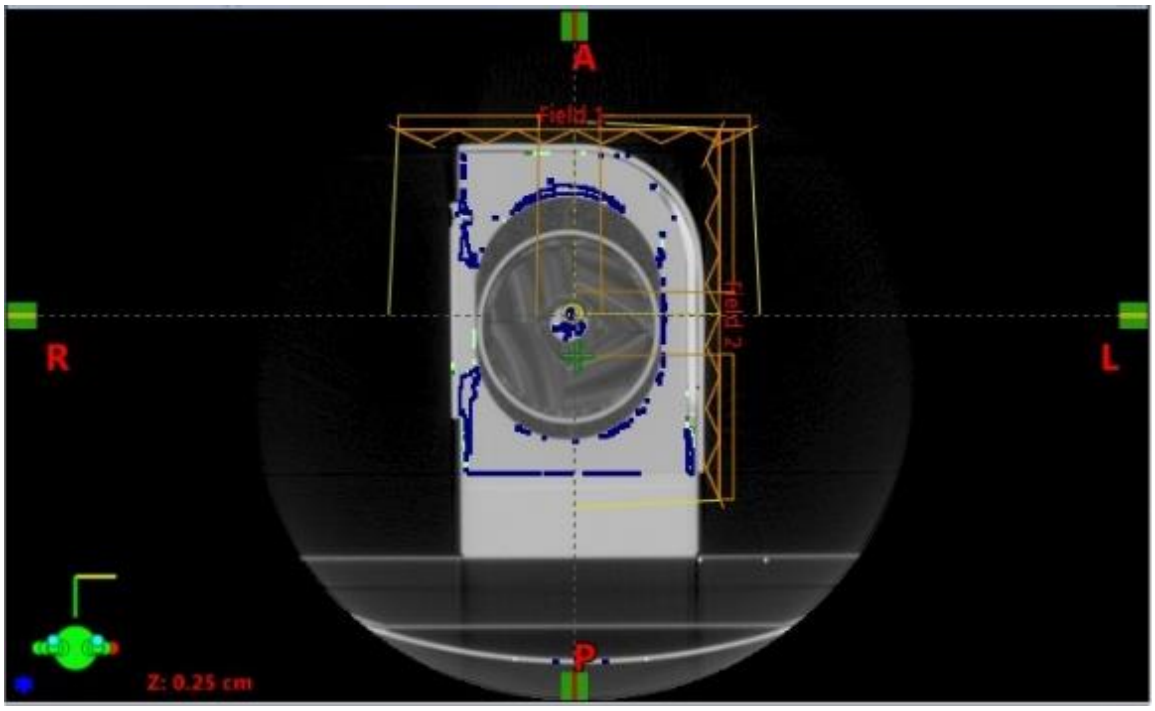

Figure 16. Contours for CT Overrides at Isocenter in Axial View

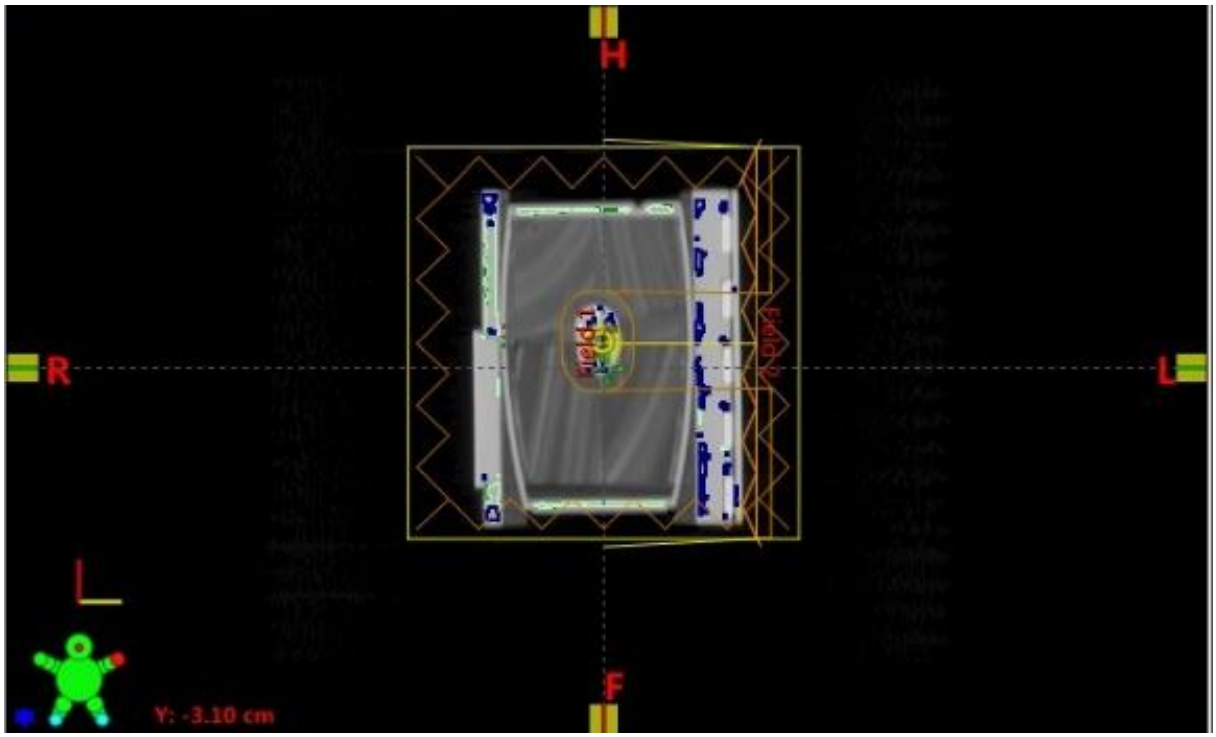

Figure 17. Contours for CT Overrides at Isocenter in Coronal View

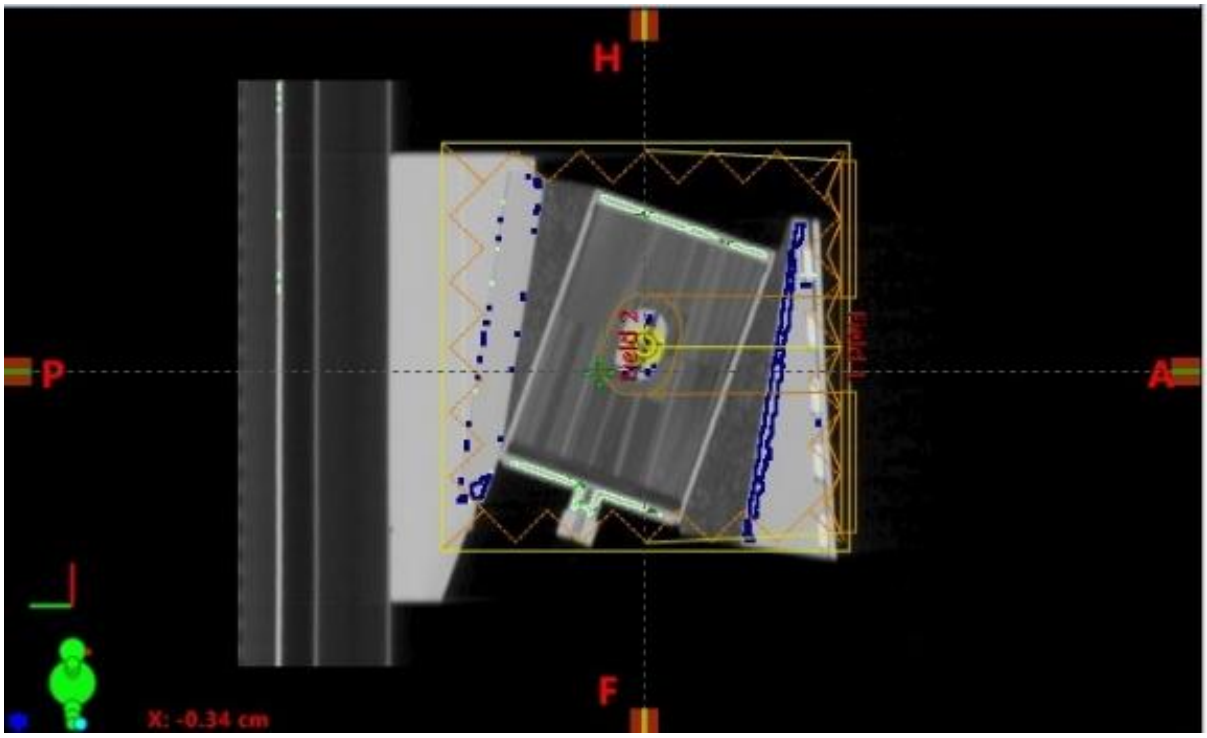

Figure 18. Contours for CT Overrides at Isocenter in Sagittal View

All 9 curves were loaded separately into the Eclipse treatment planning system under beam administration to be available for application to any treatment plan in the Research Eclipse system.

2.5 Treatment planning

The Research Eclipse treatment planning system at PTC-H was used for all treatment planning in this project. Nine treatment plans were created for the proton lung phantom, with one plan for each of 9 calibration curves created using varying combinations of CT technique and proton energy as described previously. The three data sets taken of the proton lung phantom with the CT simulator were used for treatment planning. Data sets were taken at three CT techniques: 80, 120, and 140 kV.

In this study, treatment plans using a calibration curve created with a specific CT technique were planned on the data set created at that same CT technique (for example, all plans that use a calibration curve created with a 120 kV CT technique will be planned on the 120 kV data set acquired as described in previous sections).

All plans were created using a proton energy of 140 MeV because it a typical energy used by institutions performing these lung phantom audits. Planning at the 200 and 250 MeV proton energies was not pursued in this project due to practical issues of the phantom size and design. Higher energies would not allow the SOBP to easily be placed at the target in the phantom without additional manipulation.

All plans were created with the following contours: Body, Lung, Heart, PTV, Target, and TLD. 4 additional CT override contours were created for each plan using a CT calibration curve made using 140 or 200 MeV protons. An example of all of these contours can be seen below in Figure 19 in the plan created for use with the 120 kV / 140 MeV CT calibration curve.

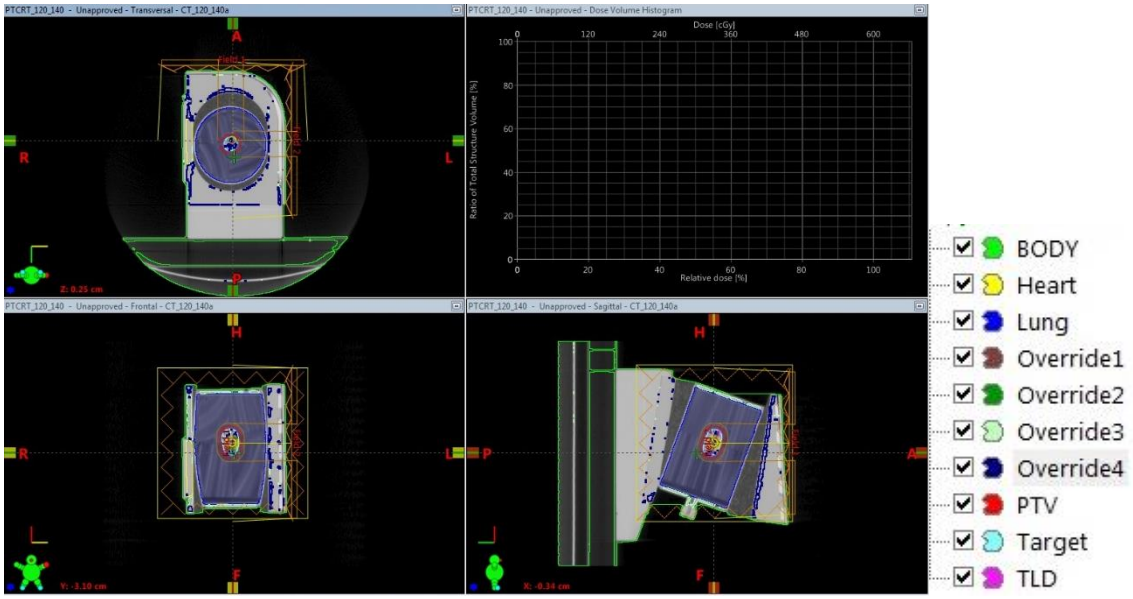

Figure 19. Contours used in treatment planning

Institutions participating in previous proton audits have created treatment plans with a variety of beam arrangements. The beam arrangement chosen for this project is a common orientation used by institutions and is the most easily reproducible for irradiations of the phantom. This study chose to create all plans with two fields, an AP beam at 0° and a left lateral beam at 90°. A compensator and block was created for each beam. Table 3 outlines parameters in every plan used for the purposes of treatment planning. All plans have identical parameters with the exception of CT dataset and CT calibration curve.

Table 3. Treatment planning parameters

Proton energy	140 MeV
Distal margin	0.6 cm
Proximal margin	0.3 cm
Reference point	Target
Nominal SAD	270 cm
Technique	Double Scattering
Machine	G2
Isocenter	(-0.34 cm, -3.10 cm, 1.85 cm)
Snout size	Medium
SOBP width	4.0 cm
Field 1 Nominal range	9.88 cm
Field 2 Nominal range	8.76 cm
Plan normalization value	97.00
Total dose	600 cGy
Fractions	1

2.6 Dose comparison

2.6.1 Dose Volume Histogram (DVH) Comparison

DVH's compare the percent volume of a specified structure that receives a given dose. These are useful in maintaining safe and effective radiation treatments for patients because they allow the monitoring of specific organs and regions. Target regions can be monitored to ensure they receive an acceptably high dose and organ doses can be monitored to ensure they remain acceptably low to avoid any adverse effects to the patient.

The DVH relationship is used in this study to ensure the created treatment plans are clinically viable and meet any clinical constraints. It also provides an additional way to compare the 9 treatment plans created for this study.

2.6.2 Gamma Analysis

2.6.2.1 3D Gamma Index Analysis

The primary goal of this study was to compare the dose distributions of treatment plans created using the different CT calibration curves created under varying parameters outlined above. The comparisons were made between the various treatment plan volumetric dose distribution data sets assessing agreement using a 3D Gamma Index analysis tool with a ±3%/5mm criteria. This is problematic for the original CERR program, but updates to the software have incorporated the ability to compare two 3D dose files.

From the Eclipse treatment planning system it is possible to export a DICOM RT dose file. Because CERR can only read one dose file at a time, it must be exported as a single total dose and not individual dose files from each field. CERR has the capability of converting these files, which are exported as DICOM files, into matlab files.

This study compared multiple plans to a single reference plan. This reference plan was defined as the plan created with a CT calibration curve corresponding to the CT scan using 120 kV and a proton energy of 140 MeV. This plan was chosen as reference because these parameters are the most appropriate clinically and most widely used for

the proton lung phantom due to its size and composition. A total of 8 comparisons to the reference plan were made using CERR's 3D gamma index analysis tool.

To perform a 3D gamma analysis in CERR the reference dose file must be converted from a DICOM RT file to a matlab file and can then be imported into the CERR viewer. Then each successive DICOM RT dataset for each treatment plan is imported and CERR gives the user the option to choose individual plans for 3D gamma comparison. The 3D gamma function provides the user with gamma statistics as well as a visual representation of the gamma results which can be found in the Appendix of this report.

2.6.2.2 2D Gamma Index Analysis

In addition to a 3D gamma analysis, a 2D gamma analysis was also performed between the reference plan axial, coronal and sagittal slices going through the isocenter and the corresponding slices for each of the other eight plans. The same gamma analysis criteria of 3%/5mm was used for these comparisons. This 2D evaluation was performed because the IROC-H anthropomorphic proton phantoms use radiochromic films in the sagittal, coronal and axial planes to measure the dose distribution delivered to the phantoms and to compare to the dose distribution calculated by the institution's treatment plan. Because the film is planar, the only comparisons that can be done are 2D gamma analyses. Therefore it was necessary to mimic how the proton phantoms are actually used and analyzed to determine whether the variations in CT technique and proton beam energy tested would have any impact on the phantom/institution comparison results. This 2D analysis was also of interest to show differences between the 3D gamma analysis versus the 2D gamma analysis because it has been shown that 3D gamma analyses result in a higher pass rate than 2D gamma analyses [32].

The 2D gamma analysis was performed with the OmniPro I'mRT software created by IBA. The region of interest (ROI) was tightened to contain only the target and adjacent low dose regions to avoid the skewing of the results from including a high number of pixels with very low dose. This was performed for a plane at isocenter in all three

spatial planes, axial, coronal and sagittal. An example of the ROI chosen can be seen below in Figures 20-22.

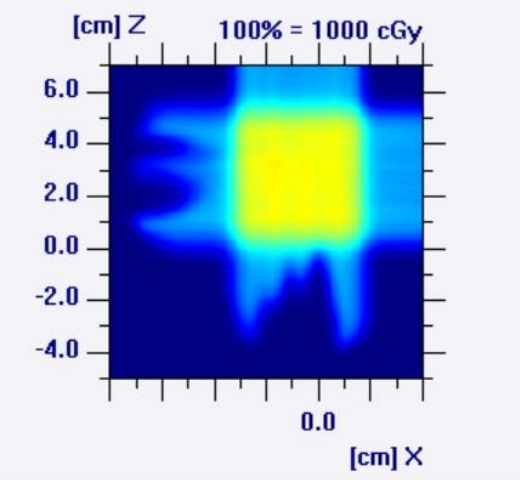

Figure 20. 2D gamma analysis of axial slice at isocenter comparing the study reference plan to the plan corresponding to 140 kV and 250 MeV.

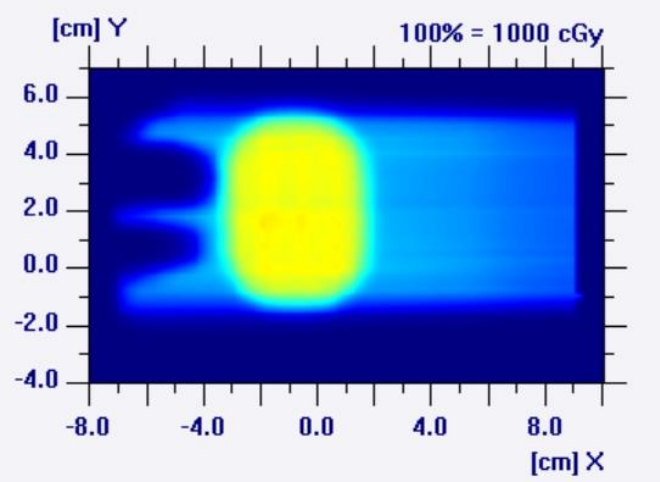

Figure 21. 2D gamma analysis of coronal slice at isocenter comparing the study reference plan to the plan corresponding to 140 kV and 250 MeV

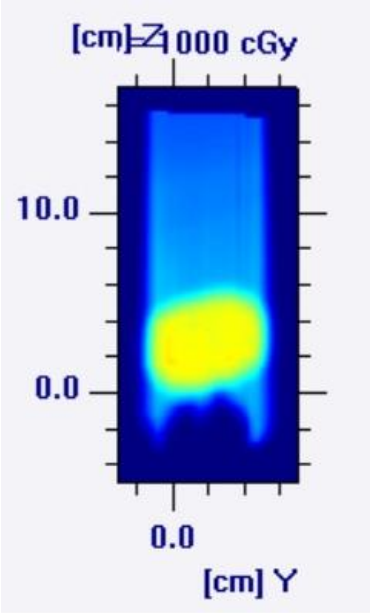

Figure 22. 2D gamma analysis of sagittal slice at isocenter comparing the study reference plan to the plan corresponding to 140 kV and 250 MeV

Chapter 3

3 Results and Discussion

3.1 Aim 1 (HU/RLSP determination and calibration curve creation)

The goal of the first specific aim was to measure the HU and RLSP of designated materials and then create custom calibration curves to be used in treatment planning. The first step in creating custom curves was to measure the HU of each material in the proton CT phantom for each of three CT techniques: 80, 120, and 140 kV. The first step in this process was to measure the constancy of the CT scanner over time and the results of this can be seen below. Measurements were taken daily for five days and then weekly for a subsequent 5 weeks. The results are pictured below in Figure 23 with the standard deviation of each material visualized in Figure 24.

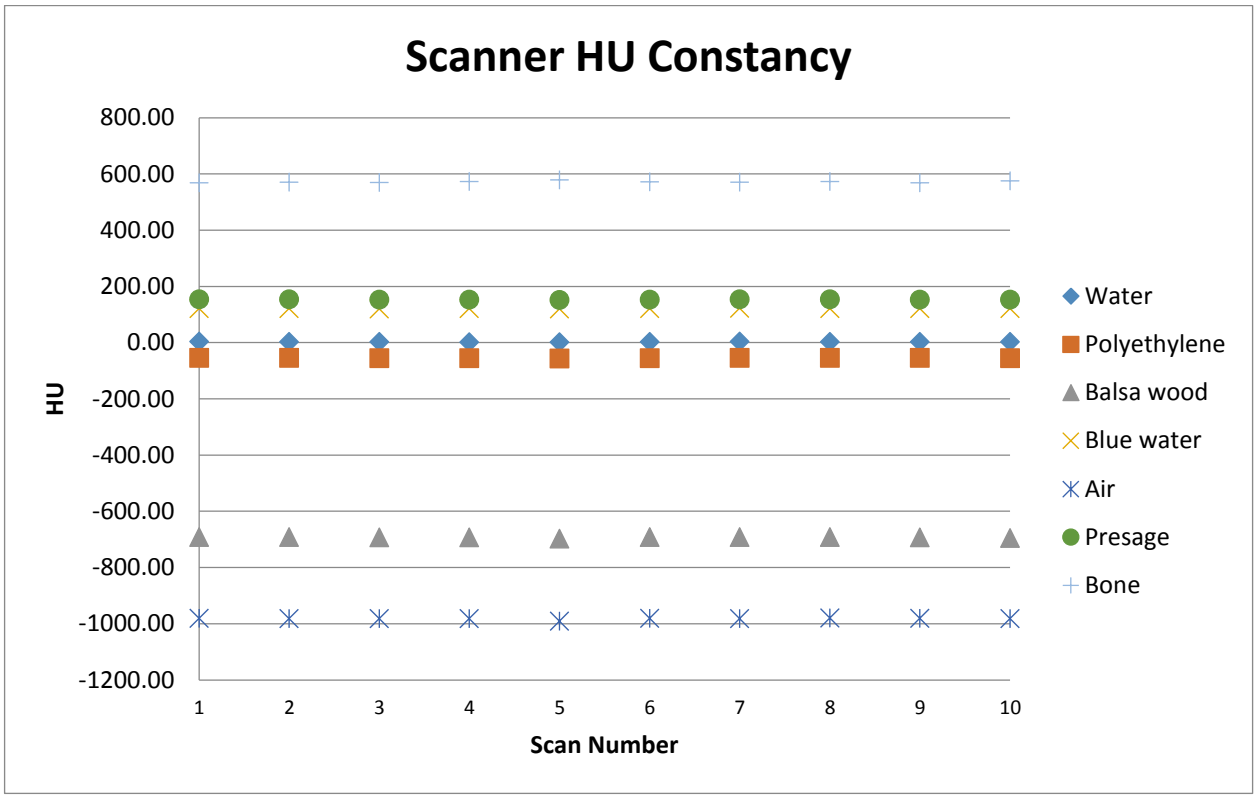

Figure 23. Constancy of HU values on MD Anderson CT simulation scanners

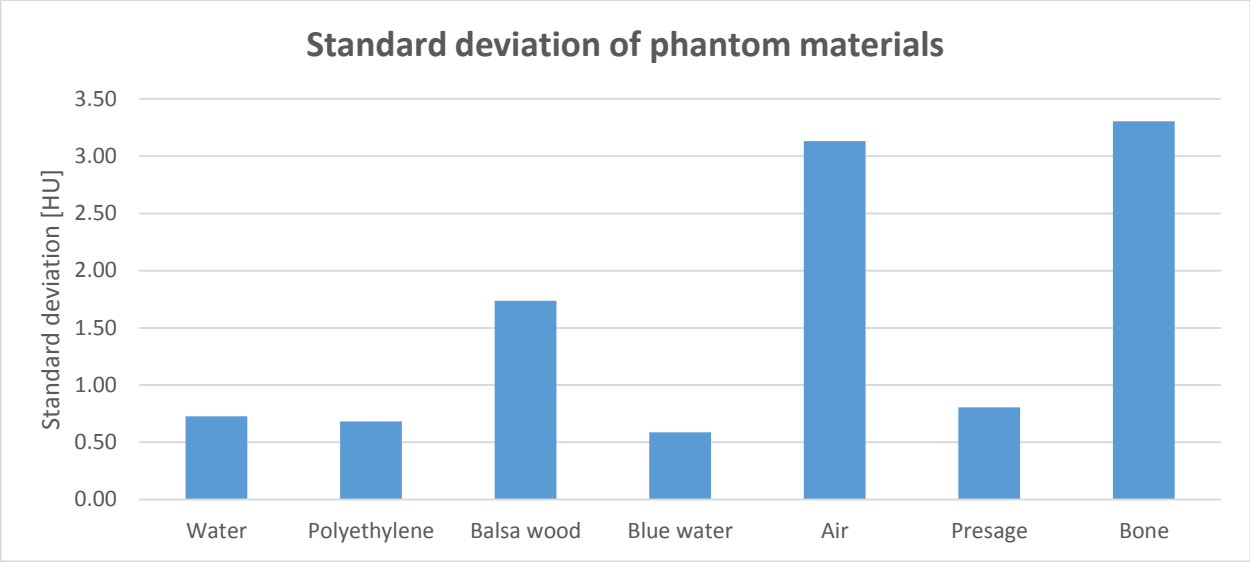

Figure 24. HU variability of CT phantom materials

These figures show that the largest deviations occur in bone. This is expected due to the high density of the material and potential for beam hardening or streaking artifacts. A similarly high deviation is seen for air. This stability over time is comparable to that seen in QA at PTC-H as well as in literature [33].

The resulting HU values measured at multiple CT energies can be seen below in Table 4. Only minor differences in the HU of the low density materials (air and balsa wood) were observed, but for the other materials, excluding water, the points of normalization, differences in HU were observed between the 3 CT energies. The largest difference, up to an approximately 80% difference, was observed between the 80 kV and the two other CT techniques. The maximum percent change between 120 and 140 kV was observed for polyethylene with a 17% change. Moyers reports a small change in RLSP due to non-standard CT techniques at low atomic numbers that increases with increasing atomic number [7]. We see this same increasing deviation as the density of material increases [34].

Table 4. Measured HU at three CT techniques

	HU		
Material	**80 kV**	**120 kV**	**140 kV**
Air	-981.90	-982.79	-980.58
Balsa wood	-695.56	-693.48	-693.28
Polyethylene	-85.29	-55.53	-47.62
Water	3.55	2.00	2.69
Blue water	159.01	120.48	111.67
Presage®	191.09	152.72	143.53
Bone	757.61	571.17	528.69

In addition to HU, the RLSP was measured for each material in the CT phantom at each of three proton energies: 140, 200, and 250 MeV. These results can be seen in Table 5 below. The resulting variation in RLSP as a function of proton energy was very small. The maximum difference was observed for the balsa wood material showing a 7.3% increase in the RLSP going from 250 MeV to 140 MeV. As the density of the materials increased, the variation in RLSP decreased to be less than 1%.

The HU for air listed in Table 4 were measured in the air hole of the proton CT phantom. Literature has reported up to a 1.8% difference in HU of air measuring inside and outside a phantom and this could therefore be an additional source of uncertainty in the HU measurements [35].

These data in Table 5, except for the lung equivalent material of balsa wood, agree with the data published by Moyer et al that reported an energy dependence of <1.2% for soft tissues [7].

Balsa wood is used to simulate lung tissue the maximum difference in RLSP due to proton energy in this material could be a cause for concern[36]. The data indicate larger differences in RLSP that would result in larger changes in proton range, altering the dose distribution.

This is relevant for the lung phantom and this material because of the possibility of larger errors in the structure of interest during lung irradiations of this IROC-H phantom.

Table 5. Measured RLSP at three proton energies for the 120 kV CT technique

	RLSP		
Material	**140 MeV**	**200 MeV**	**250 MeV**
Air	0.000	0.000	0.000
Balsa wood	0.355	0.345	0.331
Polyethylene	1.014	1.016	0.996
Water	1.000	1.000	1.000
Blue water	1.068	1.067	1.067
Presage®	1.082	1.085	1.085
Bone	1.290	1.281	1.277

Proton CT calibration curves were created by plotting HU versus RLSP for all combinations of CT technique and proton energy. These custom curves were compared to the calibration curve currently used clinically by the Eclipse proton treatment planning system at UT MD Anderson Cancer. This comparison is relevant because the currently used curve was created with the same equipment used to create the custom calibration curves for this project. Figure 25 below pictures the clinically used calibration curve as a reference compared to all 9 of the custom curves created for this experiment. The large dashed line depicts a 3% difference from the clinical reference curve and the smaller dashed line depicts a 5% difference from the clinical reference curve.

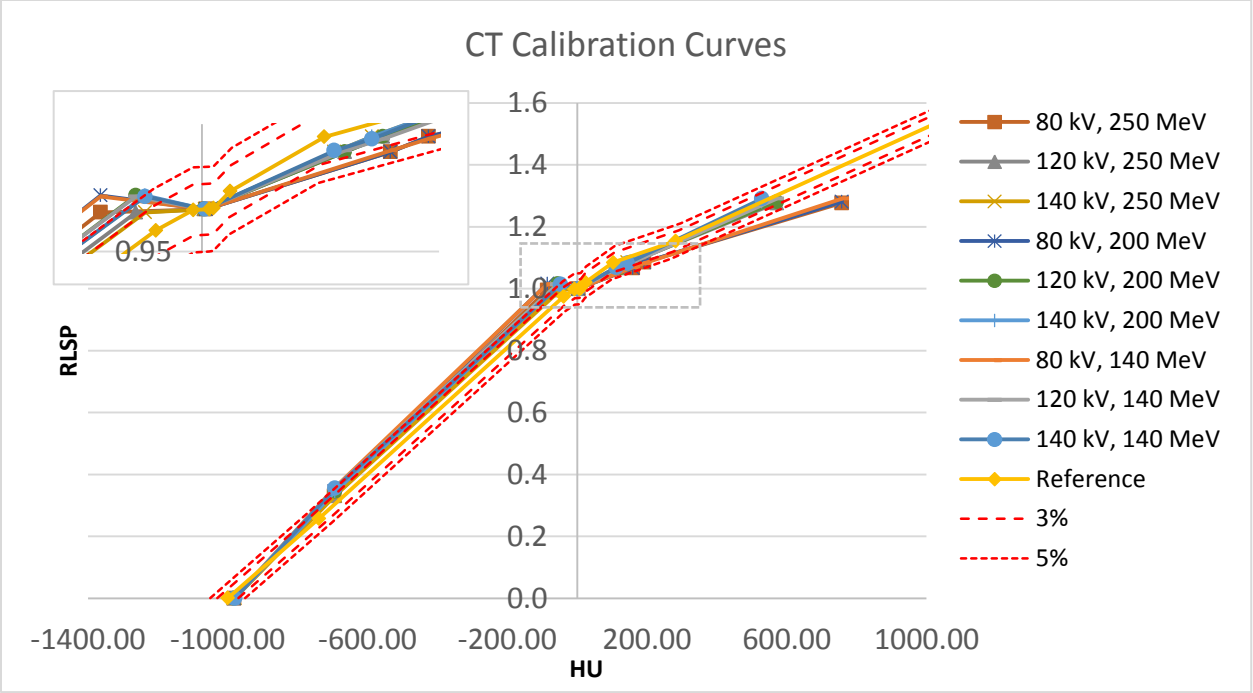

Figure 25. Custom CT calibration curves with clinical reference curve

As seen in Figure 25 above, the polyethylene material is the material with the largest difference from the clinical reference. For each curve seen above polyethylene is the material with HU ranging from -48 to -83. This data shows RLSP values for polyethylene greater than unity, causing the CT calibration curves to not have constantly increasing RLSPs. While this can be an issue for practical reasons with the treatment planning system, this is consistent with data found in the literature and therefore not a cause for concern [7]. This figure can be reexamined without the effects of polyethylene in Figure 26 below.

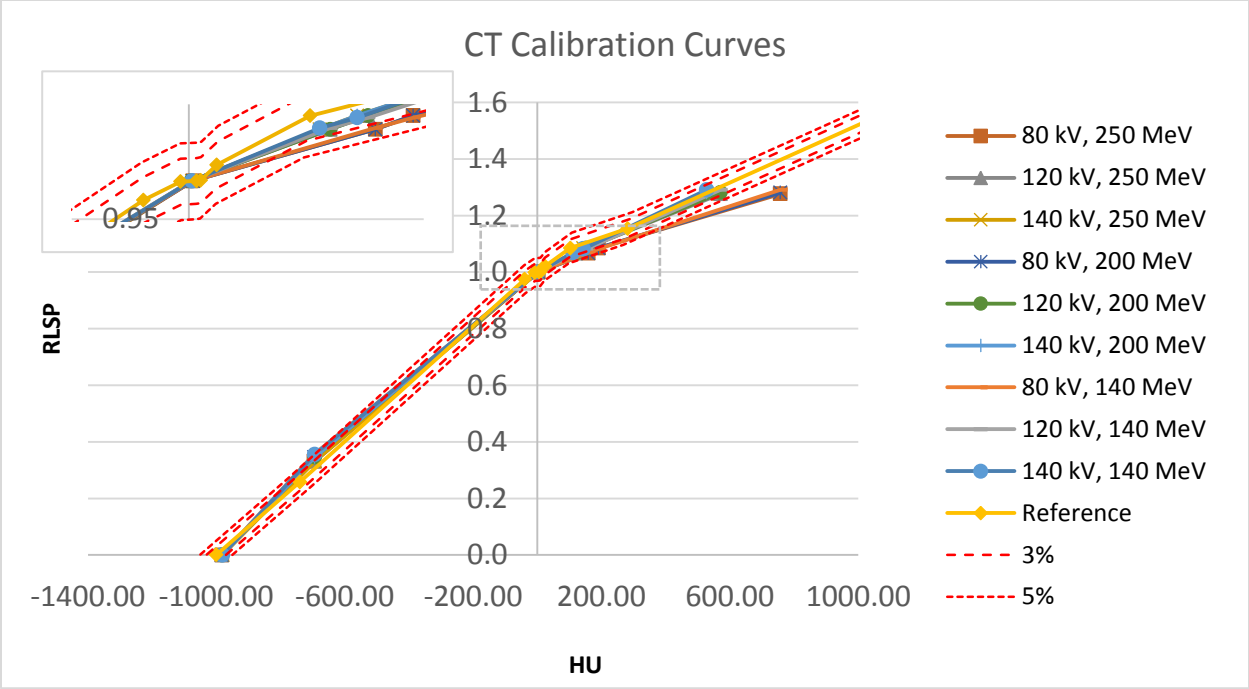

Figure 26. Custom CT Calibration curves with clinical reference curve excluding polyethylene

With the exclusion of polyethylene, most points on the curve fall within the ±5% boundary. It can be seen that at low CT techniques (80 kV) the curve begins to fall further away from the reference at higher HU values. For a given material of any HU, the maximum difference in predicted RLSP between the clinical reference curve and the custom curve is 12%. Due to the Bragg peak associated with steep proton dose gradients, errors in proton dose delivery could be significant if the edge of the peak lies close to an interface with a high density material, as this data shows RLSP has a maximum deviation in high density materials such as bone. This high deviation at low CT could pose a problem for institutions if they were imaging patients under this very low CT technique and the patient had metal implants, for example. In this scenario it would be recommended to the clinic to override high density materials for treatment planning.

The custom calibration curve can also be visually compared to the "reference" curve defined by this project as the curve created with 120 kV CT technique and 140 MeV proton energy. This difference can be seen below in Figure 27. The 3% and 5% differences are

defined from the reference curve for this study rather than the clinical reference curve here.

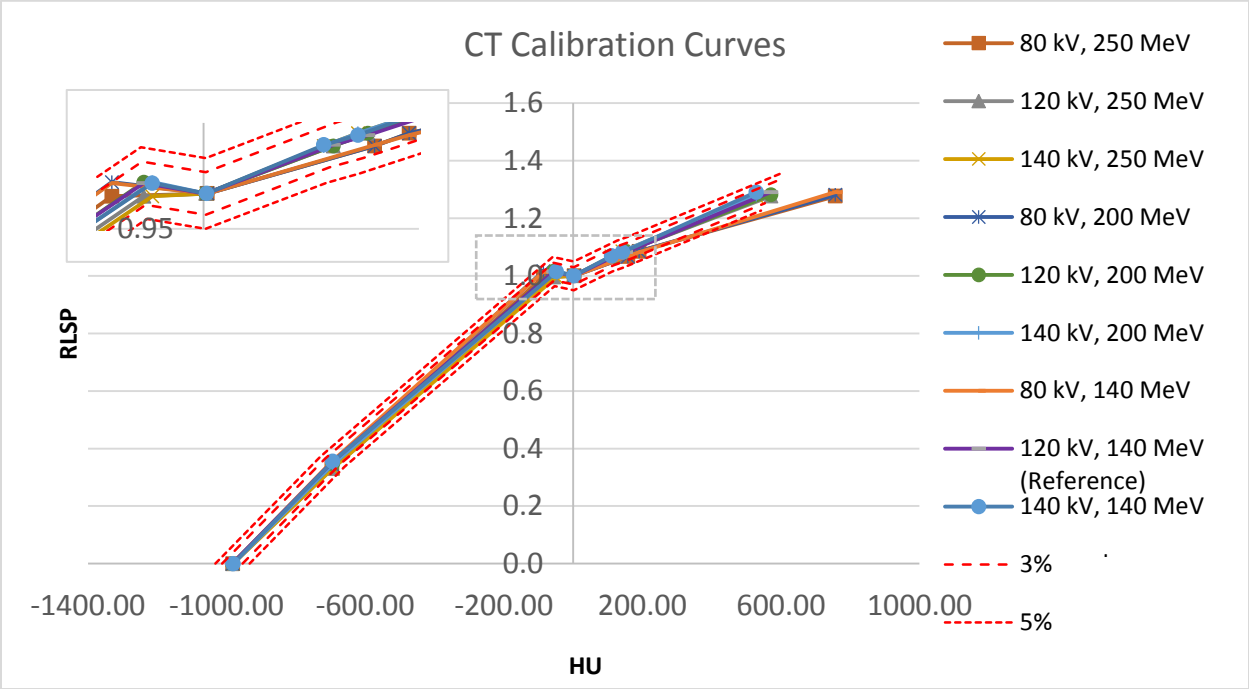

Figure 27. Custom CT Calibration curves with 120 kV/ 140 MeV reference curve including polyethylene

When polyethylene is included, the curves stay within 3% difference of the 120 kV/140 MeV reference curve pictured in Figure 27 to a much higher degree than the 3% difference line of the clinical reference curve shown in Figure 25. The same drift of RLSP corresponding to low kV (80 kV) away from the reference can be seen. For a given material of any HU, the maximum difference in predicted RLSP between the study reference curve and the custom curve is 7%, lower than that between the clinical reference curve and the custom curve.

An example of the modified calibration curves to be input into the Eclipse treatment planning system is shown below in Figure 28. It is shown compared to the reference curve currently used in the clinic at PTC-H.

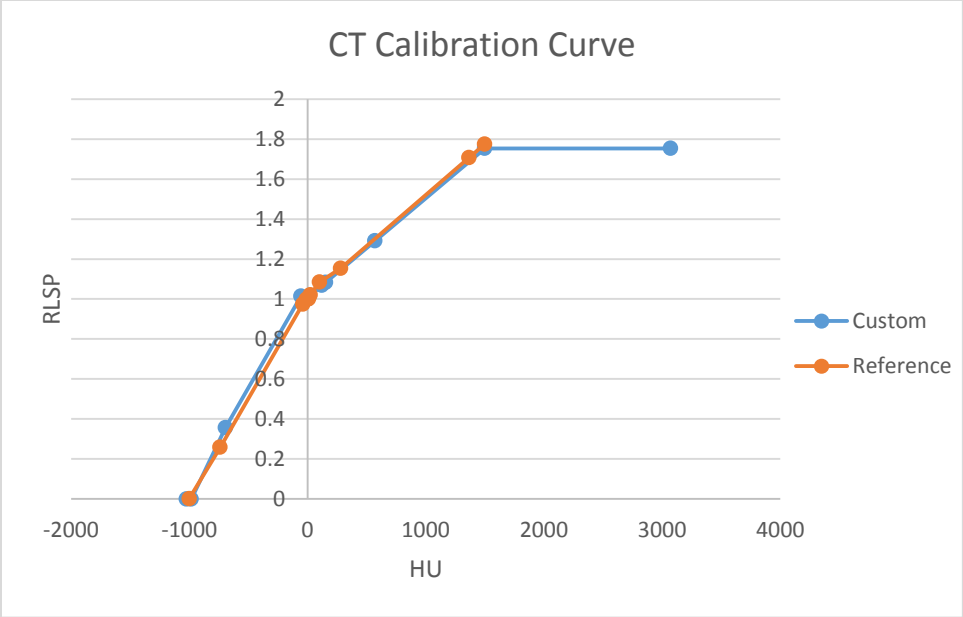

Figure 28. CT Calibration Curve for Input into Eclipse Treatment Planning System Corresponding to 120 kV CT Technique and 140 MeV Proton Energy

Additionally, the uncertainty in material thickness was examined to determine the possible effect on RLSP that would translate to deposited dose. These results can be seen below in Table 6.

Table 6. Effect of material thickness on RLSP

	140 MeV		200 MeV		250 MeV	
Material	**RLSP Difference [MeV cm^2/g]**	**RLSP Percent Difference**	**RLSP Difference [MeV cm^2/g]**	**RLSP Percent Difference**	**RLSP Difference [MeV cm^2/g]**	**RLSP Percent Difference**
Polyethylene	0.001	0.140	0.001	0.140	0.001	0.140
Balsa wood	9.27E-05	0.026	9.00E-05	0.026	8.63E-05	0.026
Blue water	0.000	0.012	0.000	0.012	0.000	0.012
HPV	0.001	0.115	0.001	0.115	0.001	0.115
Presage®	0.001	0.095	0.001	0.095	0.001	0.095

Table 6 shows that the uncertainty in the material thickness leads to a maximum change in RLSP of 0.001 across all materials and proton energies. 0.001 is the smallest unit of RLSP difference that the Eclipse treatment planning system can differentiate and therefore would not lead to a meaningful change in dose distribution.

3.2 Aim 2 (Creation of plans)

The goal of aim 2 was to incorporate the custom CT calibration curves into the Eclipse treatment planning system to create 9 different treatment plans to evaluate their effects on the resulting dose distributions to see if there were any measurable differences. The 9 different dose distributions were calculated by the planning system based on the given RLSP provided by the custom curve and the subsequent calculated proton range and deposited dose.

3.2.1 Dose Volume Histograms (DVH)

The DVHs for three organs (heart, lung, and target) for each plan was examined in the treatment planning system and compared to clinical standards to assess the quality of the treatment plan. The DVHs between the 9 plans were also compared as a measure of differences due to the varying CT technique and different proton energy. An example DVH of the plan corresponding to 120 kV CT technique and 140 MeV proton energy can be seen below in Figure 29. The remaining 8 DVH's for all plans can be found in the Appendix. In Figure 29, the dose to the heart is shown in yellow, the dose to the lung is shown in blue, and the dose to the target is shown in cyan. This color scheme is followed for all DVH's shown for this study.

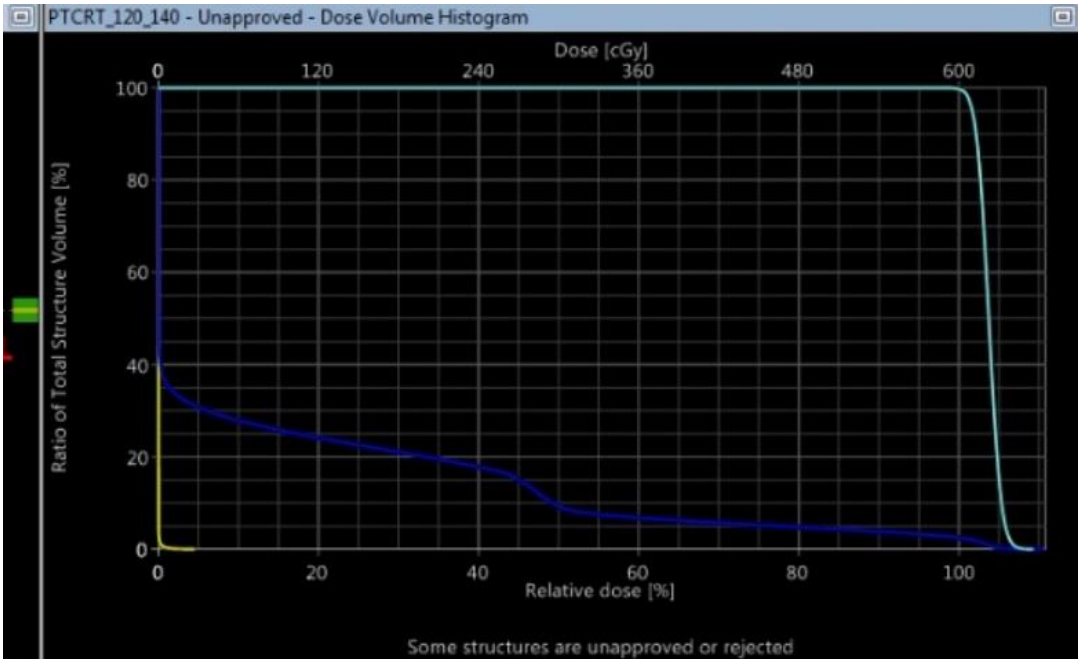

Figure 29. Heart, lung, and target DVH of plan corresponding to 120 kV CT technique and 140 MeV proton energy

Based on the DVH in Figure 29 above, the 3 organ structures met the clinical constraints and goals. The heart dose is very low, and remains so for all plans, and is below clinical critical limits [37]. The target dose achieved its goal of >100% of the prescription dose of 600 cGy and this too is consistent throughout all 9 plans. However, the lung dose, as measured with the V20% (percent of the lung volume receiving 20% of the prescription dose), varied slightly between plans as shown below in Table 7.

Table 7. DVH of lung for various treatment plans

Plan [kV_MeV]	V20% [%]
80_140	24
80_200	25
80_250	26
120_140	24

120_200	24
120_250	24
140_140	24
140_200	25
140_250	26

V20% is a metric describing the dose is a standard used clinically to predict lung complications and is kept below 30-35% at MD Anderson Cancer Center for treatment with radiation therapy alone [37][38]. All V20% values for plans in this study are below this 40% threshold and these plans are therefore considered acceptable. The variation noted in V20% between the different plans ranged from 24% to 26% with the reference lung treatment parameters of 120 kV/140 MeV having a V20% of 24%. These data suggest that regardless of the proton beam energy or CT technique used, the resulting proton dose distributions would not impact the lung dose in any great amount.

3.2.2 HU Overrides

3.3 Aim 3 (Analysis of plan differences)

3.3.1 3D gamma analysis

A 3D gamma analysis, using the CERR software, was performed as described in previous sections between the reference lung treatment plan corresponding to 120 kV CT technique and 140 MeV proton energy.

Recall that this study is examining the hypothesis that the variations in the treatment plans caused by the different CT techniques and proton beam energy RLSP values will reduce the percent of passing pixels by 10% using a gamma criteria of ±3%/5mm. A threshold of 5% was used for both 3D and 2D gamma analyses.

Shown below in Figure 30 are the results of the percent of pixels passing the 3D gamma index criteria of ±3%/5mm for each of four contoured structures for each of the 8 plans as compared to the 120 kV/140 MeV.

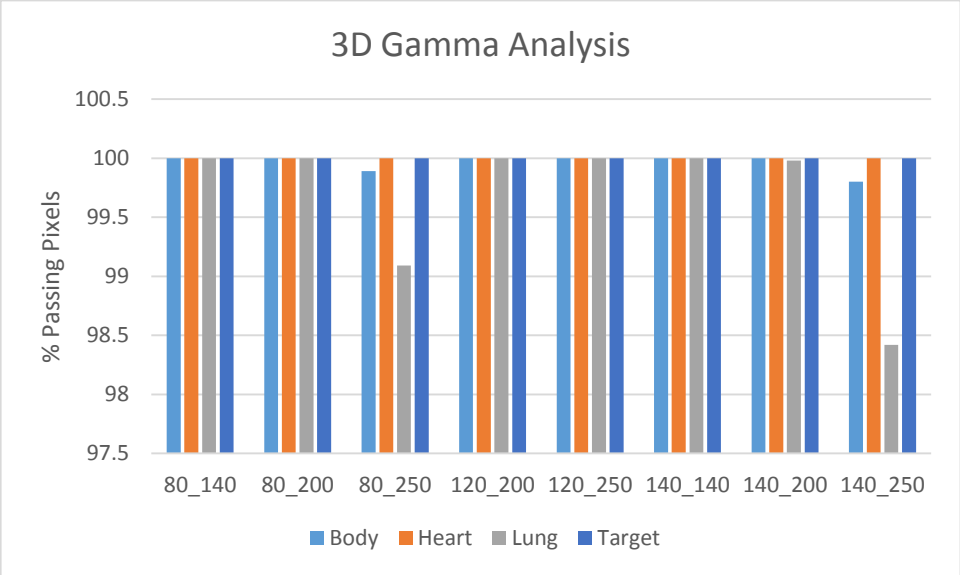

Figure 30. 3D gamma analysis of 120 kV/ 140 MeV treatment plan compared to all other treatment plans created for this study with a gamma criteria of 3%/5mm

These 3D gamma analysis results are displayed for different contours in the plan. The primary contour of interest is the Target contour as this is the section of the phantom used for analysis in IROC-H audits using the proton lung phantom. As shown above, every plan has a Target with a 100% rate of passing pixels. The variation in CT technique and proton beam energy had no effect on the Target dose. The lowest passing rate of pixels is found in the lung, likely due to the large volume and heterogeneous nature of the lung material. However, this pass rate is still very high, 98.4%, far below our hypothesized 10% reduction. Although not of primary interest, the gamma evaluation of the Body and Heart contours are also included in Figure 30 for reference with the goal of pinpointing any failing pixels. An example of the spatial representation of this gamma analysis with a ±3%/5mm criteria can be seen in Figure 31 below. While not included in the ROI of the

gamma analysis, there were areas at the distal end of each proton beam that showed some disagreement. This was to be expected due to the observed differences in the RLSPs as a function of beam energy for the low density tissue substitutes. While there appear to be some localized differences, the impact on the overall lung dose is minimal and has no impact on the Target dose. A full set of visual representations of these gamma analyses at isocenter can be seen in the Appendix.

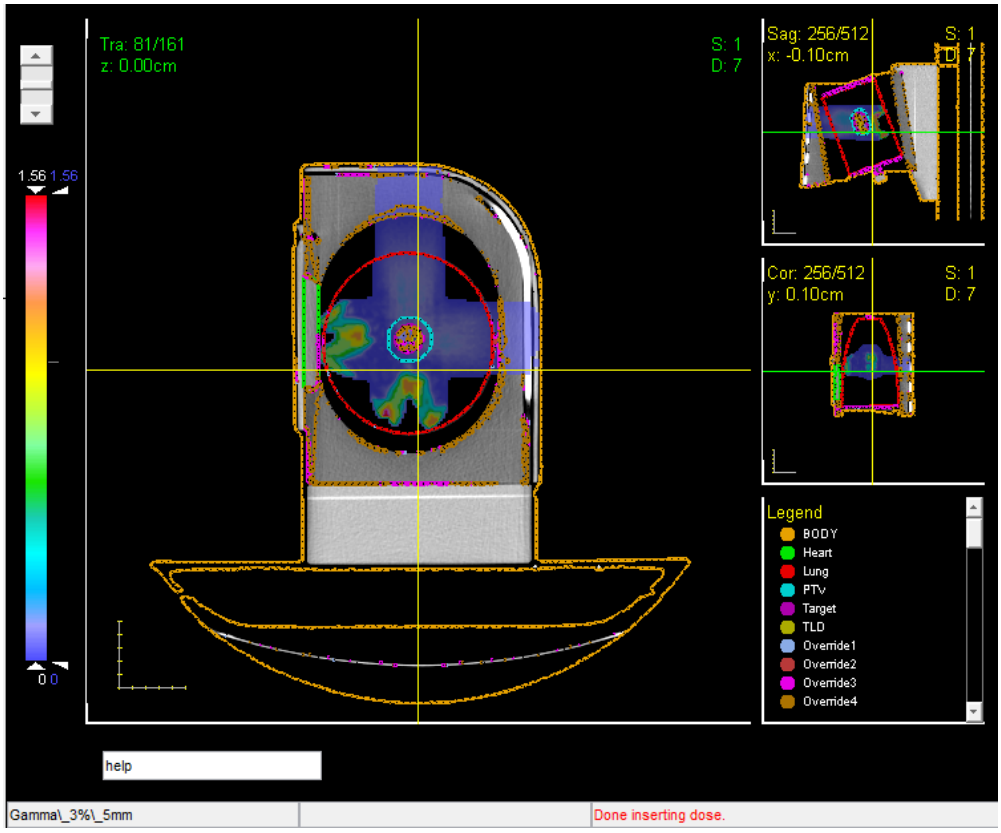

Figure 31. Gamma analysis at isocenter of plan corresponding to study lung reference curve compared with plan corresponding to 80 kV and 250 MeV with gamma criteria 3%/5mm

Because the percent of passing pixels was so high for the hypothesis criteria, there was interest in the effects of variable gamma criteria. Shown below in Figure 32 are the results of a gamma analysis performed on the same plans as described previously, but with an extremely tight gamma criteria of ±1%/1mm.

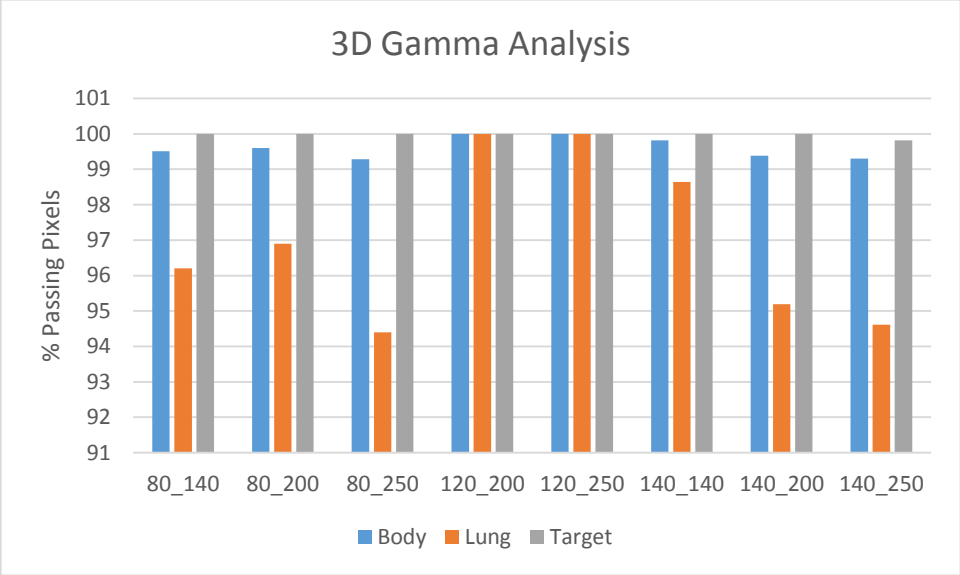

Figure 32. 3D gamma analysis of 120 kV/ 140 MeV treatment plan compared to all other treatment plans created for this study with a gamma criteria of 1%/1mm

From these gamma tests, it can be seen that although the majority of the Targets maintains a 100% pixel passing rate (one Target had a percent of passing pixels of 99.5%), the lung becomes a good representation of the change experienced due to the varying treatment plans. From this it can be seen that the lowest passing rate is associated with the 250 MeV proton energy, for both 80 kV and 140 kV, yet no plans resulted in greater than a 5.6% change, still less than the hypothesized 10% change. This lack of dependence on CT technique is in contrast to the CT calibration curves alone, which showed a large difference at a low CT technique. The lower pass rate also seen here at the highest proton energy, 250 MeV, for all CT techniques, is not reflected in the CT calibration curve differences noted earlier. It is possible that the percent of pixels passing at 1%/1mm criteria is not an appropriate metric when comparing the variations in the CT calibration curves and the resulting treatment planning system calculated dose distributions. There are approximations in the planning system dose calculations that possibly cannot

distinguish differences at the 1%/1mm level. These approximations would be especially problematic for such tight criteria if registering of images was involved.

An example of the spatial representation of this gamma analysis with 1%/1mm criteria at the isocenter can be seen in Figure 33 below. A full set of visual representations of these gamma analyses at isocenter can be seen in the Appendix.

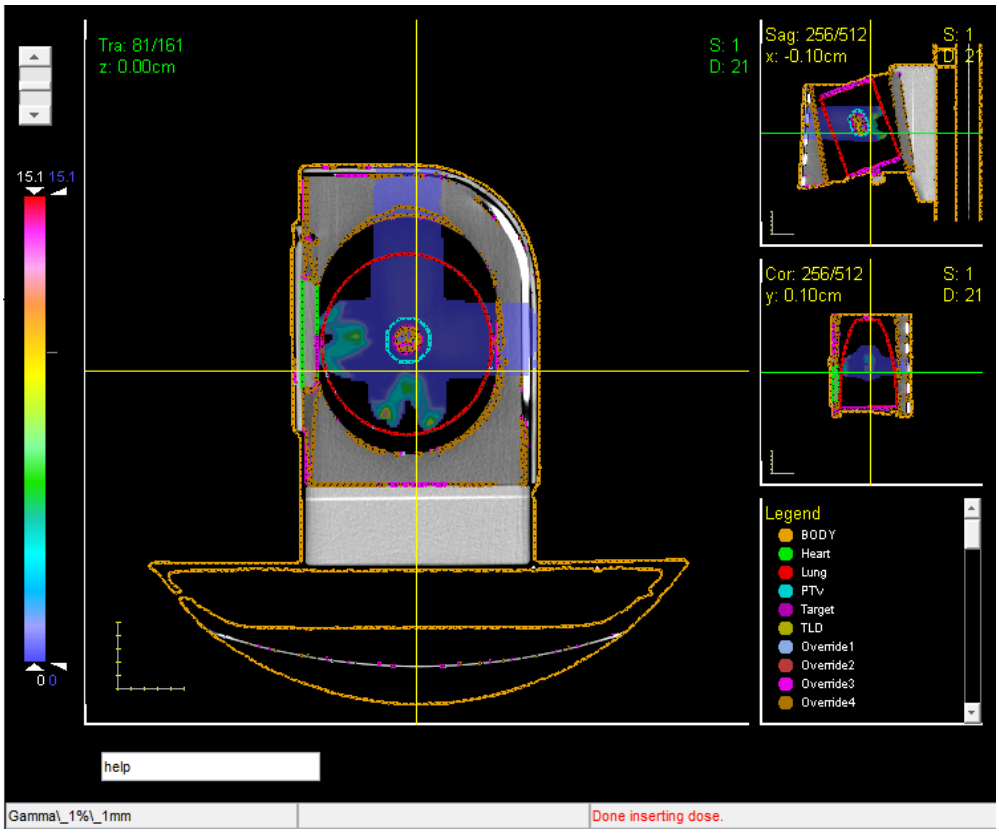

Figure 33. Gamma analysis at isocenter of plan corresponding to study reference curve compared with plan corresponding to 80 kV and 250 MeV with gamma criteria 1%/1mm

The gamma criteria were then further tightened with the goal of approaching the point of failing, defined as <90% of passing pixels. This test was only performed for the study reference curve compared to the curve corresponding to 80 kV and 250 MeV due to its already established lower passing rate. With the criteria tightened to 0.5%/0.5mm, the results of a gamma test for all contours in this comparison are

shown below in Figure 34. Even with this unrealistic gamma criteria, the difference in pixels did not ever exceed 10%. Varying the CT technique and proton beam energy did not negatively impact any of the comparisons for any of the 9 plans.

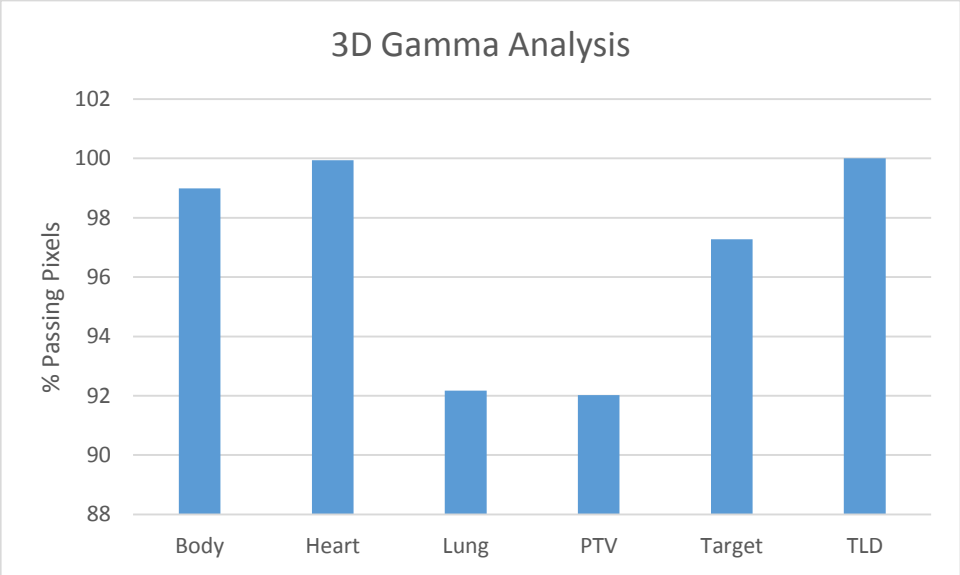

Figure 34. Results of 3D gamma analysis of plan using study reference curve compared to the curve corresponding to 80 kV CT technique and 250 MeV proton energy

An example of the spatial representation of this gamma analysis with 0.5%/0.5mm criteria at the isocenter can be seen in Figure 35 below.

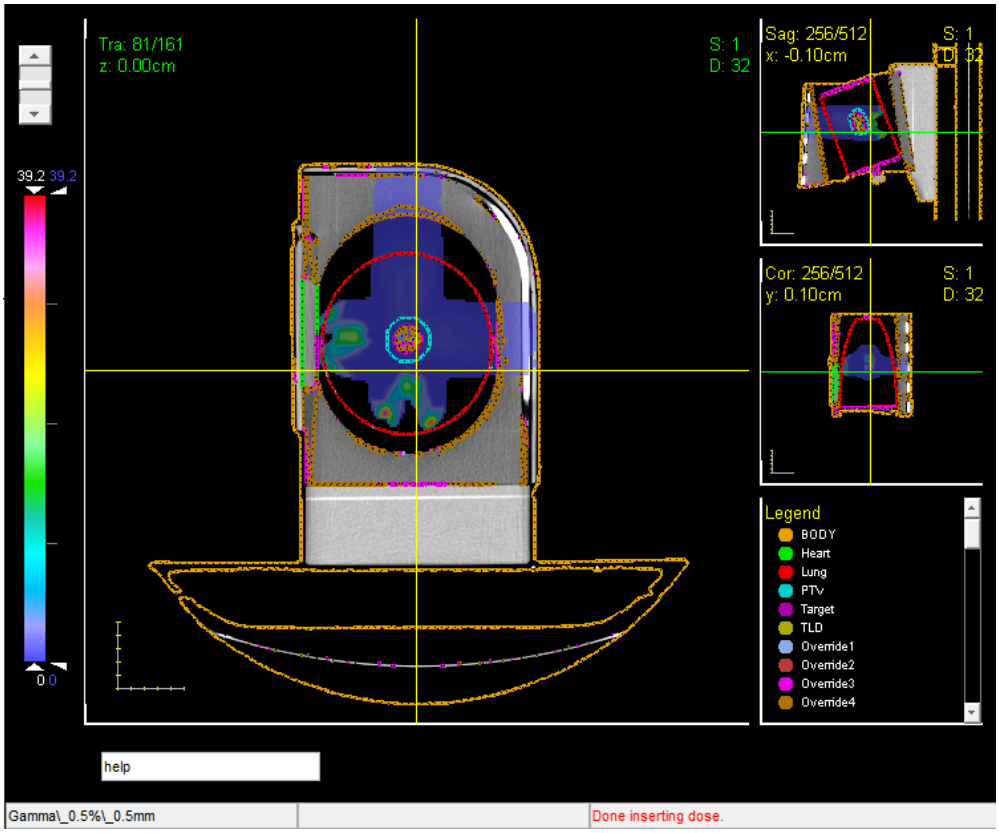

Figure 35. Gamma analysis at isocenter of plan corresponding to study reference curve compared with plan corresponding to 80 kV and 250 MeV with gamma criteria 0.5%/0.5mm

3.3.2 2D gamma analysis

Due to the very high pass rates of the 3D gamma analysis the difference between 3D analyses and 2D analyses was investigated.

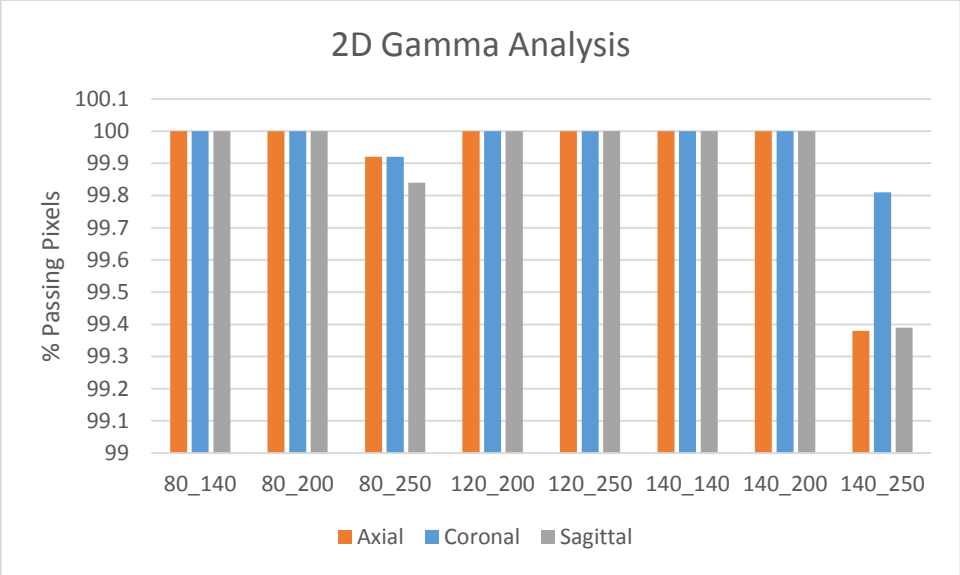

Figure 36. 2D gamma analysis of 120 kV/ 140 MeV treatment plan compared to all other treatment plans created for this study with a gamma criteria of 3%/5mm

Recall that this gamma analysis was done for all three planes, axial, coronal and sagittal, comparing the study lung reference plan (120 kV/140 MeV) to all other plans created for the study. As shown in Figure 36, it is possible to see that the lowest number of passing pixels using a gamma index criteria of ±3%/5mm occurs for the comparison between the study reference plan and the plan corresponding to 140 kV and 250 MeV, contradicting the maximum difference seen in the CT calibration curves at a low 80 kV technique, but consistent with the results of the 3D gamma analysis. At the hypothesis gamma criteria of 3%/5mm, a spatial representation of this gamma analysis can be seen below in Figures 37-39 for the three spatial planes. The only differences noted are at the distal ends of each treatment beam because of the measured differences in lung RLSPs. The remaining 2D gamma representations and profiles can be seen in the Appendix.

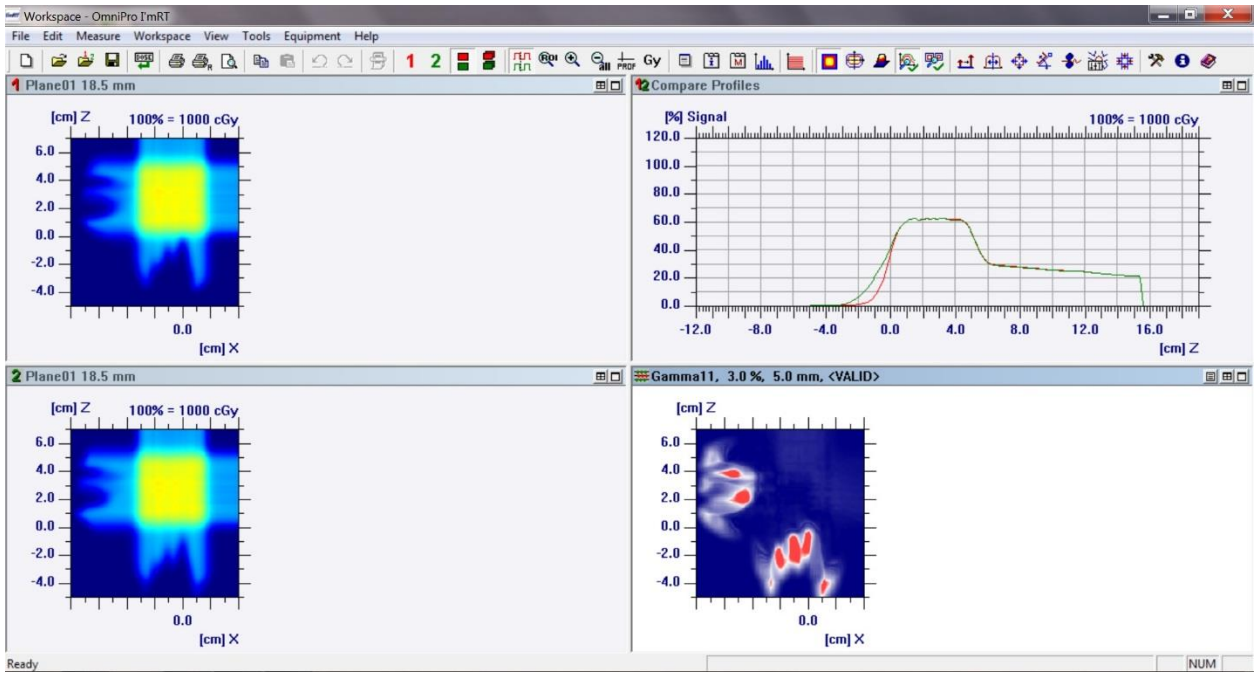

Figure 37. 2D gamma analysis of axial slice at isocenter comparing the study reference plan to the plan corresponding to 140 kV and 250 MeV with gamma criteria of 3%/5mm

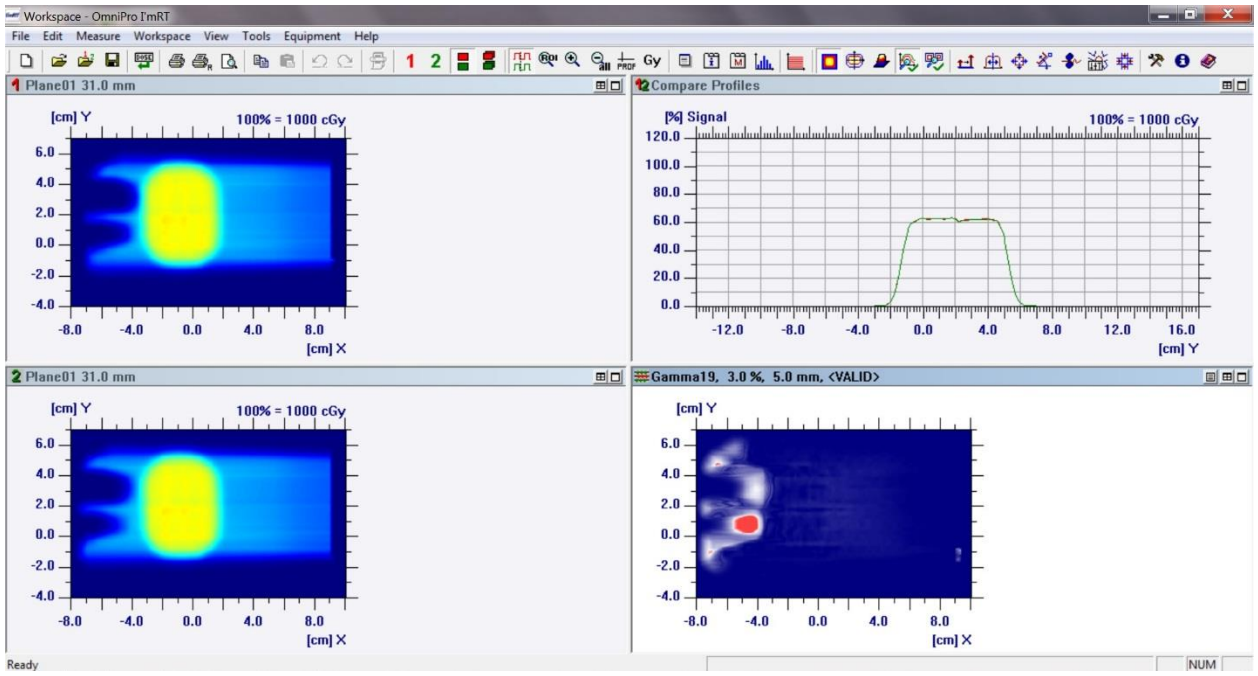

Figure 38. 2D gamma analysis of coronal slice at isocenter comparing the study reference plan to the plan corresponding to 140 kV and 250 MeV with gamma criteria of 3%/5mm

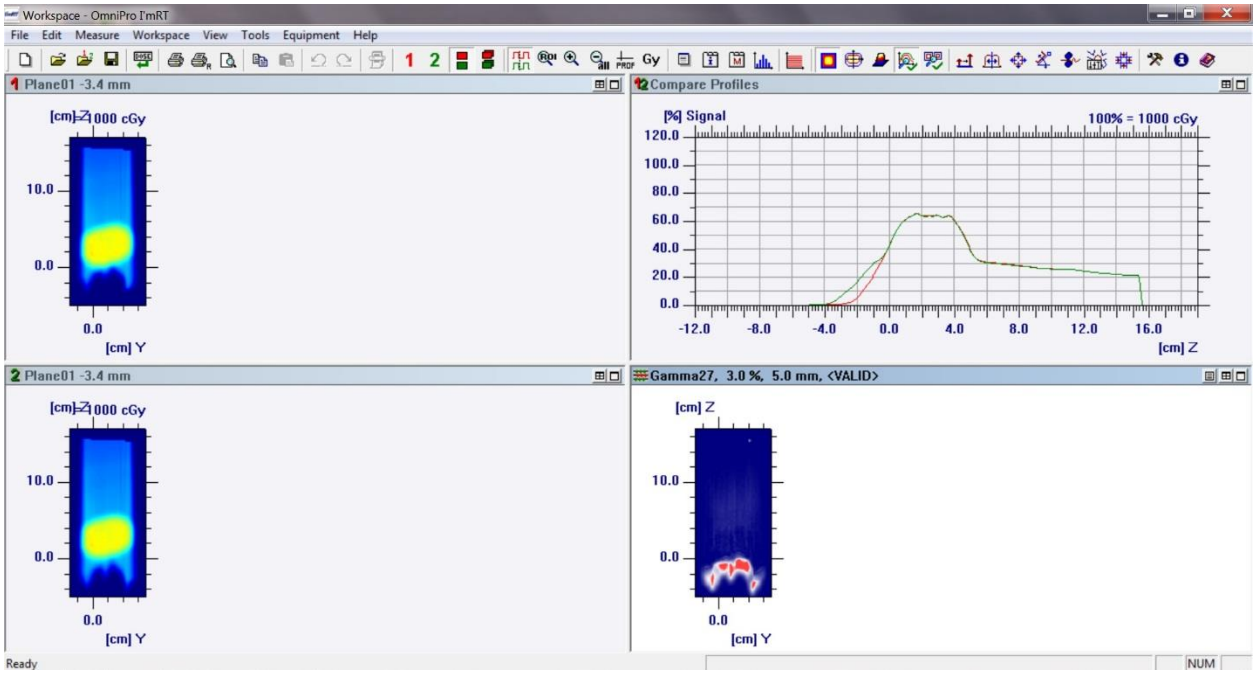

Figure 39. 2D gamma analysis of sagittal slice at isocenter comparing the study reference plan to the plan corresponding to 140 kV and 250 MeV with gamma criteria of 3%/5mm

The 2D gamma analysis was repeated with a tighter gamma criteria, as was performed with the 3D analysis. The plan with the maximum difference, as determined by the percent of passing pixels using a ±3%/5mm gamma index analysis, is seen in Figure 36 to be the plan corresponding to 140 kV and 250 MeV. A threshold of 5% was used. The gamma analysis was also run with the tightened criteria of 1%/1mm with the same threshold for the same two plans and the results are seen below in Figures 40-42. The actual % of pixels passing the 1%/1mm criteria are listed in Table 8.

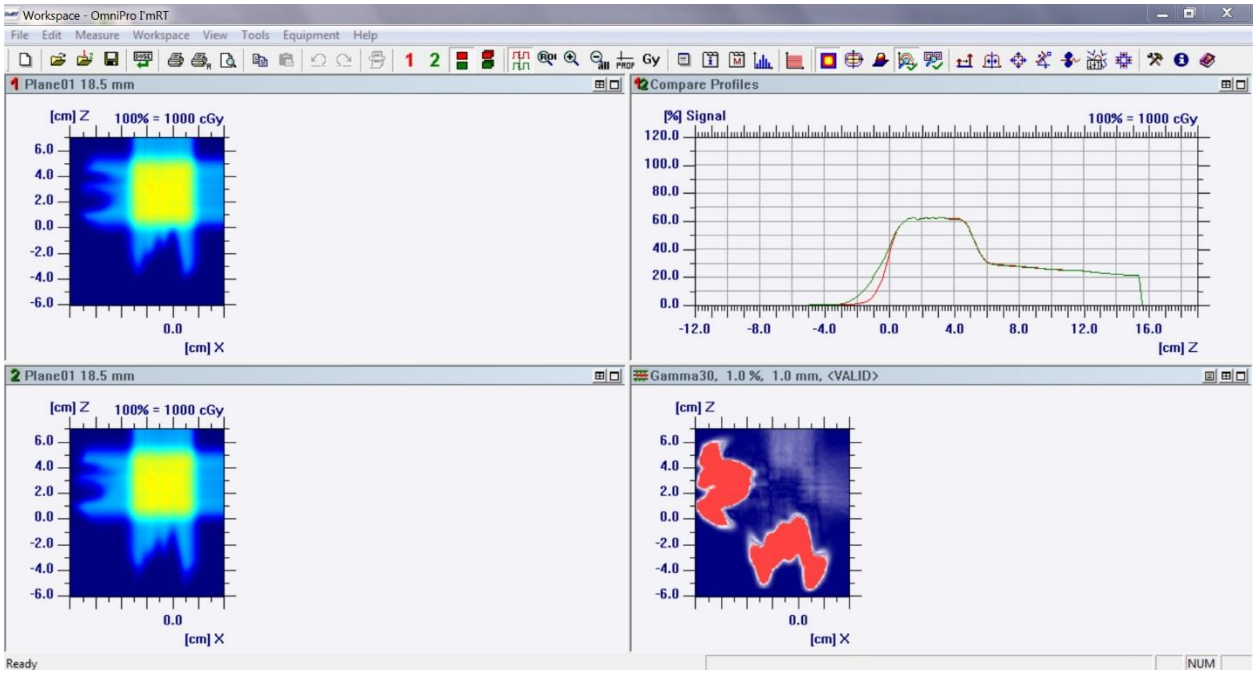

Figure 40. 2D gamma analysis of axial slice at isocenter comparing study reference plan to the plan corresponding to 140 kV and 250 MeV with gamma criteria of 1%/1mm

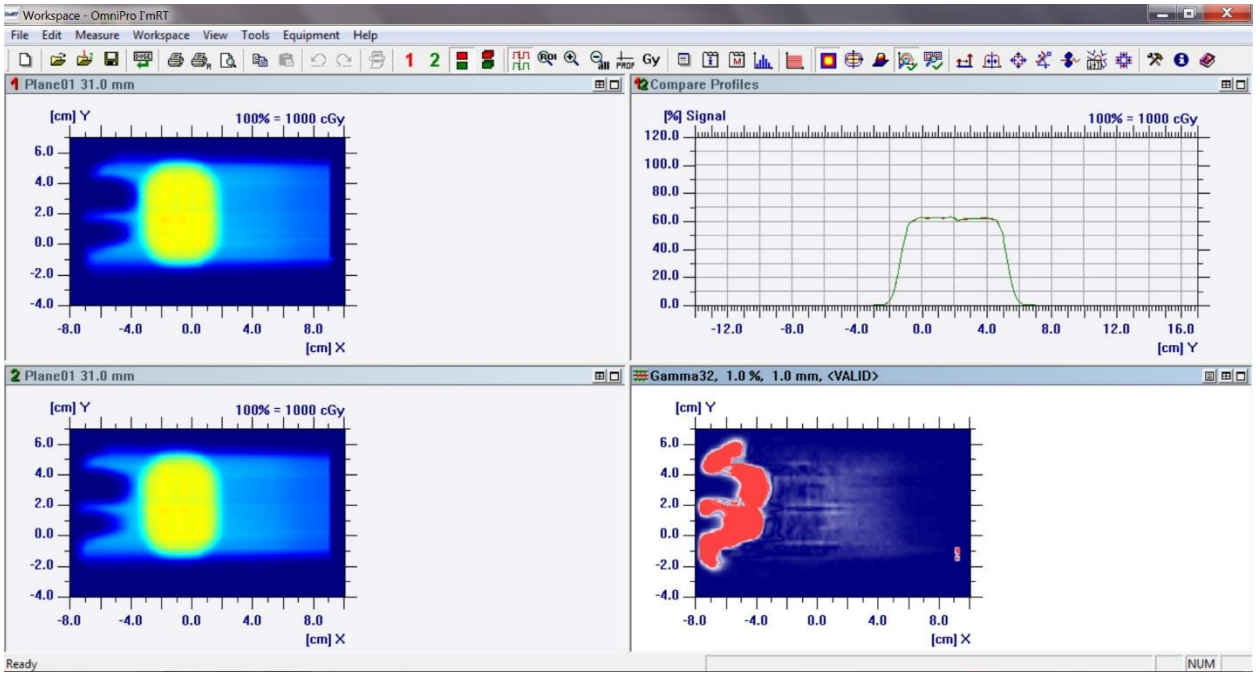

Figure 41. 2D gamma analysis of coronal slice at isocenter comparing study reference plan to the plan corresponding to 140 kV and 250 MeV with gamma criteria of 1%/1mm

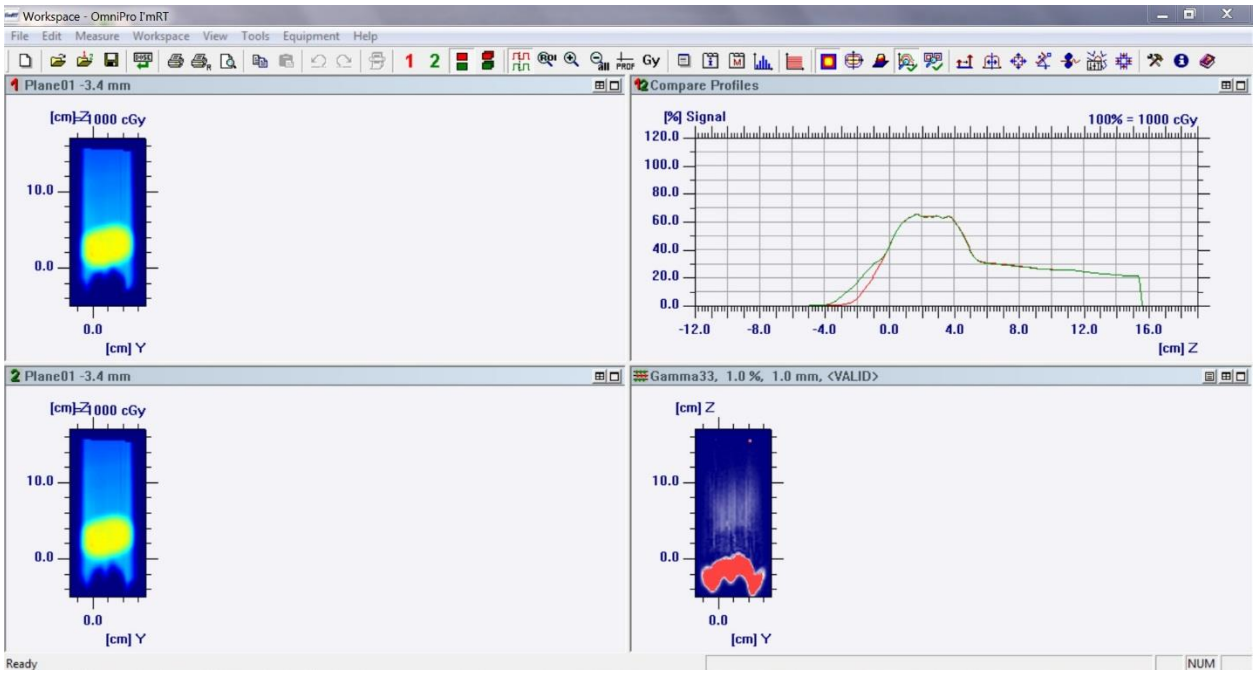

Figure 42. 2D gamma analysis of sagittal slice at isocenter comparing study reference plan to the plan corresponding to 140 kV and 250 MeV with gamma criteria of 1%/1mm

This tightened criteria of 1%/1mm is quantified in Table 8 below.

Table 8. 2D Gamma results for study reference plan compared to 140 kV and 250 MeV plan with gamma criteria of 1%/1mm

	% Passing Pixels
Axial	96.22
Coronal	97.91
Sagittal	97.58

A gamma criteria of 1%/1mm is much tighter than that used clinically or by IROC-H. Even at this very tight criteria, the passing pixel percentage was well above the

hypothesized 90% needed for the plan to pass, indicating a low level of influence due to variable CT technique and proton energy in the creation of CT calibration curves even using a 2D gamma analysis.

Chapter 4

4 Conclusions

4.1 Meeting of specific aims

The goal of this project was to understand the uncertainty in the proton CT calibration curves at proton institutions and its influence on the credentialing and auditing process (E2E anthropomorphic QA phantom irradiation) performed by IROC-H that might stem from variable CT technique and proton energy. This project further looked at how this uncertainty might translate to uncertainties in dose distributions. The hypothesis of this project was to determine if this variable CT technique and proton energy would lead to a change in dose distribution resulting in more than 10% of failing pixels with a gamma analysis criteria of ±3%/5mm.

The first specific aim was to measure the HU and RLSP of phantom materials and create custom calibration curves. This was accomplished with the proton CT phantom containing 6 proton equivalent materials currently used by IROC-H on proton institution site visits. All of the custom curves were compared to the clinical reference curve used at MD Anderson's PTC-H and the reference curve (120 kV and 140 MeV) used for this study. It was found that the maximum difference in predicted RLSP between the clinical reference curve and the custom curves was no more than 12%. The maximum difference in predicted RLSP between the study's reference curve and the custom curves was 7%. This completed specific aim one and laid the ground work for aims two and three as well as provided as initial reference when comparing dose differences.

The second specific aim involved the creation of 9 treatment plans for IROC-H's proton lung phantom and was accomplished simultaneously with the first part of specific aim three which required uploading the custom calibration curves into the Eclipse treatment planning system and calculating the plans, each using a different proton CT calibration curve. This was accomplished through the beam administration functions of

Eclipse as described in previous chapters. Once the custom curves were uploaded and assigned to treatment plans it was possible to calculate the plans and get dose distributions specific to each set of parameters.

Specific aim 3 was the evaluation and analysis of the treatment plans created in specific aim two. Both 3D and 2D gamma analyses were performed to evaluate the hypothesis as described in previous chapters. The hypothesis stated that the passing rate must be reduced by more than 10% passing pixels at a gamma criteria of 3%/5mm, meaning a pass rate of less than 90% for any treatment plan compared to the study's reference plan. At this gamma criteria, the percent of passing pixels for the Target structure was 100%. Zero percent of pixels failing implies that the changing plans from the various CT techniques and/or proton beam energy have no substantial effect on the dose distribution. Following from this, we can conclude that the use of proton CT calibration curves with variable CT technique and proton energy is not a substantial source of uncertainty in IROC-H's end to end (E2E) credentialing and auditing QA processes that use the proton anatomic phantoms and is not contributing to any institution failing a proton audit.

This refutes the hypothesis defined for this study that states:

Variations in CT technique and proton energy will alter the delivered dose distributions of typical proton treatments by reducing the percent of passing pixels by 10% using a gamma analysis criteria of ±3%/5 mm as measured using a heterogeneous proton QA phantom.

4.2 Clinical significance

IROC-H provides QA services to institutions participating in NCI funded clinical trials involving proton therapy. The purpose of IROC-H is to ensure that institutions are delivering accurate and comparable doses, which is accomplished in part by phantom

dosimetry audits. In this process it is critical for IROC-H to understand the potential uncertainties in the QA phantoms and in the E2E process in order to provide accurate feedback. This study adds to the understanding of the uncertainty in this process with the goal of improving institution feedback and therefore improving clinical trial data and cancer care.

4.3 Future work

The results of this project resulted in conclusions that rejected the stated hypothesis and therefore open the door for additional studies to address the problem described in Chapter 1. The increased failure rate of institutions participating in proton QA through IROC-H continues to have an unknown source and steps should be taken in the future to investigate this uncertainty further.

It could be valuable to determine how this uncertainty is seen in a scanning beam, although expected differences would be low because the measurement of RLSP would remain consistent. Additionally the addition of motion, frequently used in IROC-H proton audits with the lung phantom, could also add a level of uncertainty not evaluated in this project.

The continued presence of an uncertainty in the auditing process of IROC-H can lead to additional institution failures and reduces the reliability of the QA services provided by IROC-H and may negatively affect the availability and quality of data provided to NCI funded clinical trials.

Chapter 5

5 Appendix

5.1 Incline

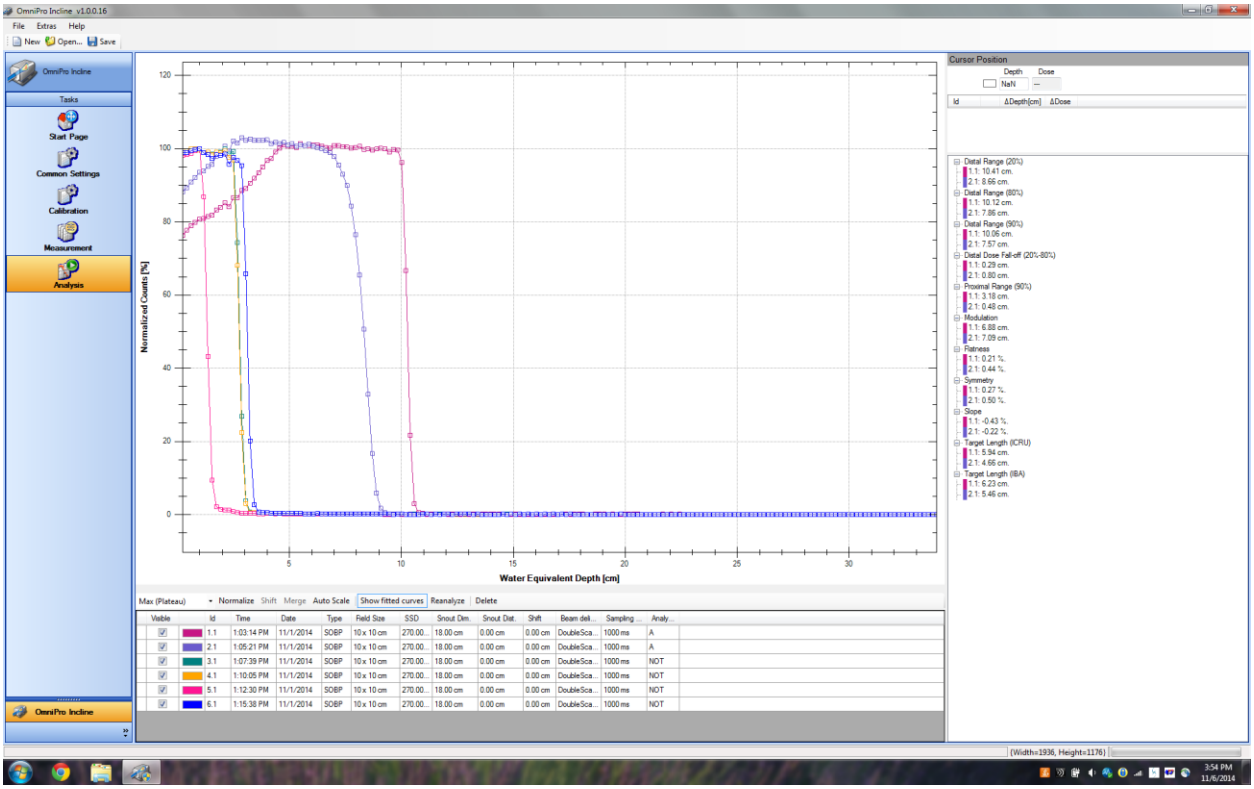

Figure 43. Depth Dose Measured by Zebra at 140 MeV for Various Materials

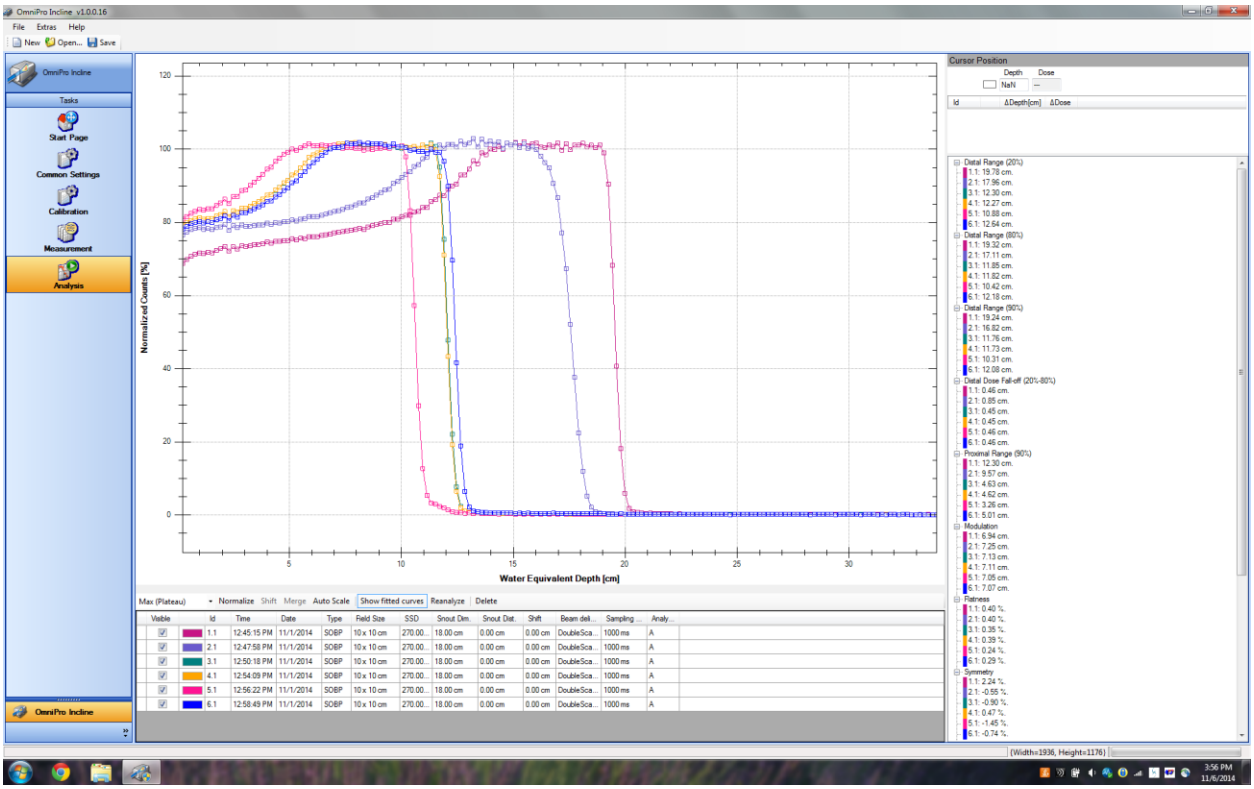

Figure 44. Depth Dose Measured by Zebra at 200 MeV for Various Materials

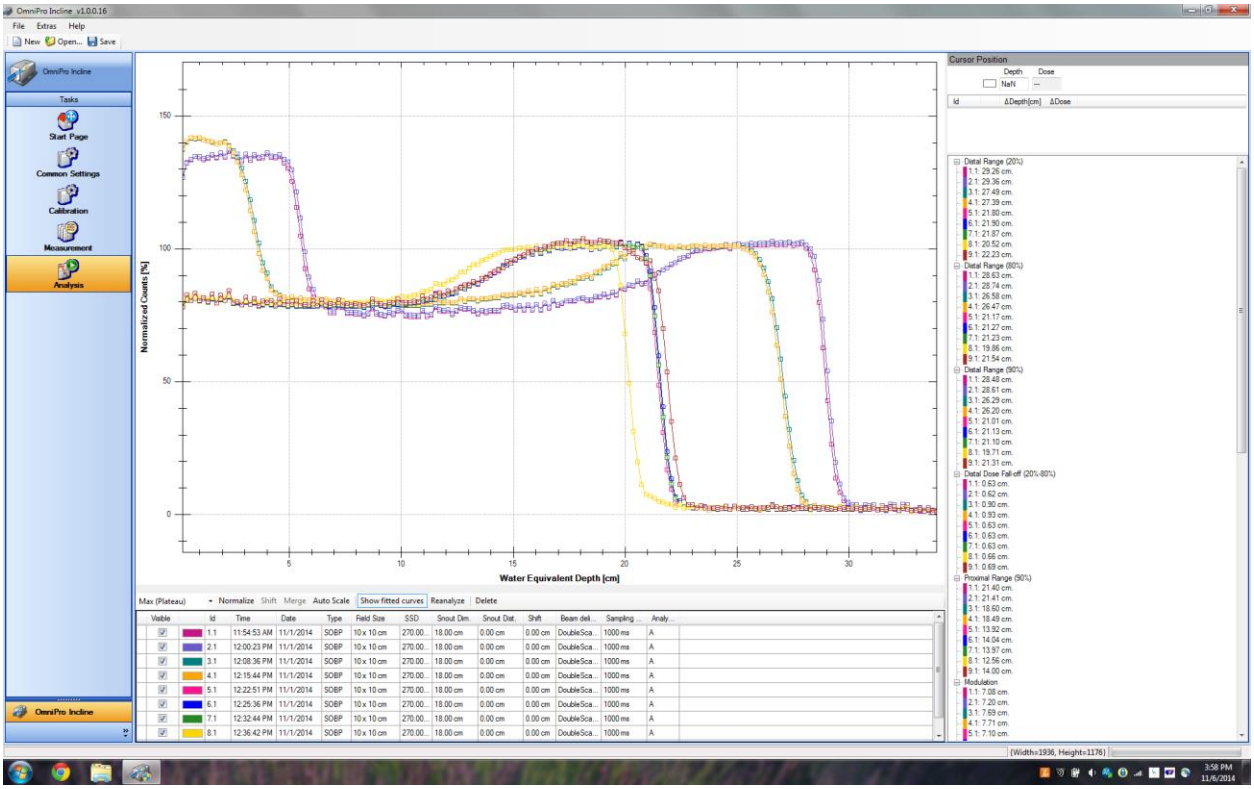

Figure 45. Depth Dose Measured by Zebra at 250 MeV for Various Materials

5.2 Custom curves

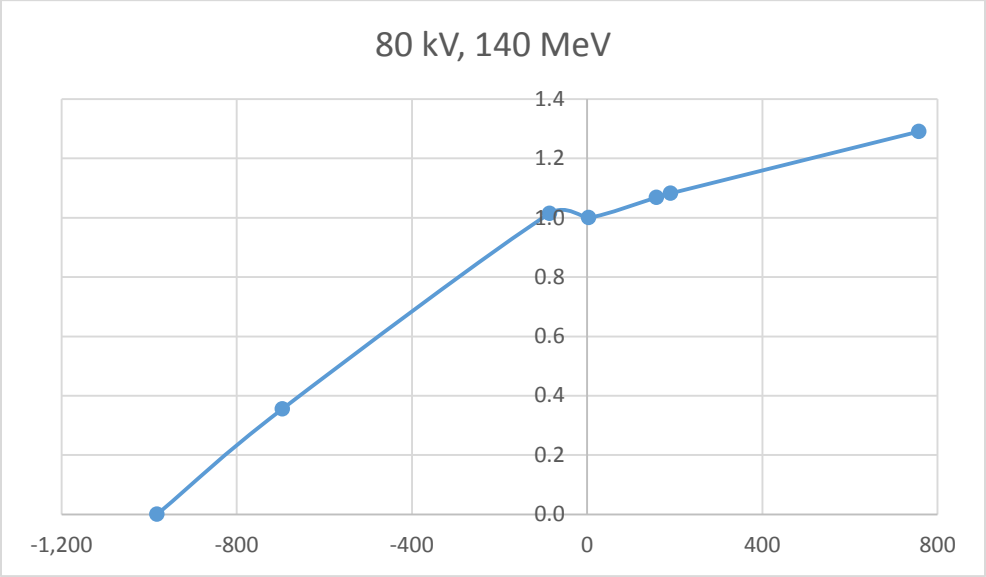

Figure 46. CT Calibration Curve with HU Corresponding to 80 kV and RLSP corresponding to 140 MeV

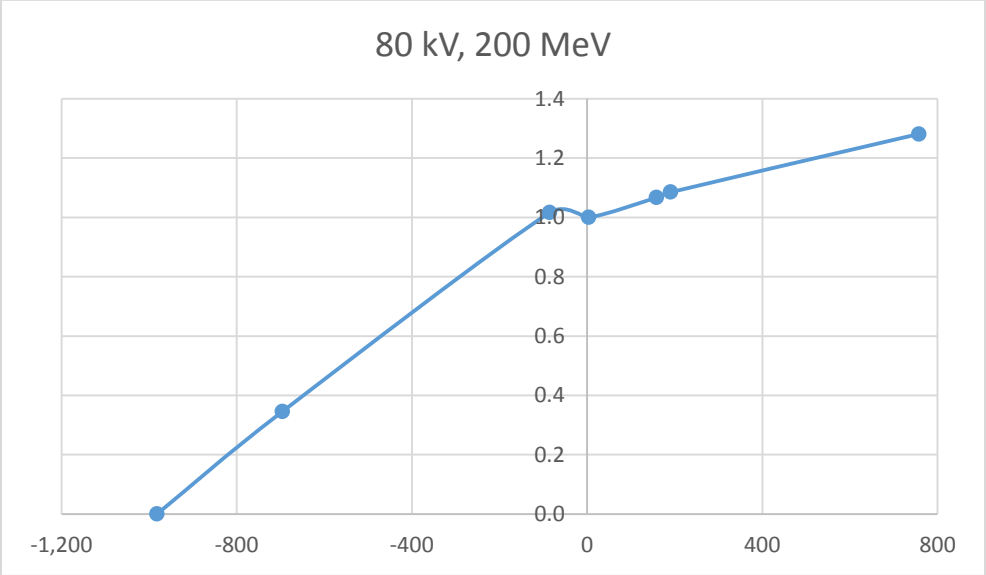

Figure 47. CT Calibration Curve with HU Corresponding to 80 kV and RLSP corresponding to 200 MeV

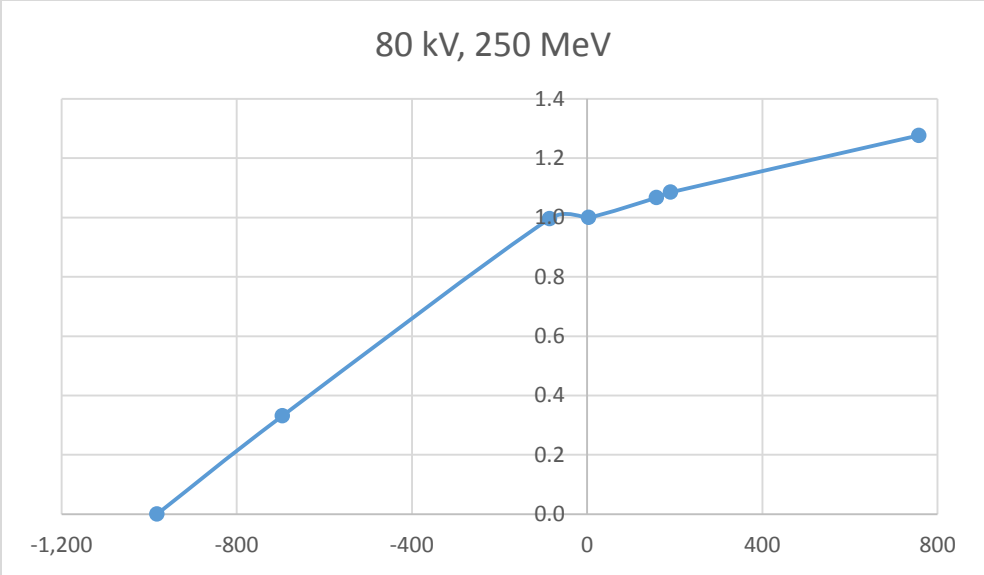

Figure 48. CT Calibration Curve with HU Corresponding to 80 kV and RLSP corresponding to 250 MeV

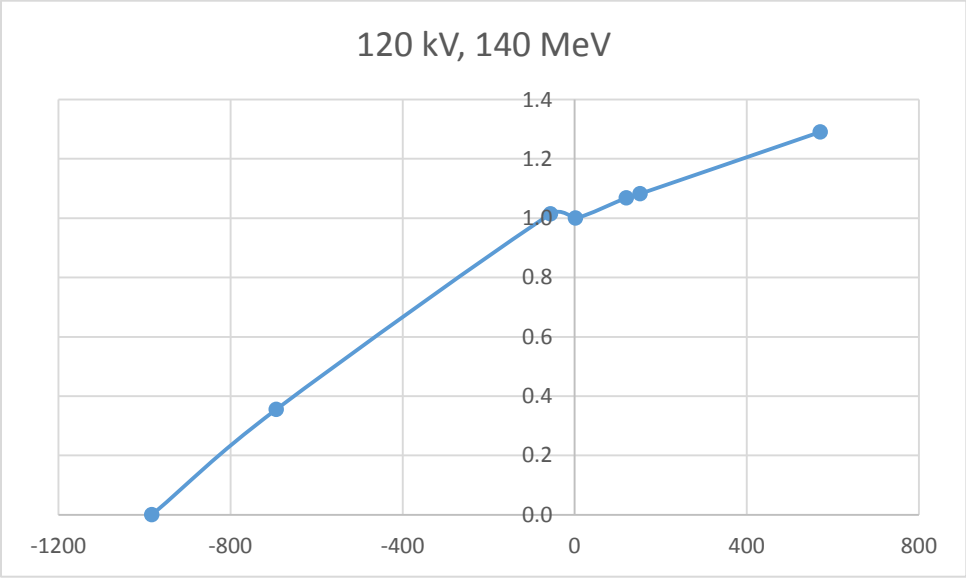

Figure 49. CT Calibration Curve with HU Corresponding to 120 kV and RLSP corresponding to 140 MeV

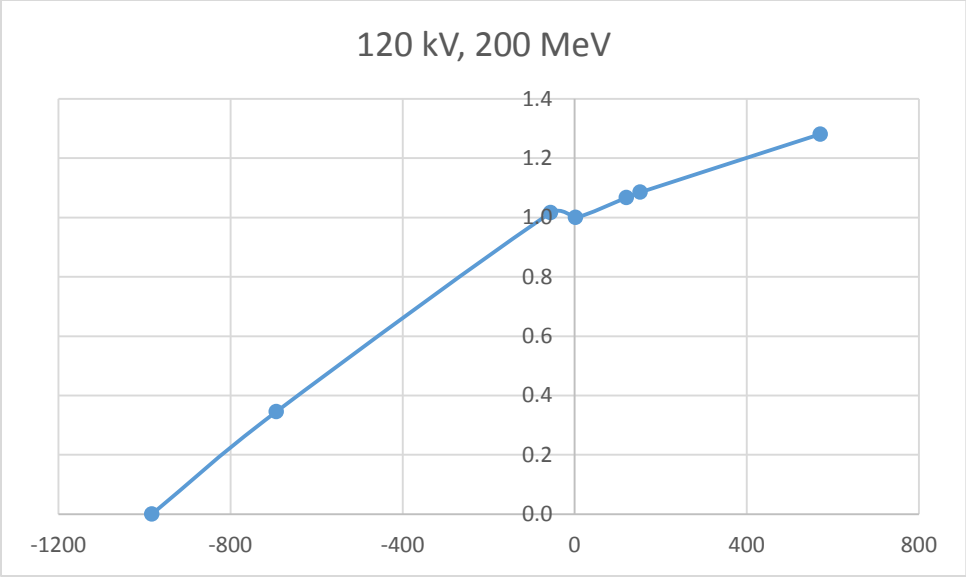

Figure 50. CT Calibration Curve with HU Corresponding to 120 kV and RLSP corresponding to 200 MeV

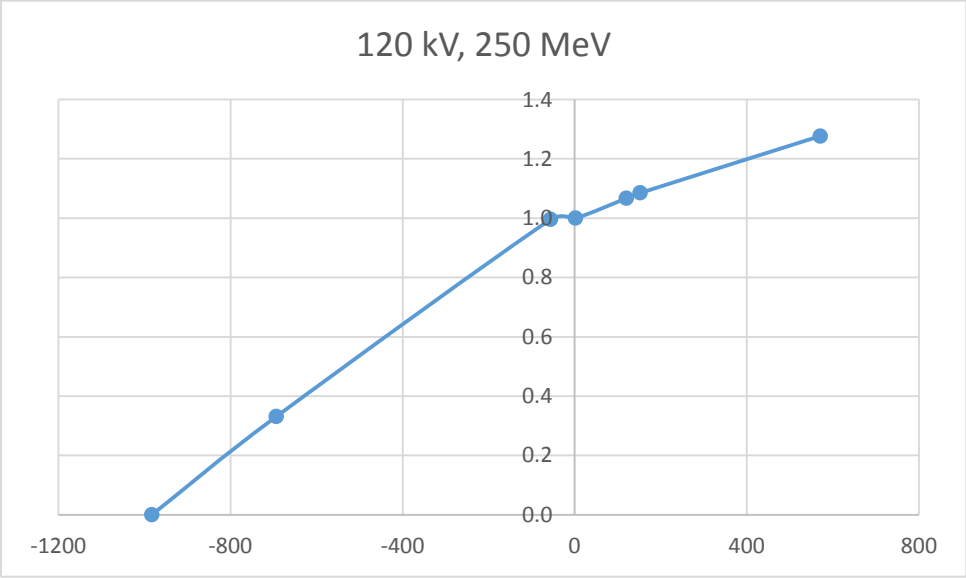

Figure 51. CT Calibration Curve with HU Corresponding to 120 kV and RLSP corresponding to 250 MeV

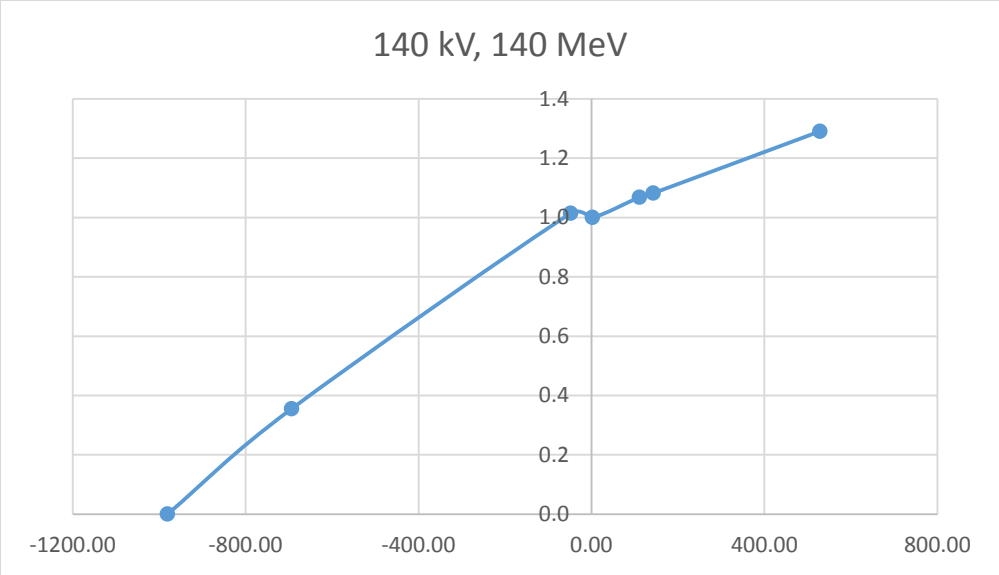

Figure 52. CT Calibration Curve with HU Corresponding to 140 kV and RLSP corresponding to 140 MeV

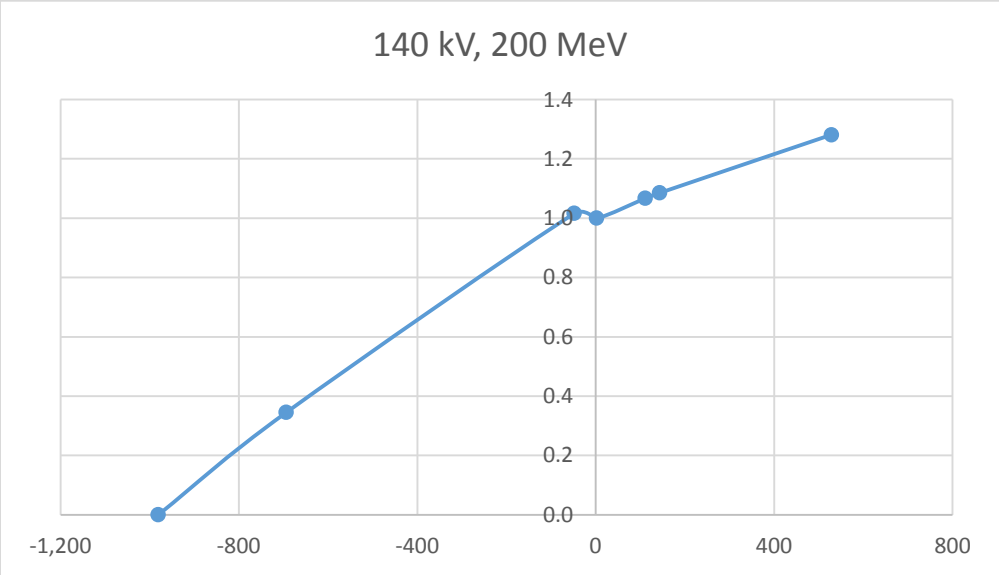

Figure 53. CT Calibration Curve with HU Corresponding to 140 kV and RLSP corresponding to 200 MeV

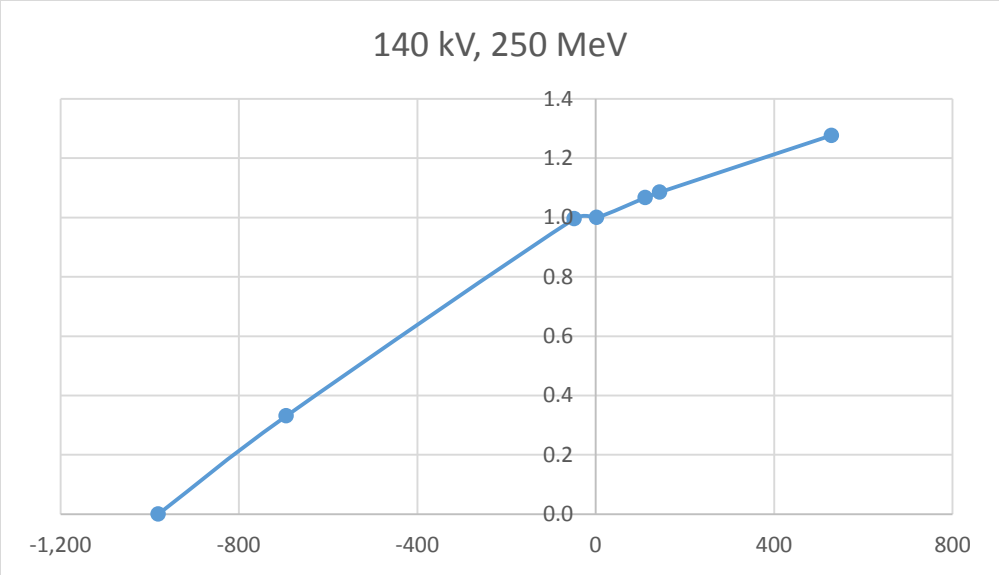

Figure 54. CT Calibration Curve with HU Corresponding to 140 kV and RLSP corresponding to 250 MeV

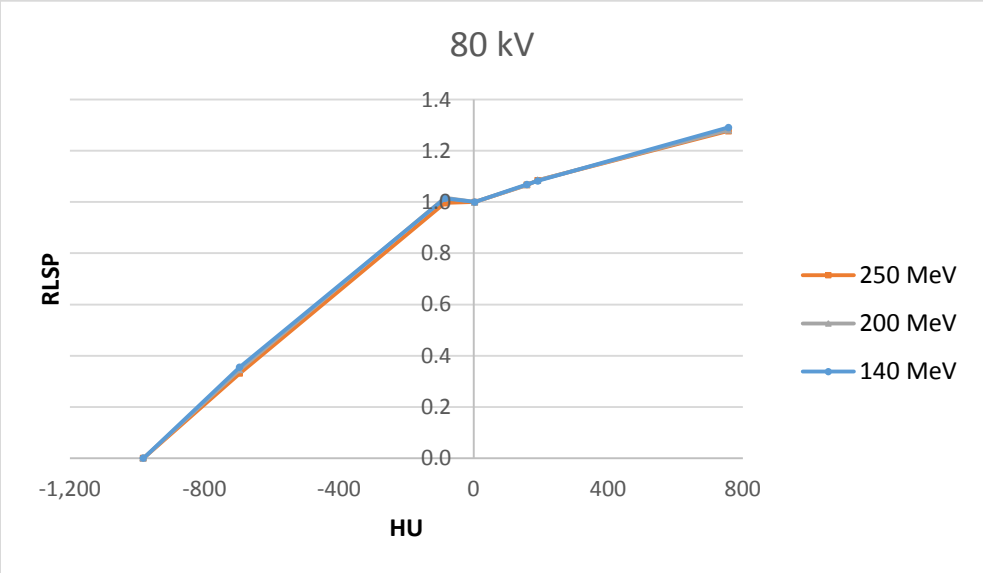

Figure 55. CT Calibration Curves with HU Corresponding to 80 kV

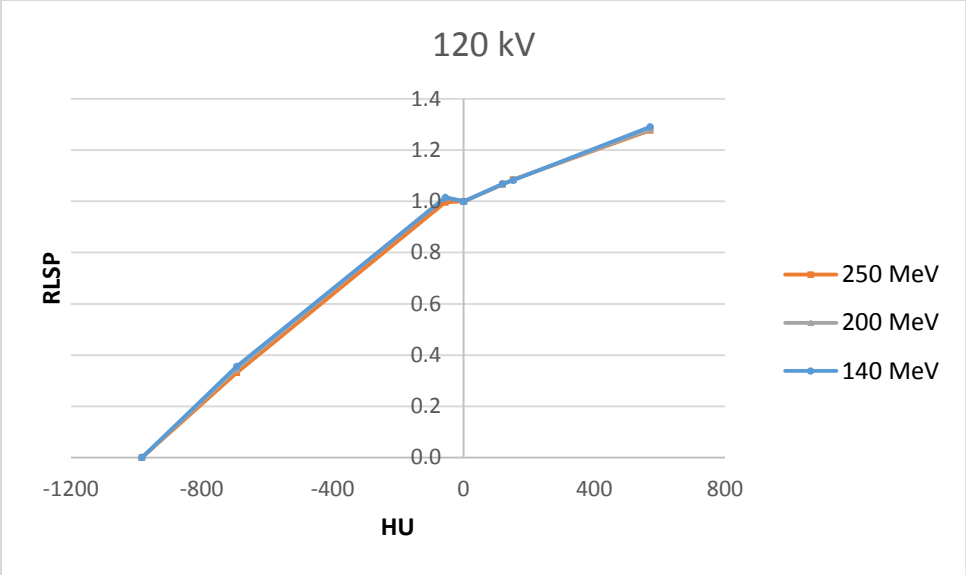

Figure 56. CT Calibration Curves with HU Corresponding to 120 kV

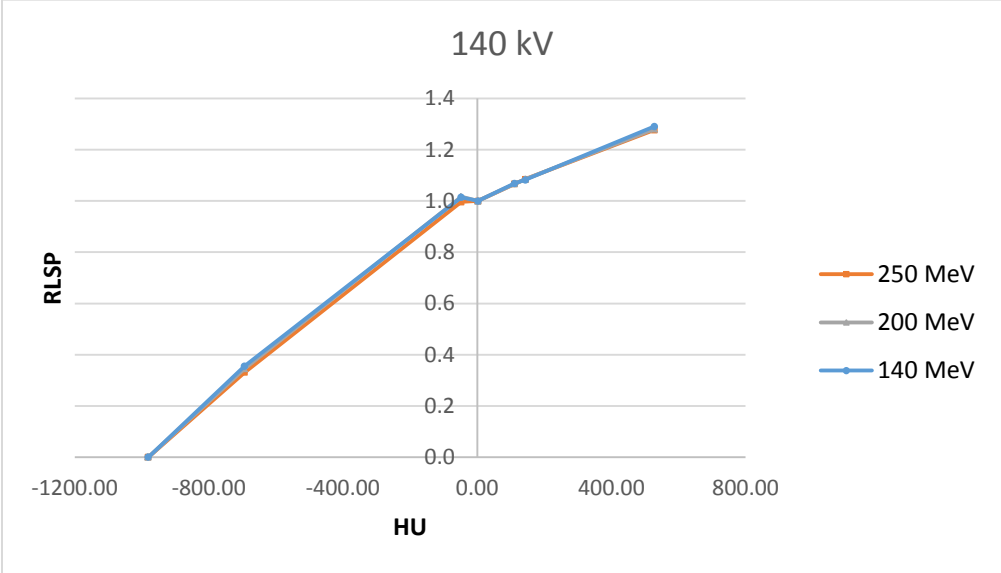

Figure 57. CT Calibration Curves with HU Corresponding to 140 kV

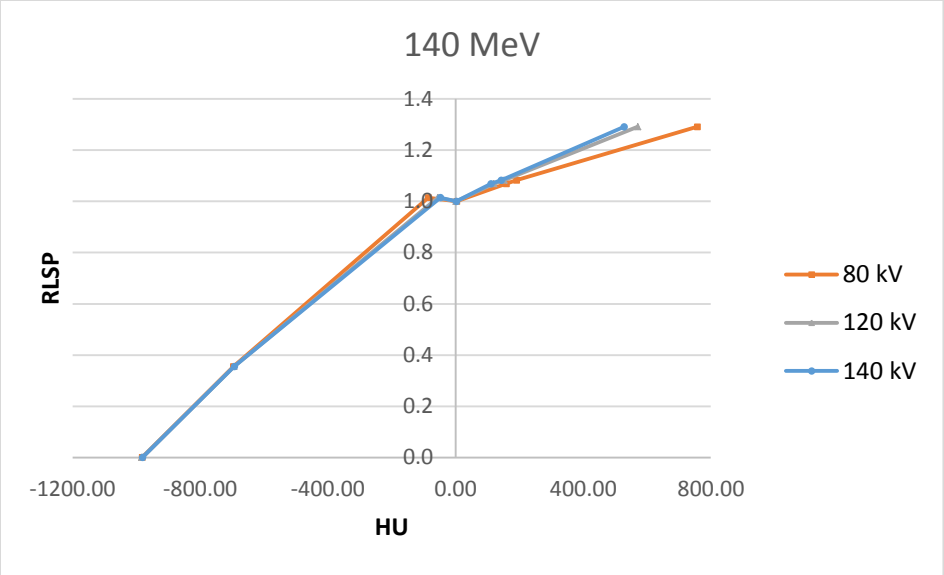

Figure 58. CT Calibration Curves with RLSP Corresponding to 140 MeV

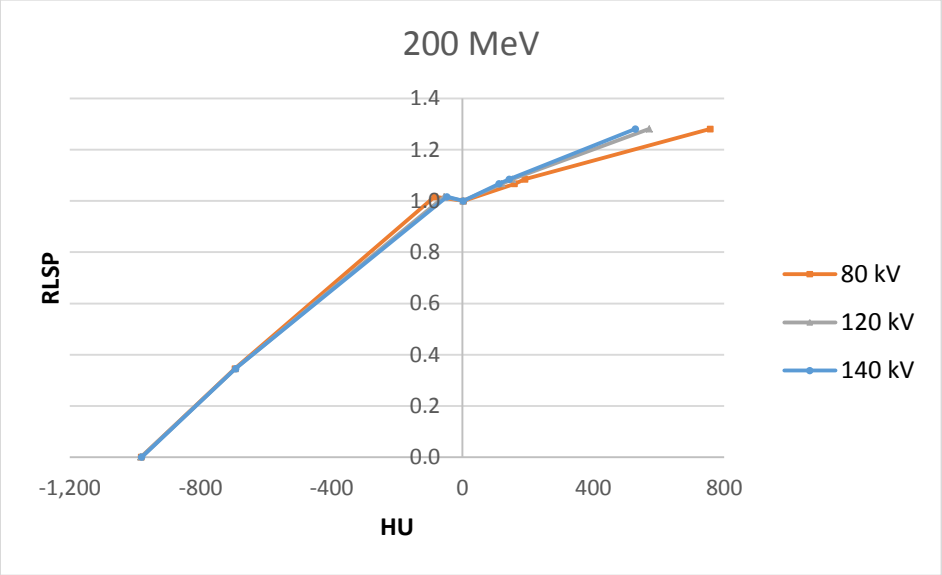

Figure 59. CT Calibration Curves with RLSP Corresponding to 200 MeV

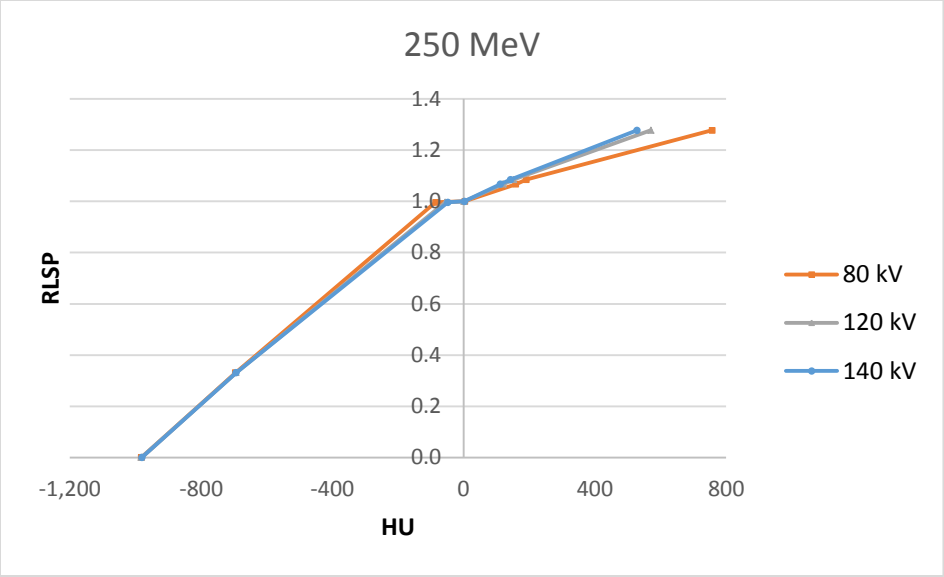

Figure 60. CT Calibration Curves with RLSP Corresponding to 250 MeV

5.3 Dose at Isocenter

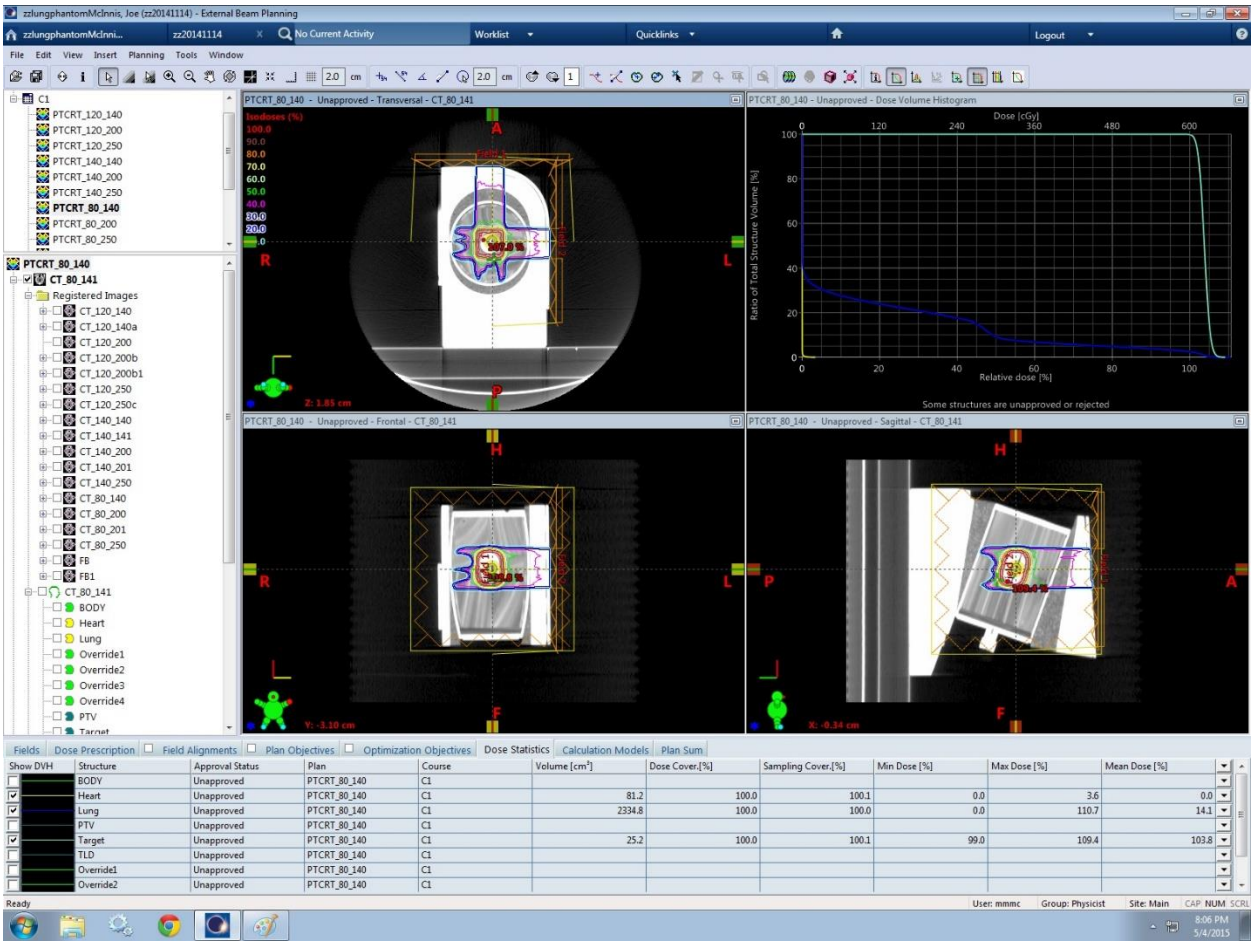

Figure 61. Dose Distribution at Isocenter of Plan Using CT Calibration Curve Corresponding to 80 kV CT Technique and 140 MeV Proton Energy

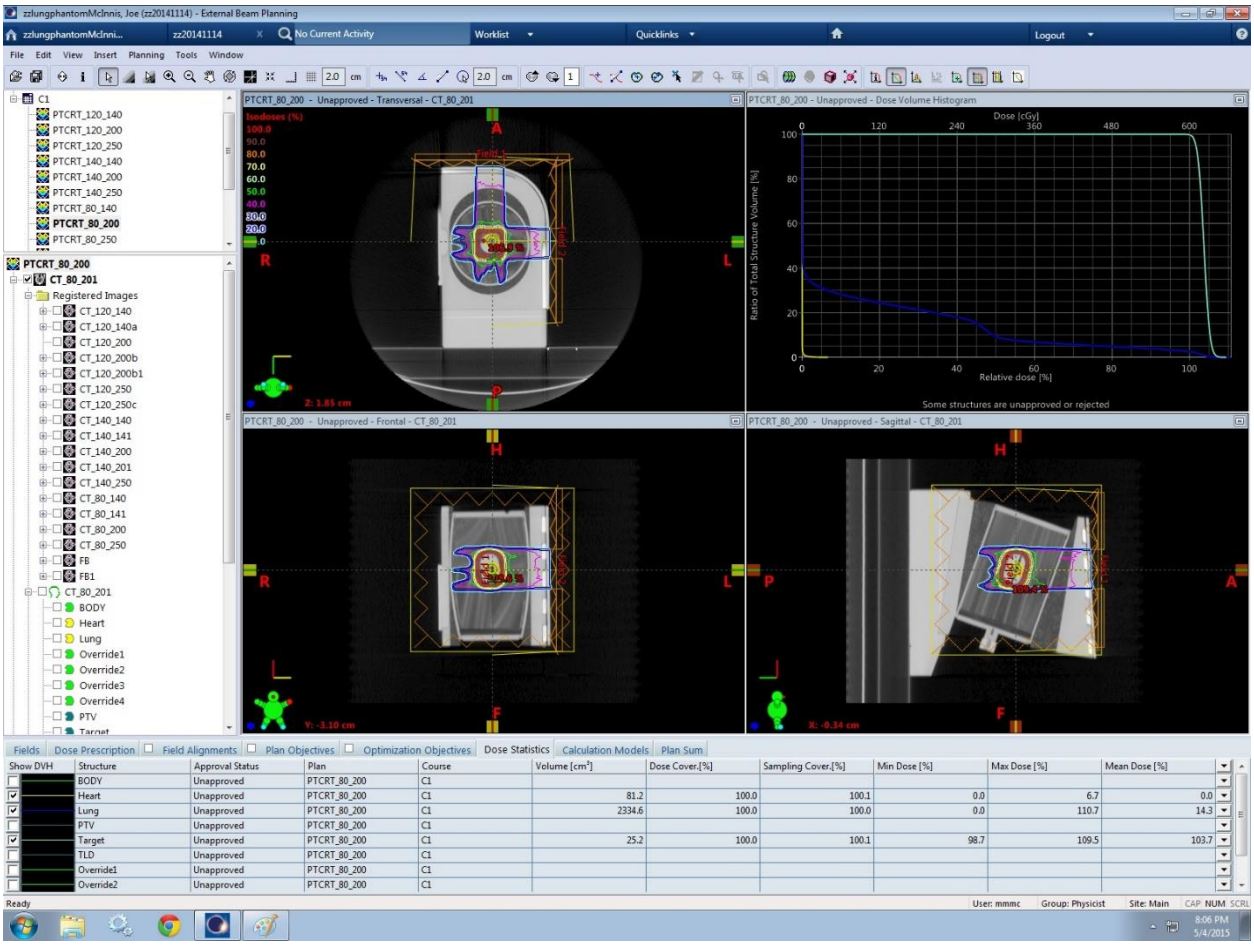

Figure 62. Dose Distribution at Isocenter of Plan Using CT Calibration Curve Corresponding to 80 kV CT Technique and 200 MeV Proton Energy

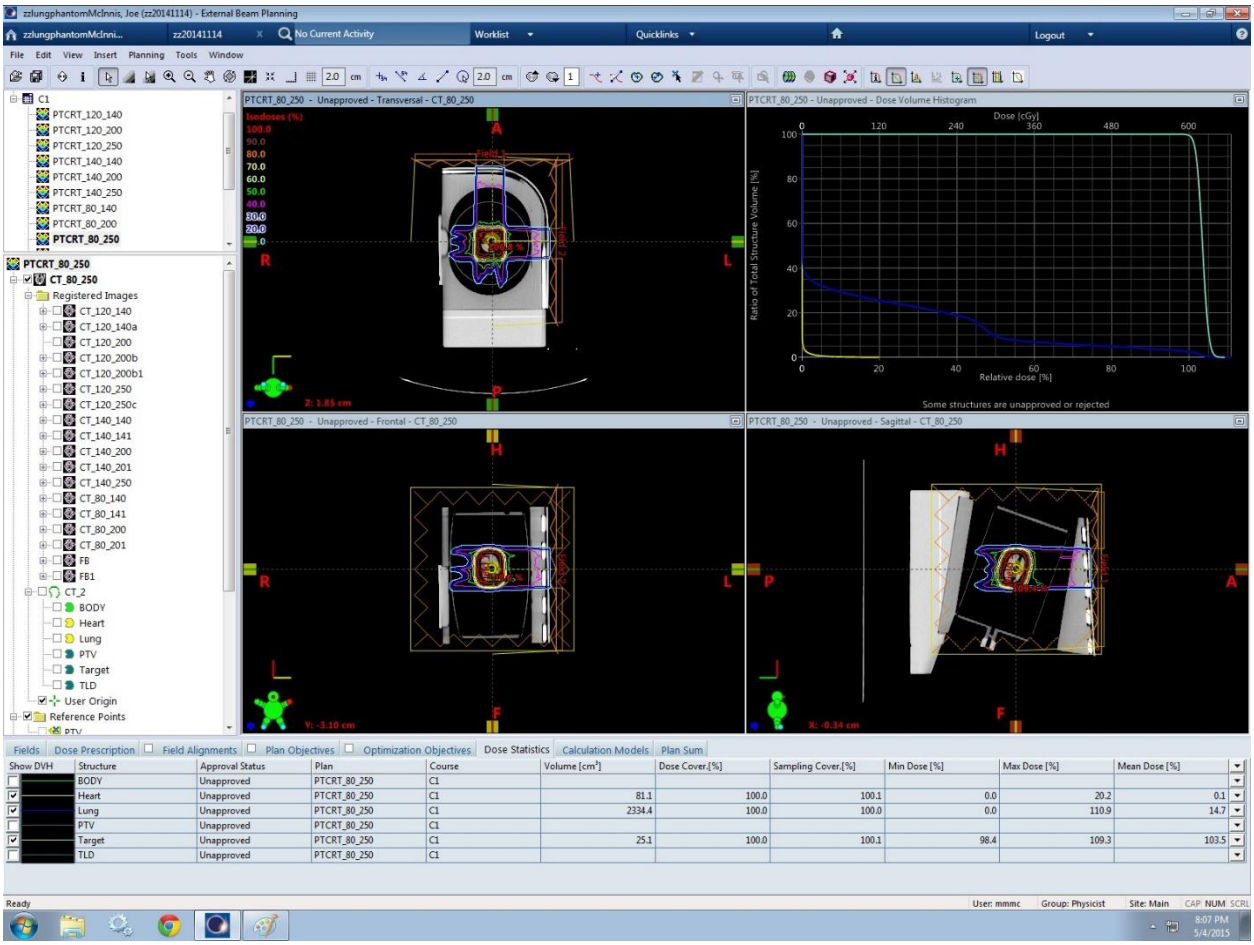

Figure 63. Dose Distribution at Isocenter of Plan Using CT Calibration Curve Corresponding to 80 kV CT Technique and 250 MeV Proton Energy

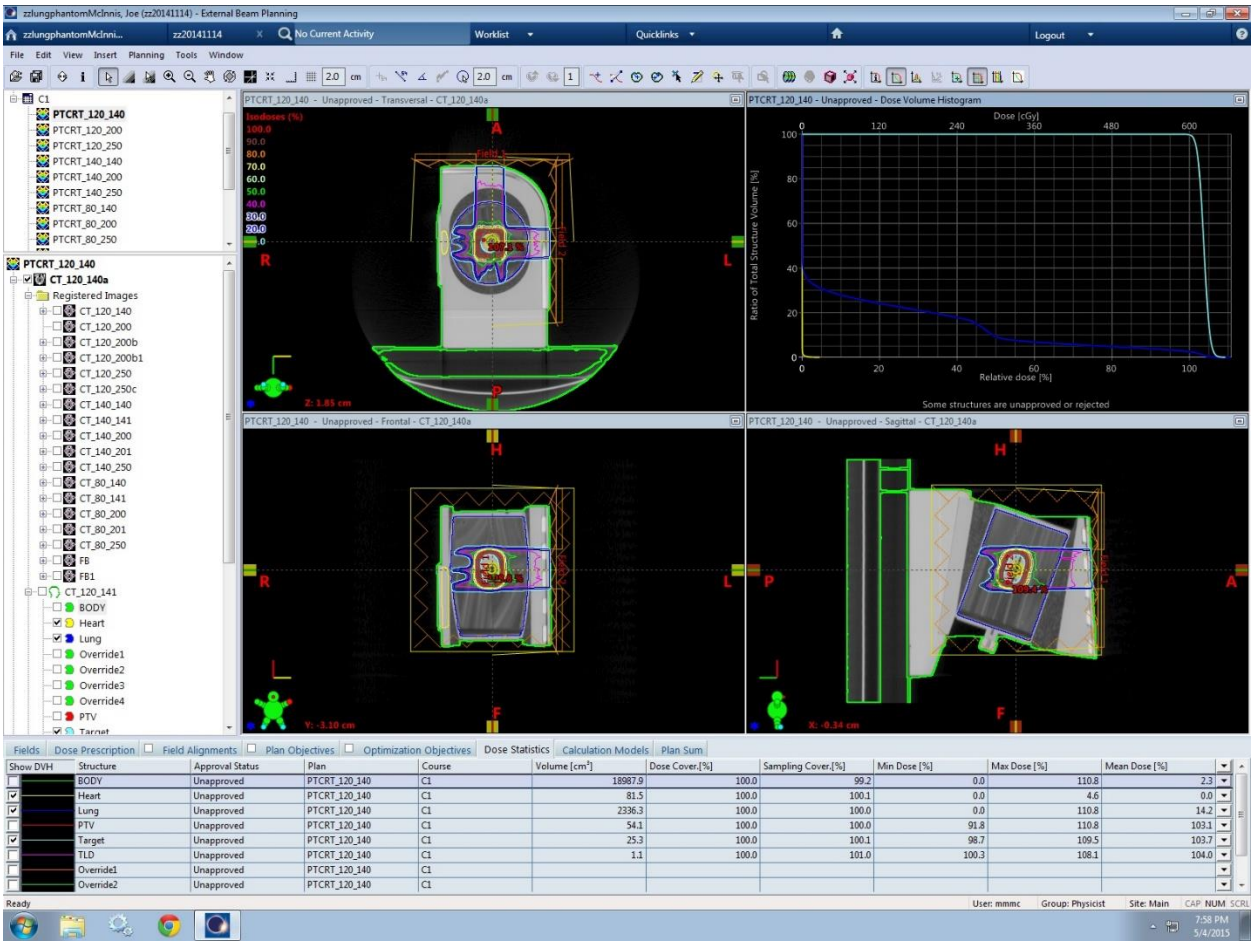

Figure 64. Dose Distribution at Isocenter of Plan Using CT Calibration Curve Corresponding to 120 kV CT Technique and 140 MeV Proton Energy

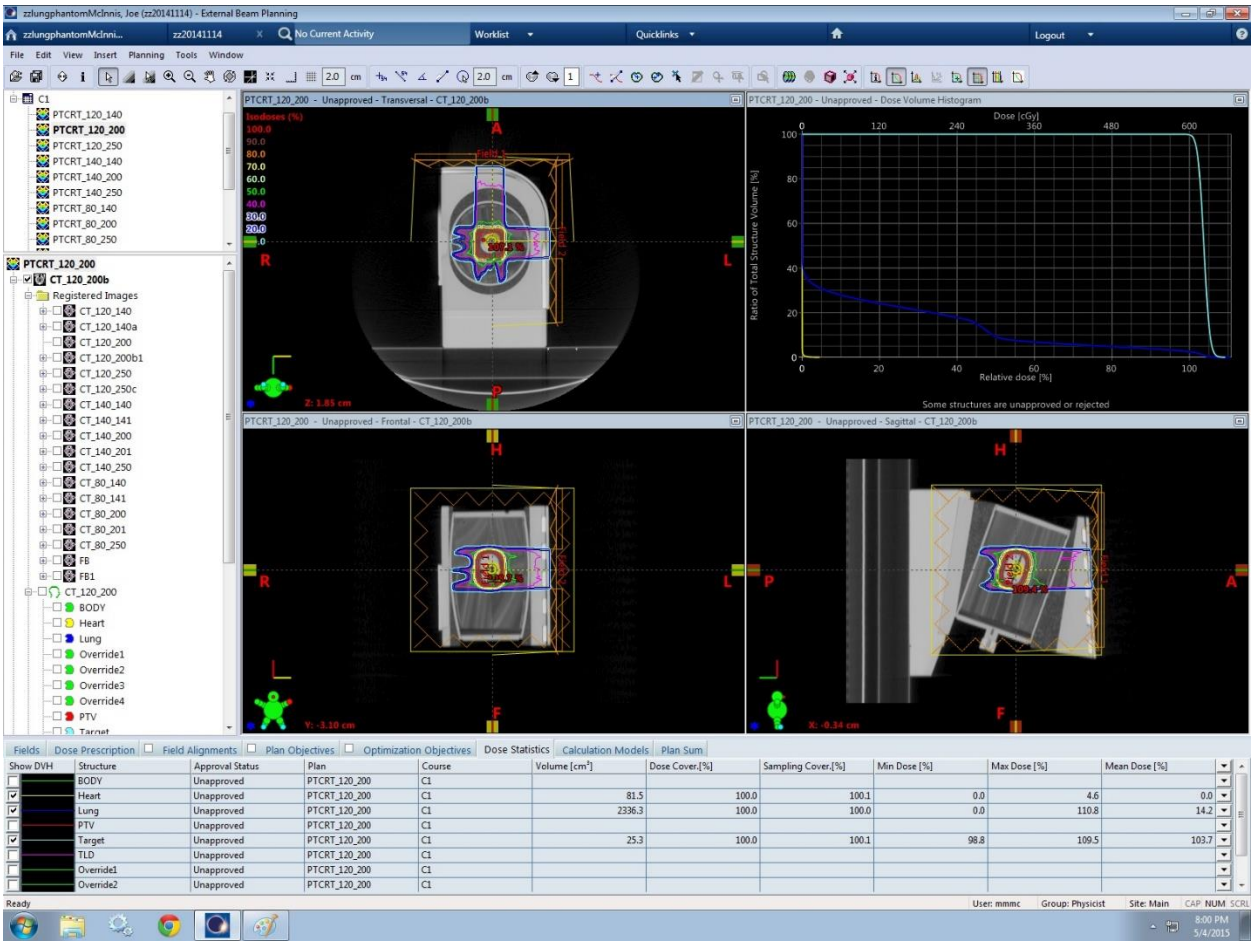

Figure 65. Dose Distribution at Isocenter of Plan Using CT Calibration Curve Corresponding to 120 kV CT Technique and 200 MeV Proton Energy

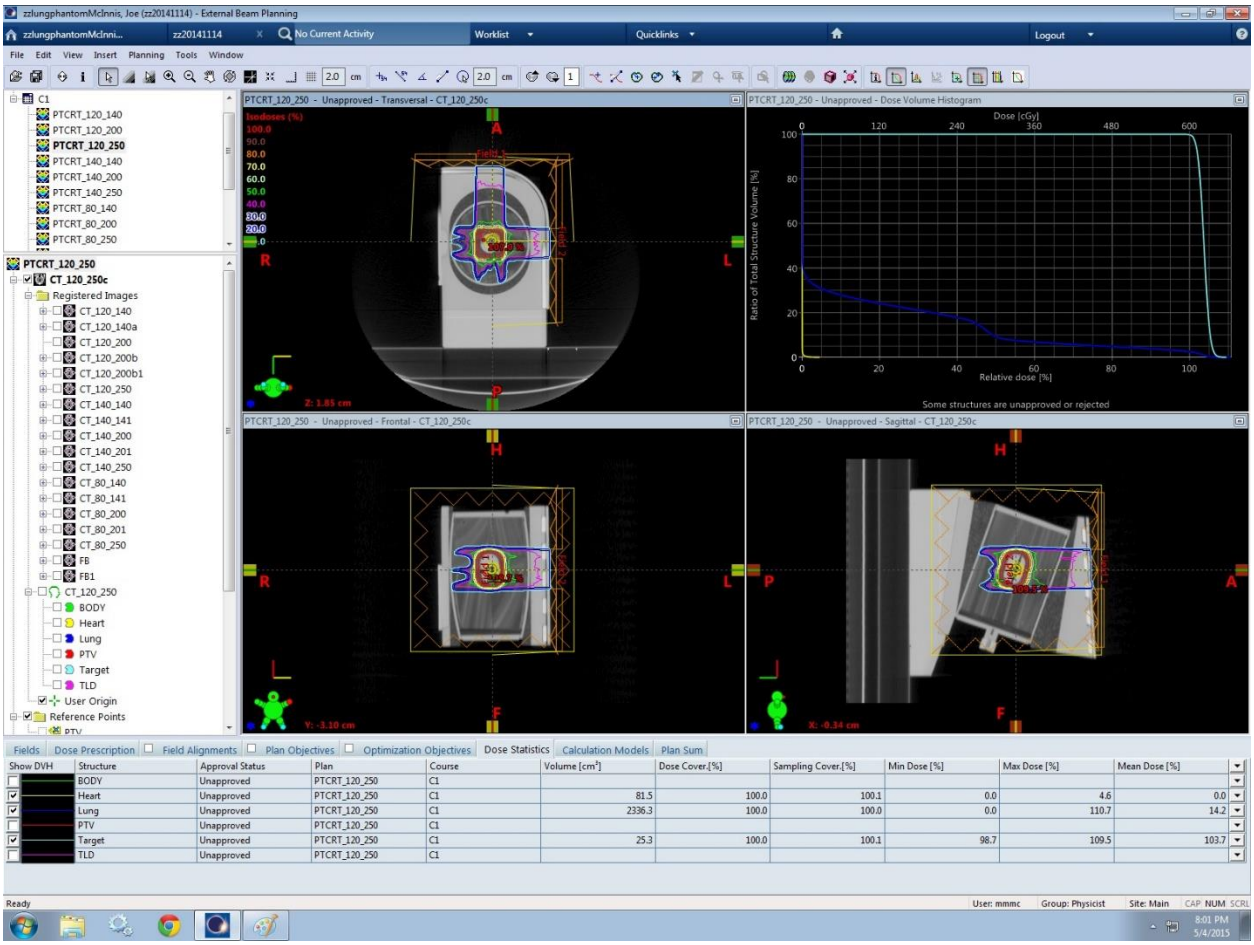

Figure 66. Dose Distribution at Isocenter of Plan Using CT Calibration Curve Corresponding to 120 kV CT Technique and 250 MeV Proton Energy

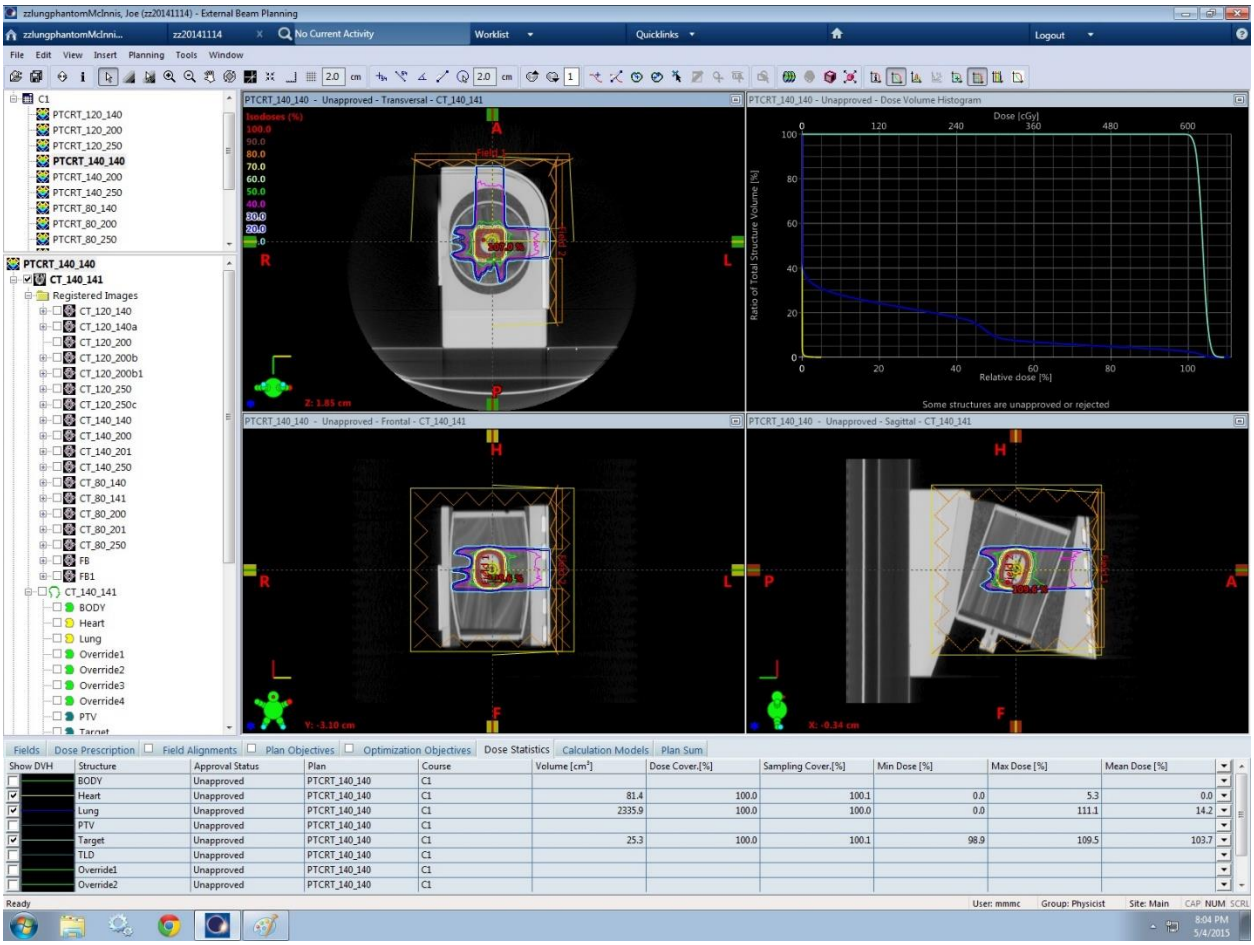

Figure 67. Dose Distribution at Isocenter of Plan Using CT Calibration Curve Corresponding to 140 kV CT Technique and 140 MeV Proton Energy

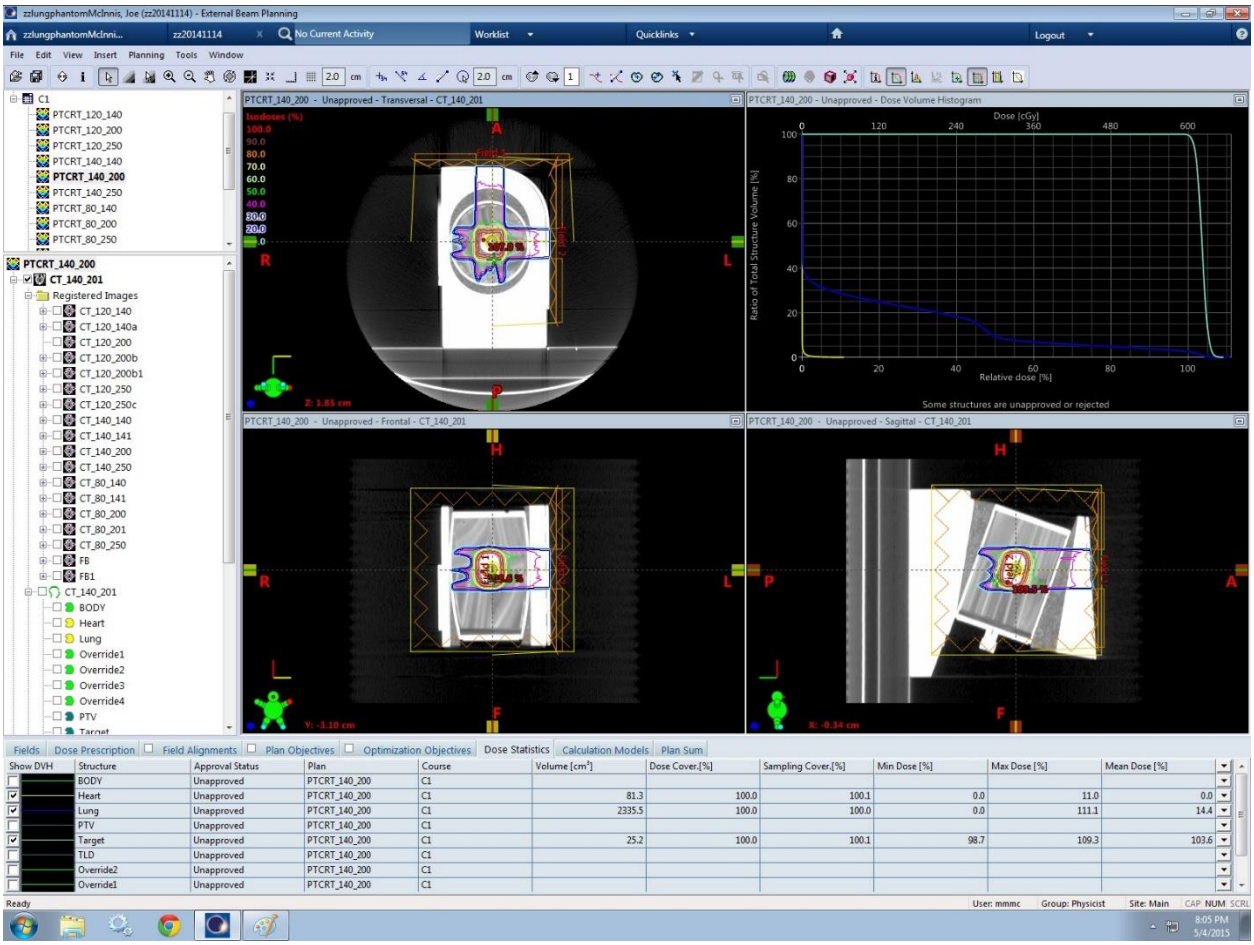

Figure 68. Dose Distribution at Isocenter of Plan Using CT Calibration Curve Corresponding to 140 kV CT Technique and 200 MeV Proton Energy

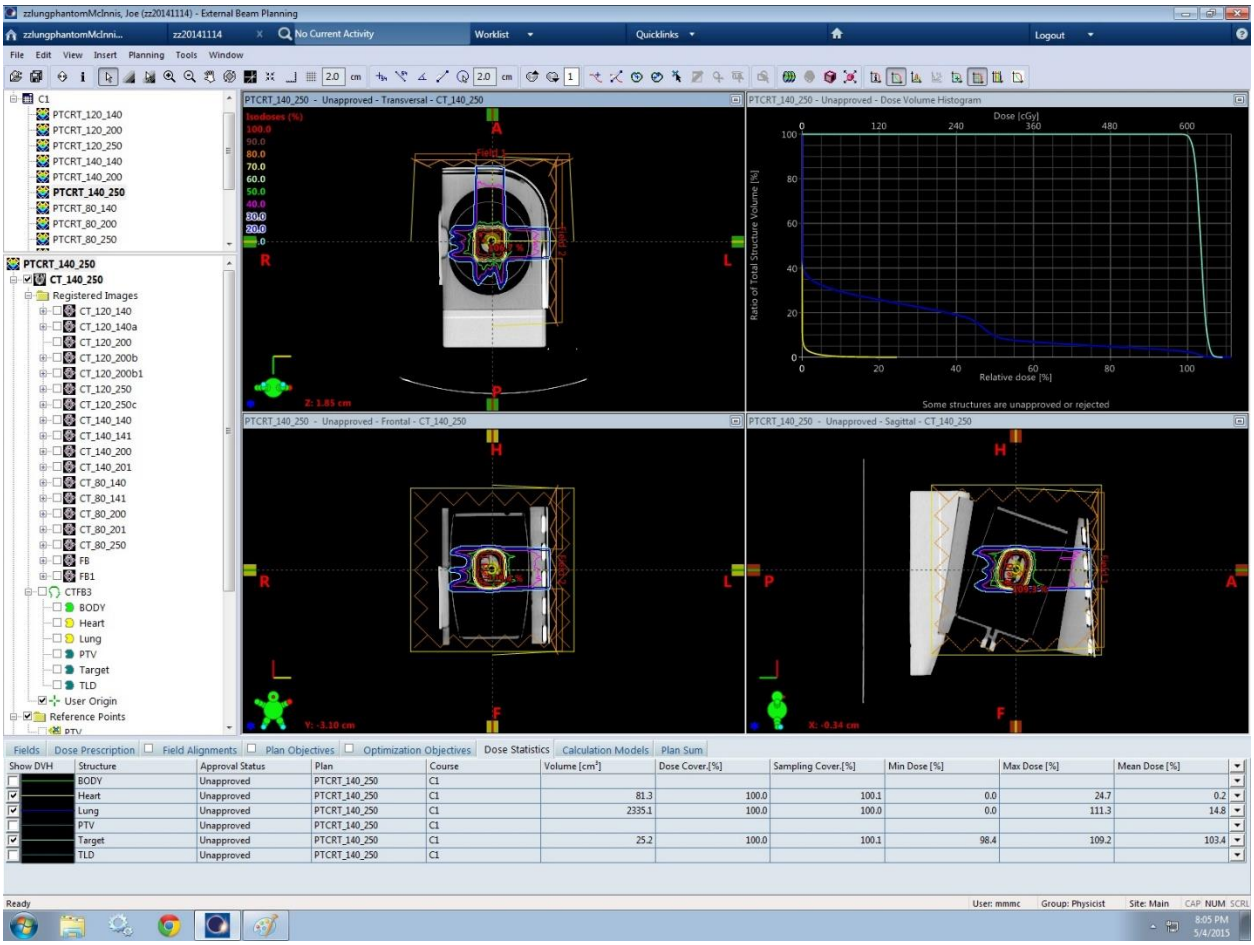

Figure 69. Dose Distribution at Isocenter of Plan Using CT Calibration Curve Corresponding to 140 kV CT Technique and 250 MeV Proton Energy

5.4 CERR Dose Distributions

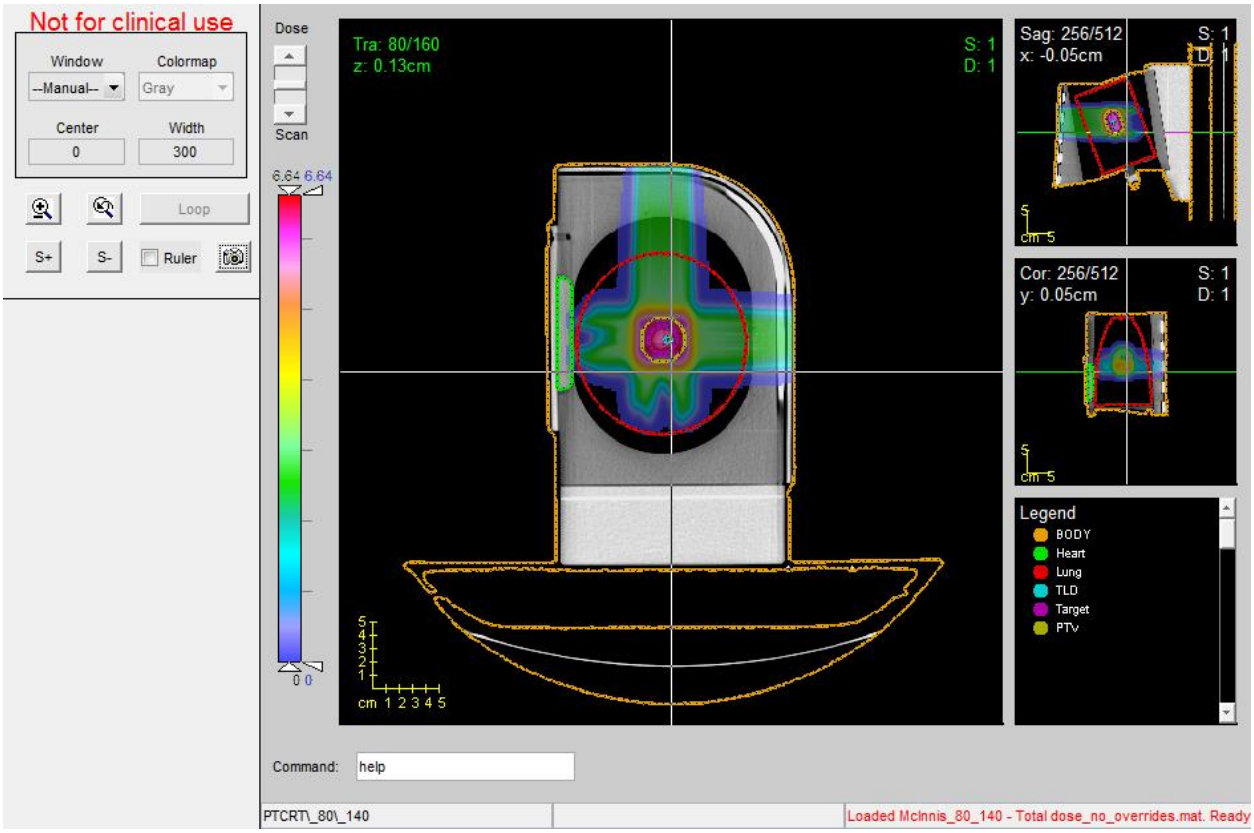

Figure 70. Dose smear provided by CERR for the plan corresponding to 80 kV CT technique and 140 MeV proton energy

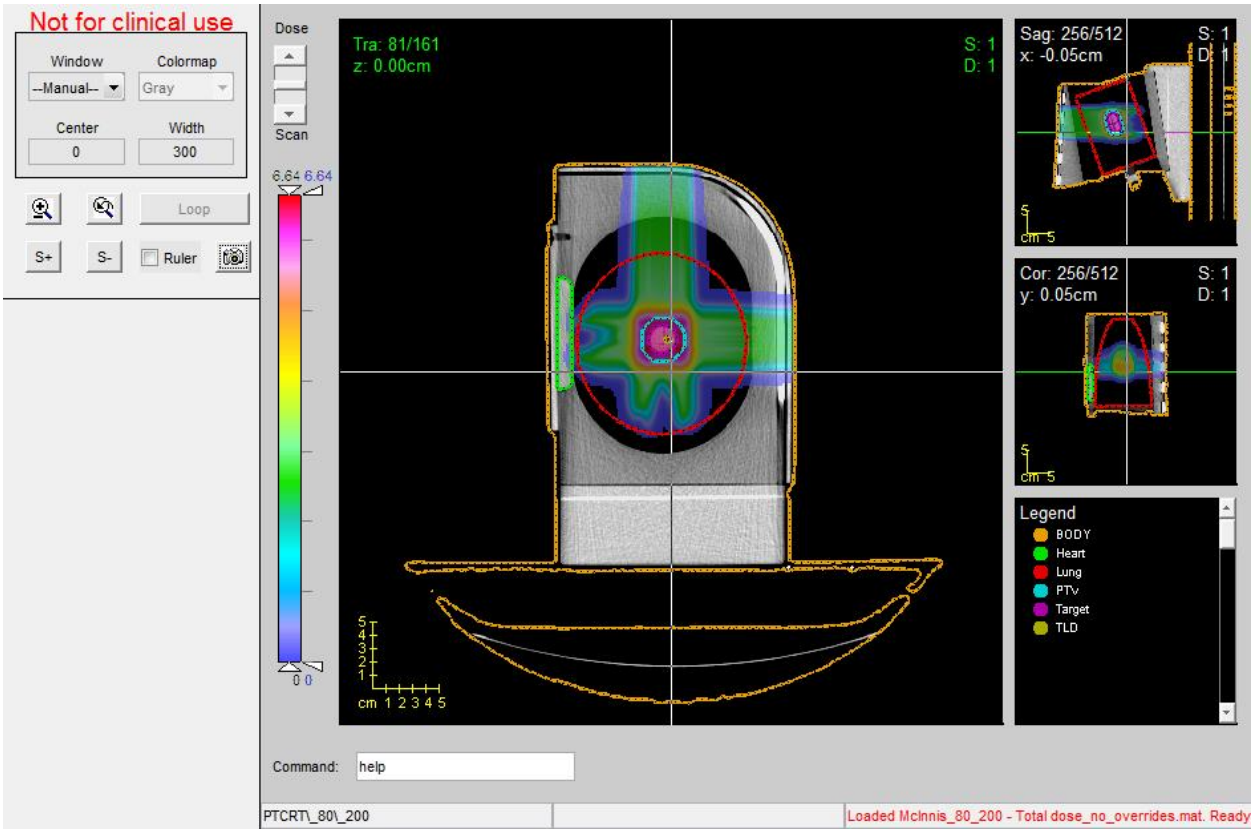

Figure 71. Dose smear provided by CERR for the plan corresponding to 80 kV CT technique and 200 MeV proton energy

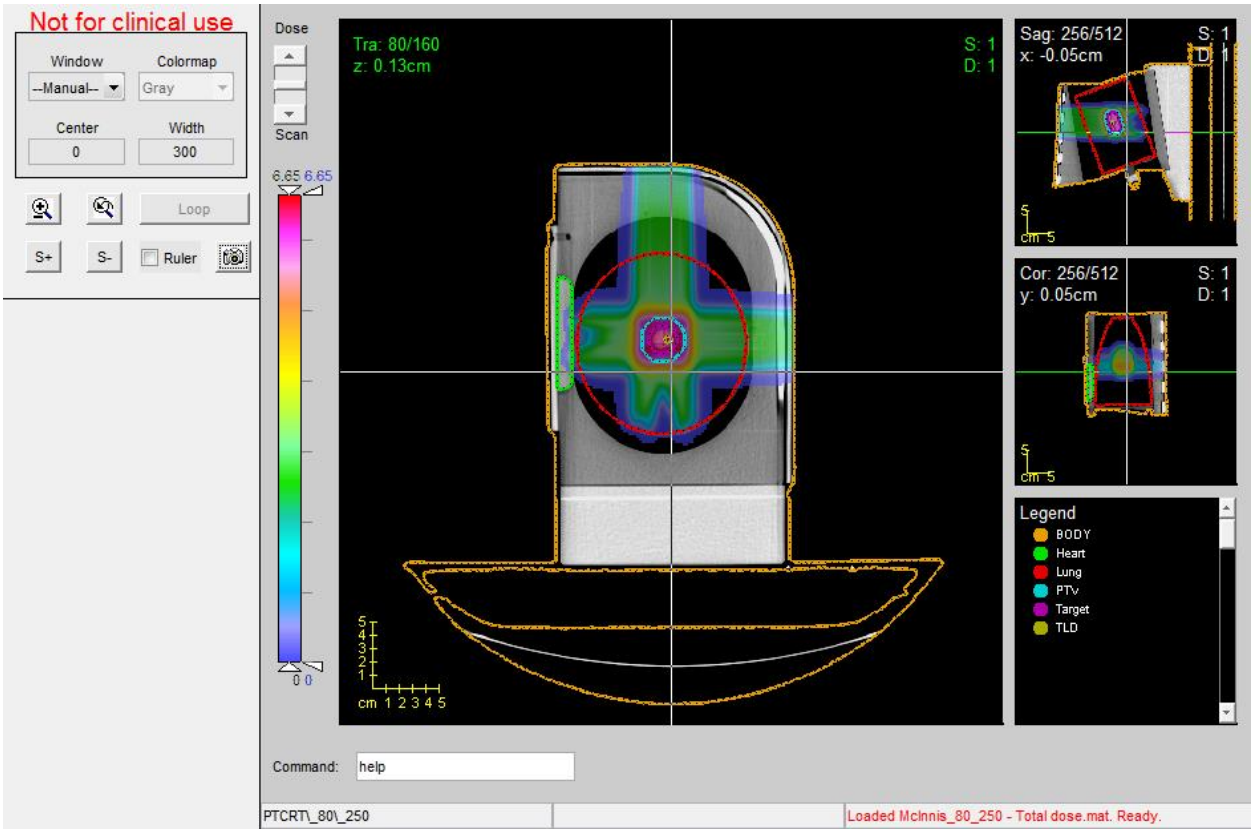

Figure 72. Dose smear provided by CERR for the plan corresponding to 80 kV CT technique and 250 MeV proton energy

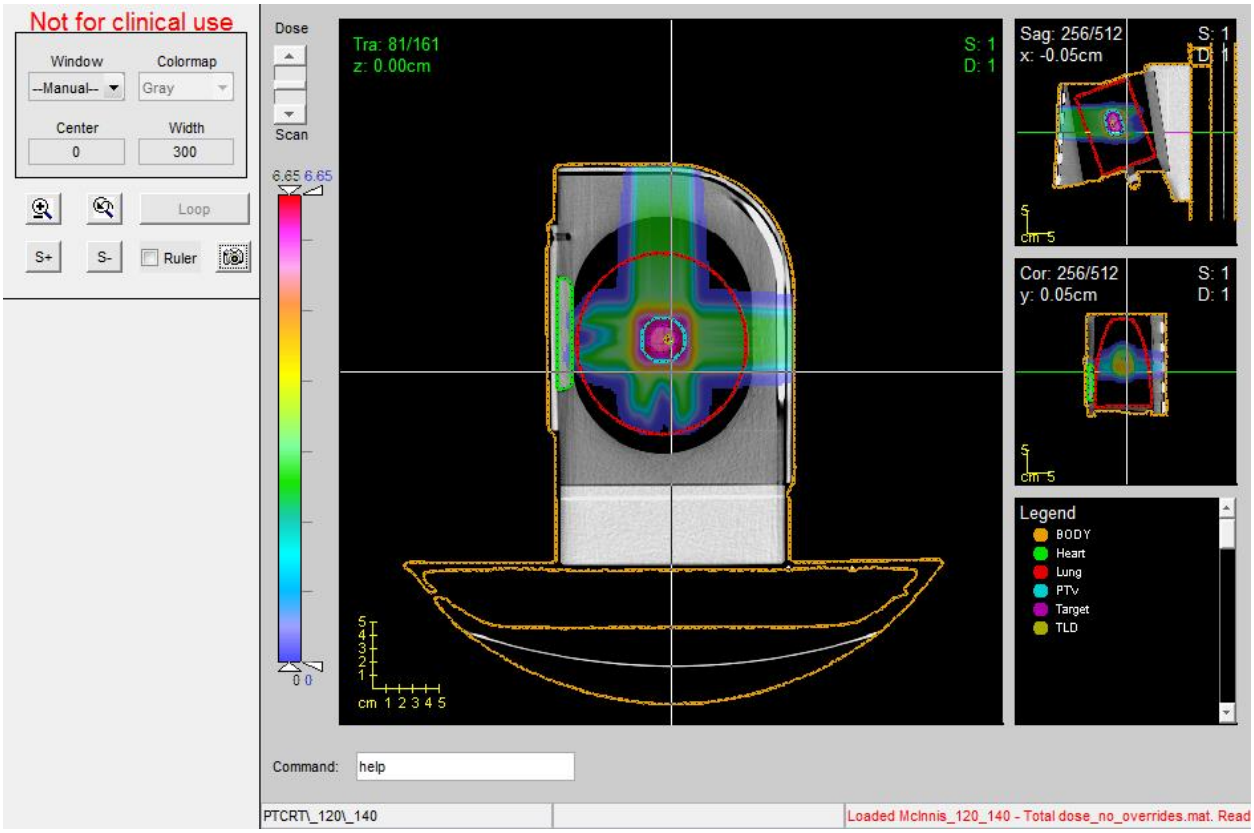

Figure 73. Dose smear provided by CERR for the plan corresponding to 120 kV CT technique and 140 MeV proton energy

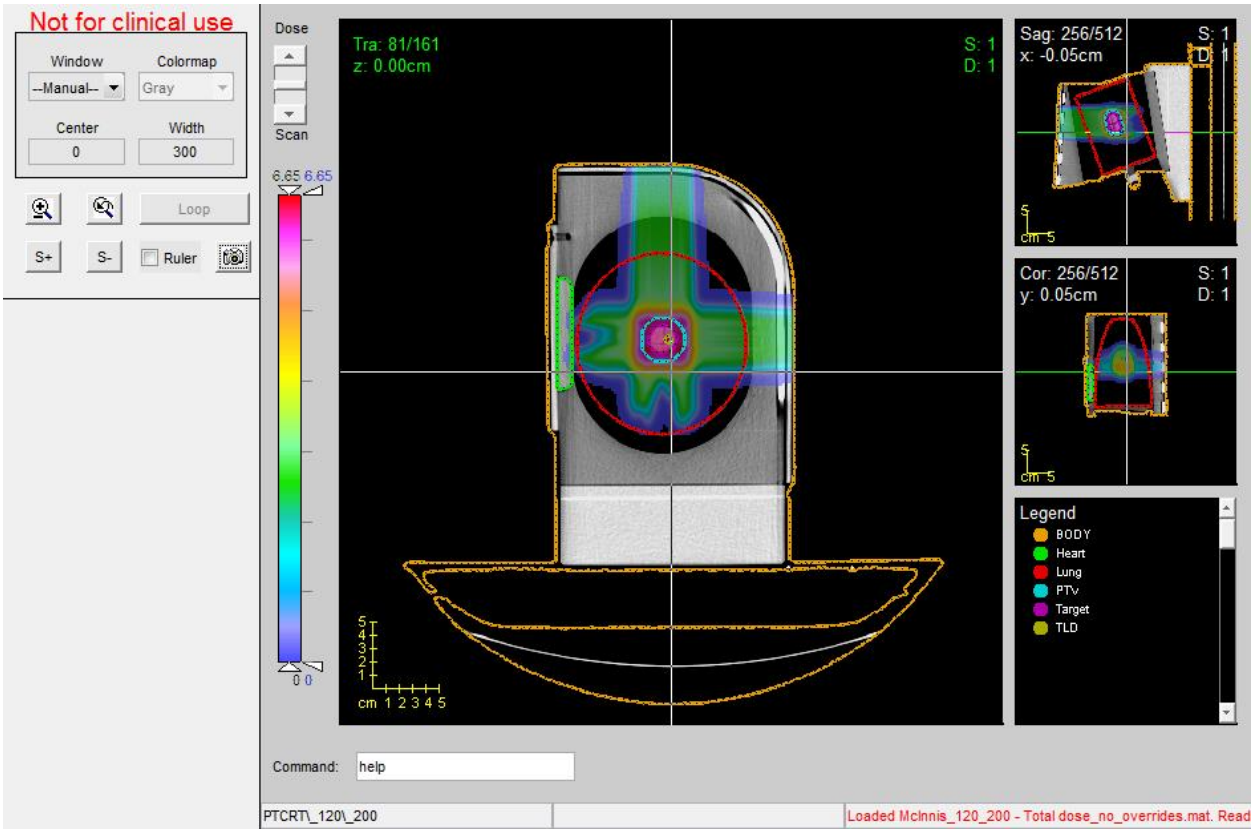

Figure 74. Dose smear provided by CERR for the plan corresponding to 120 kV CT technique and 200 MeV proton energy

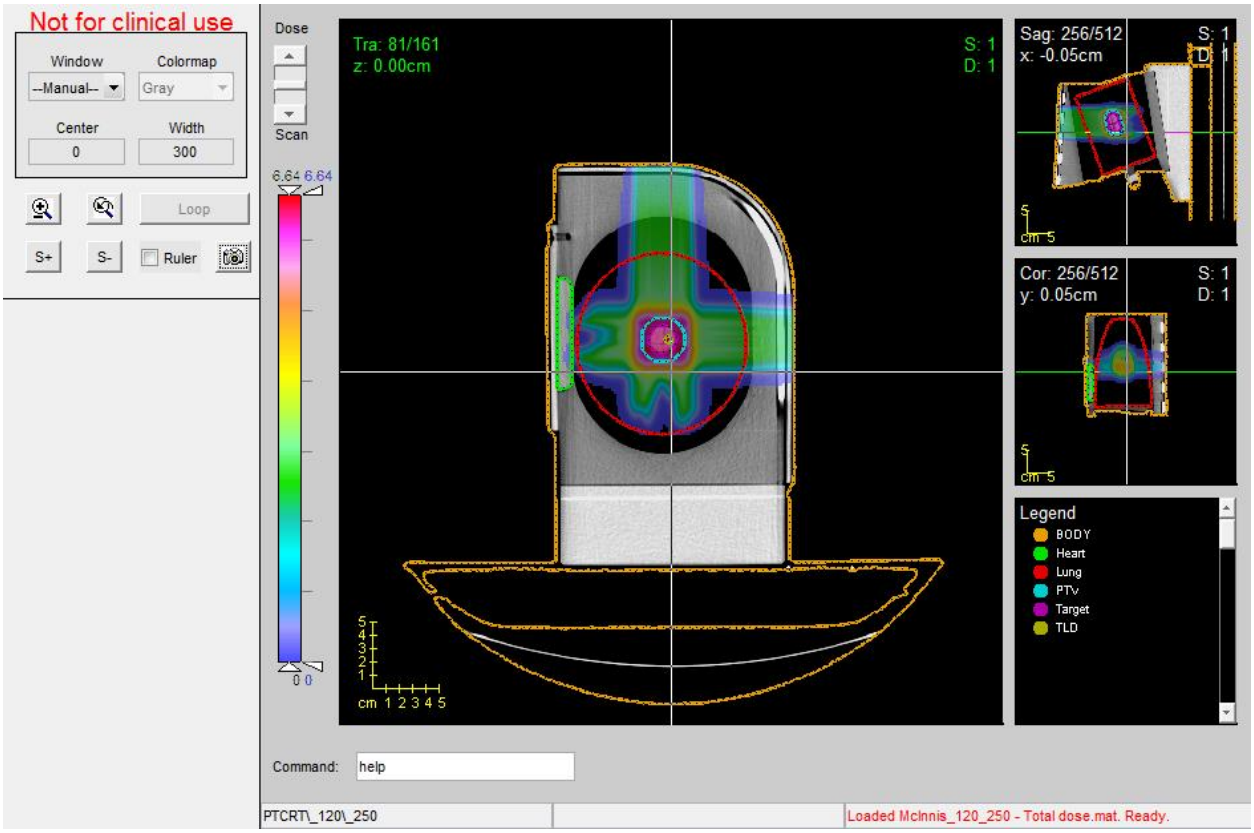

Figure 75. Dose smear provided by CERR for the plan corresponding to 120 kV CT technique and 250 MeV proton energy

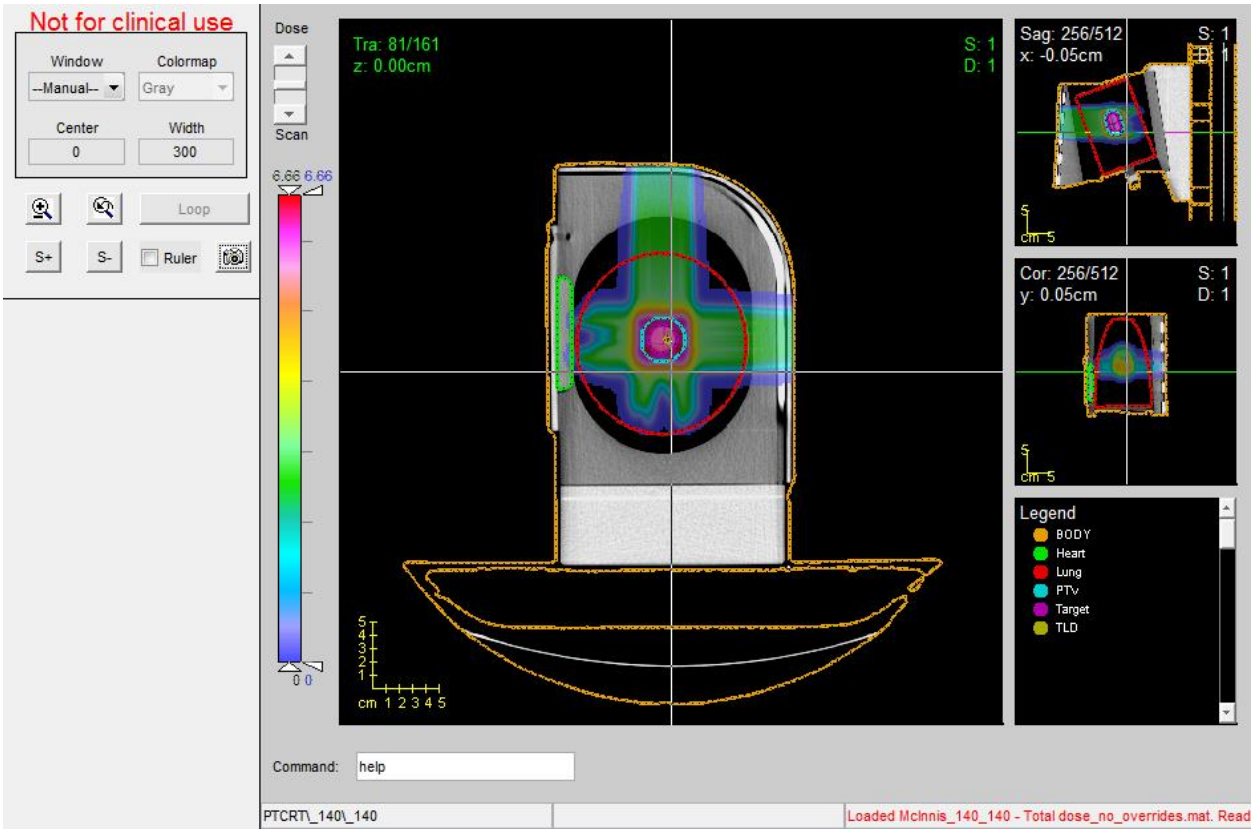

Figure 76. Dose smear provided by CERR for the plan corresponding to 140 kV CT technique and 140 MeV proton energy

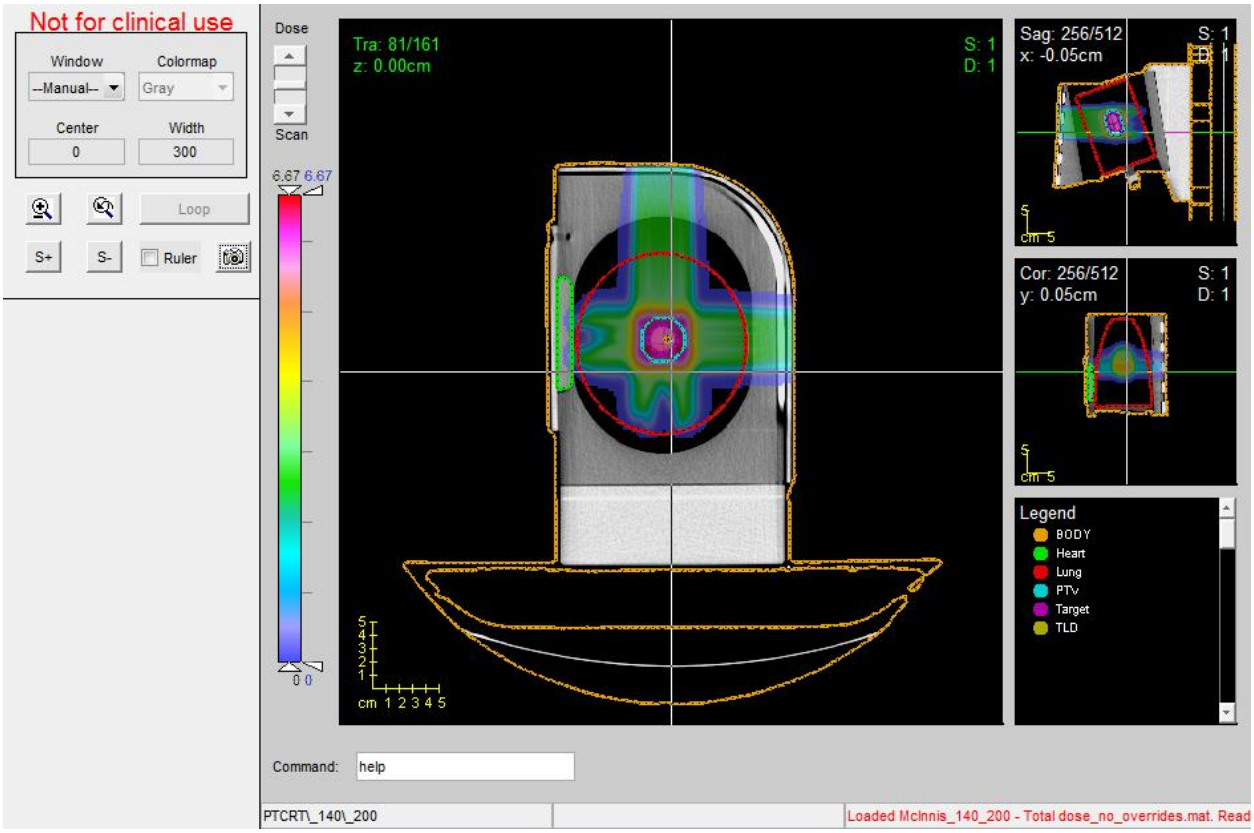

Figure 77. Dose smear provided by CERR for the plan corresponding to 140 kV CT technique and 200 MeV proton energy

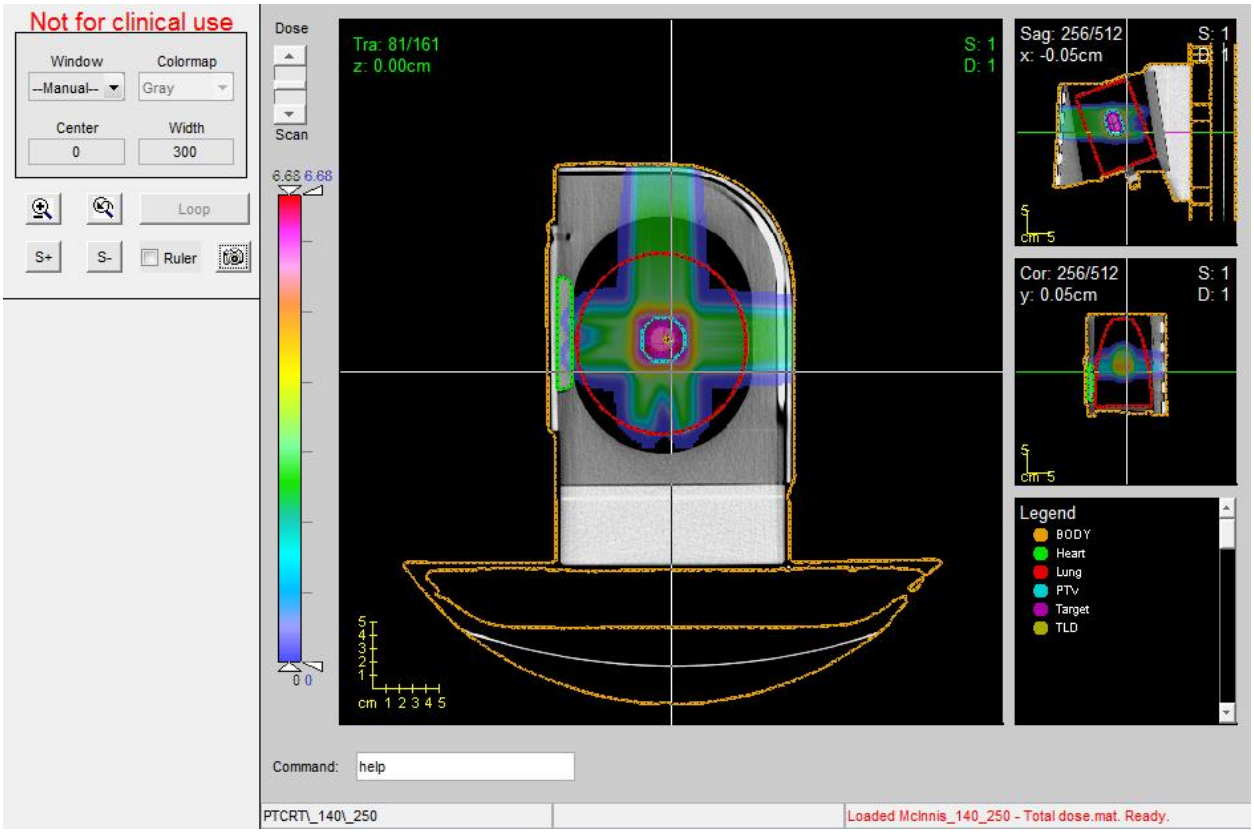

Figure 78. Dose smear provided by CERR for the plan corresponding to 140 kV CT technique and 250 MeV proton energy

5.5 CERR 3D Gamma Analysis

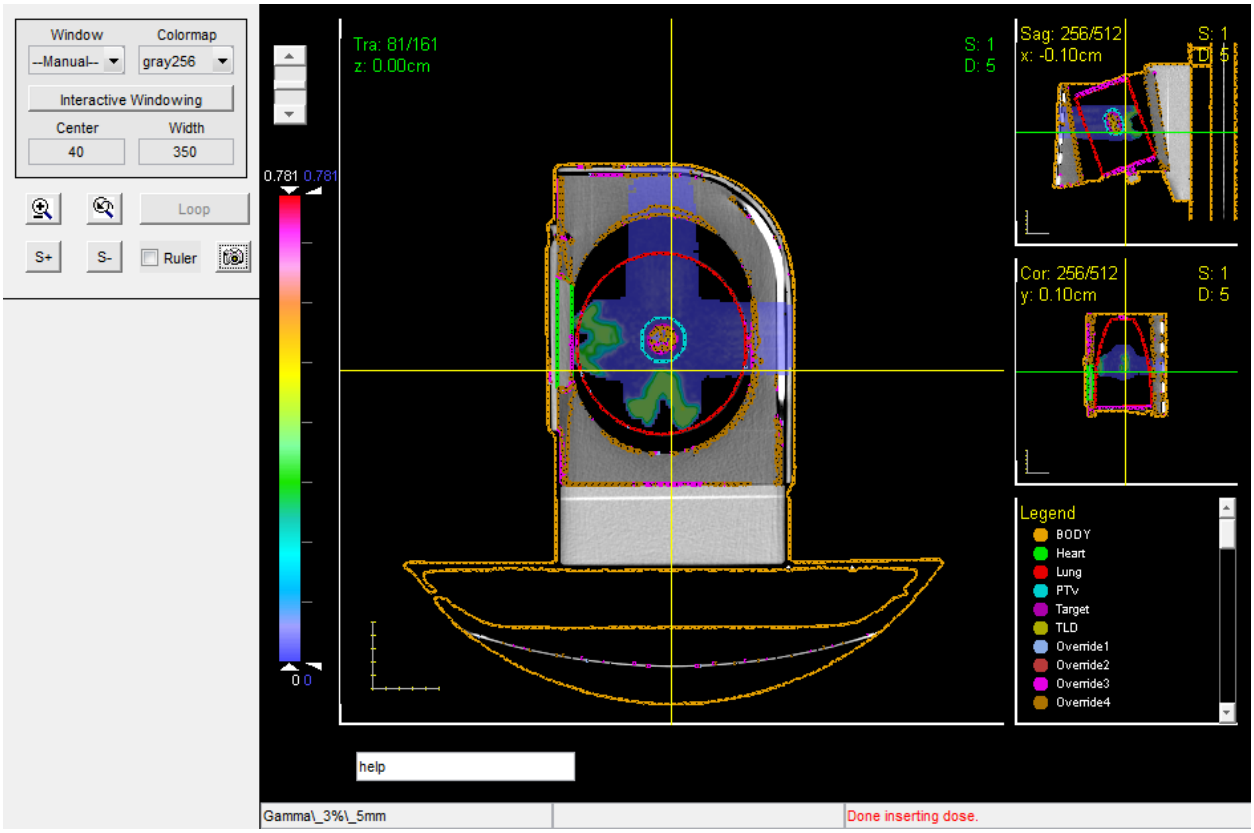

Figure 79. Gamma analysis at isocenter of plan corresponding to study reference curve compared with plan corresponding to 80 kV and 140 MeV with gamma criteria 3%/5mm

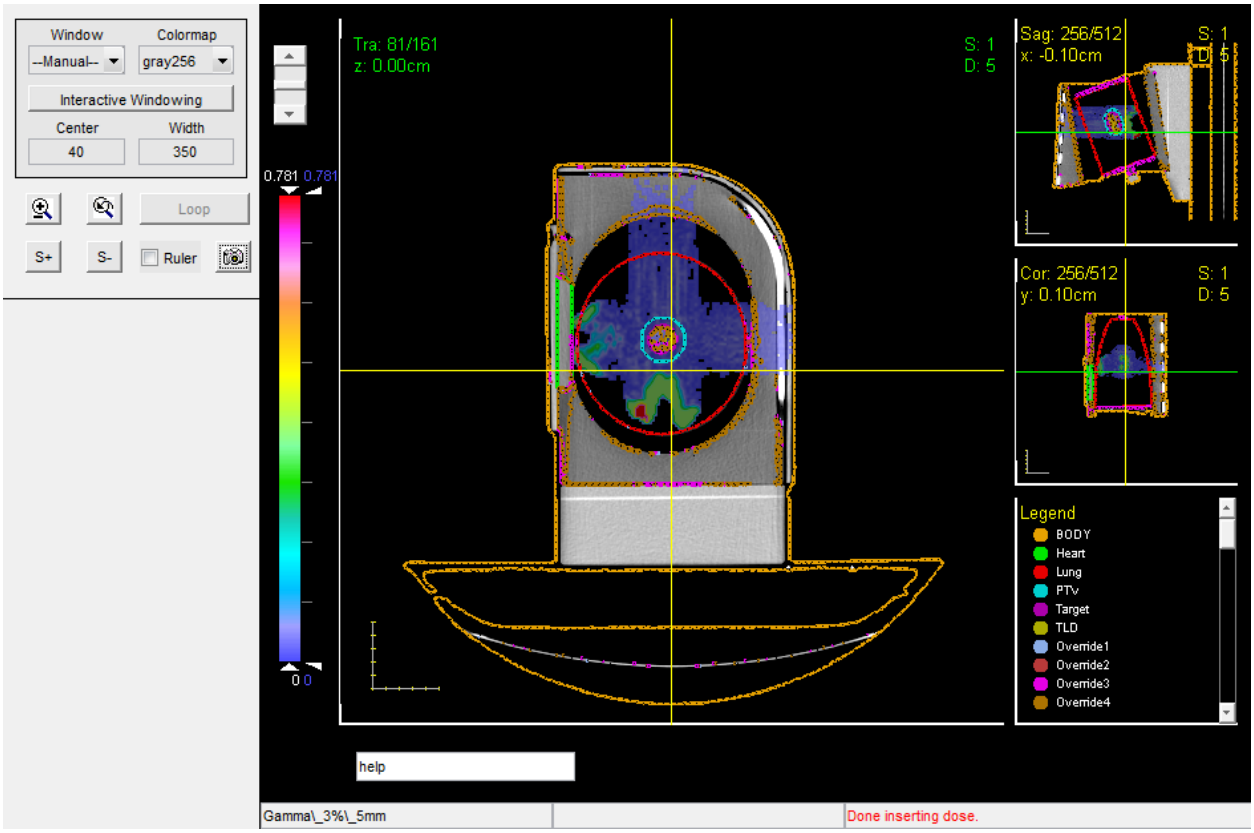

Figure 80. Gamma analysis at isocenter of plan corresponding to study reference curve compared with plan corresponding to 80 kV and 200 MeV with gamma criteria 3%/5mm

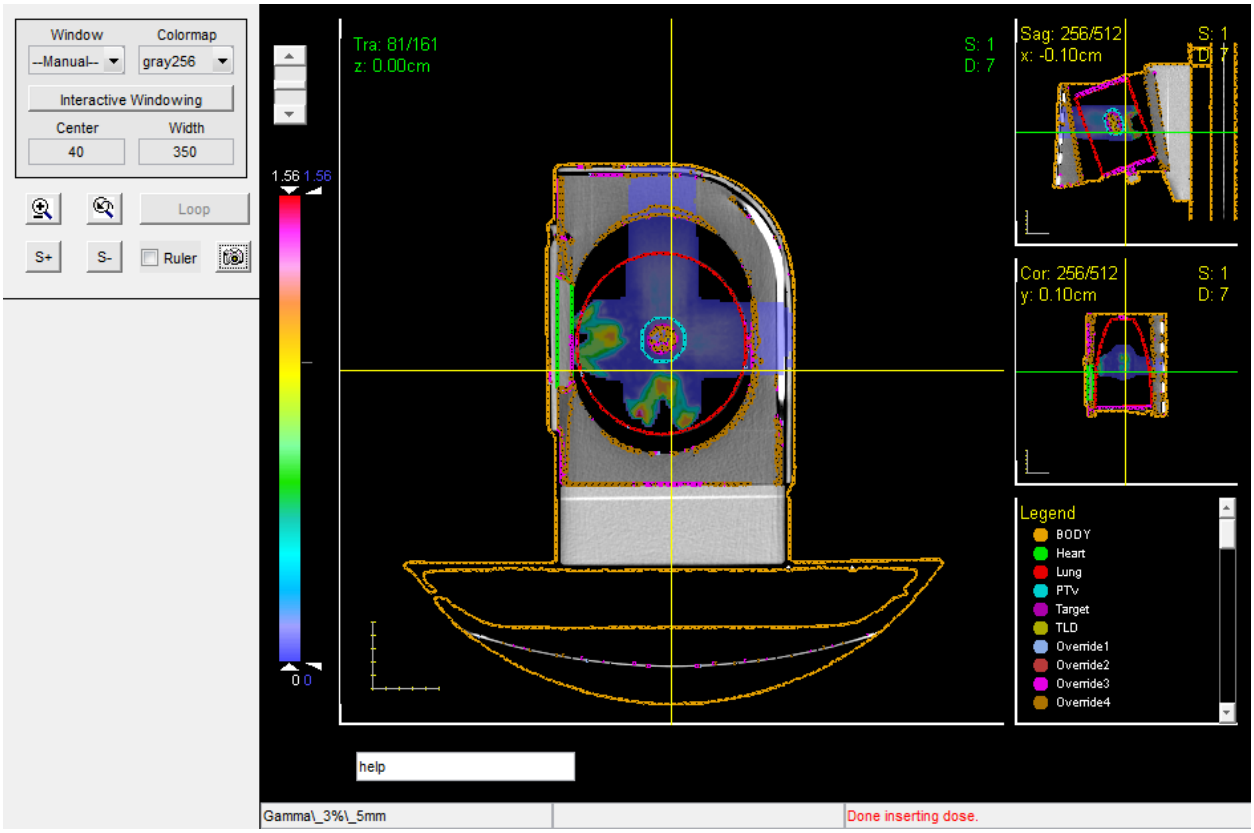

Figure 81. Gamma analysis at isocenter of plan corresponding to study reference curve compared with plan corresponding to 80 kV and 250 MeV with gamma criteria 3%/5mm

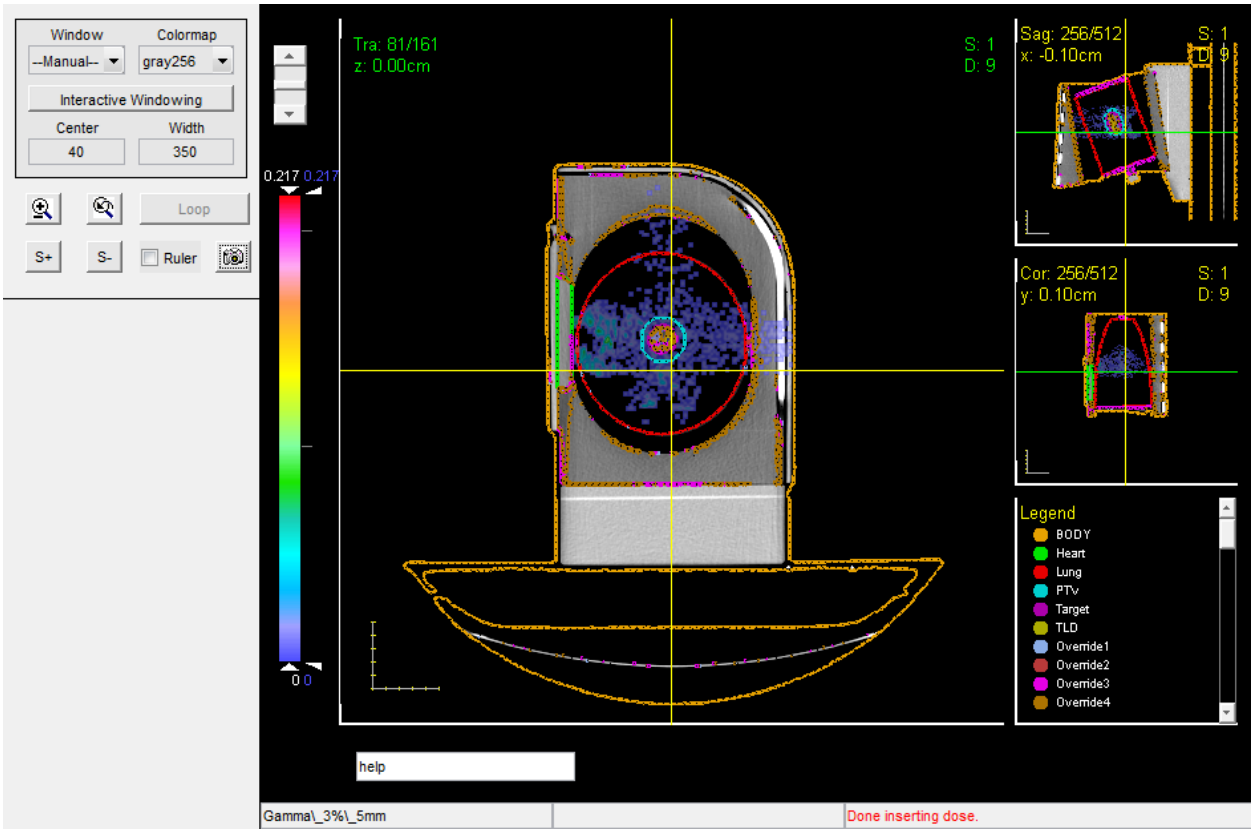

Figure 82. Gamma analysis at isocenter of plan corresponding to study reference curve compared with plan corresponding to 120 kV and 200 MeV with gamma criteria 3%/5mm

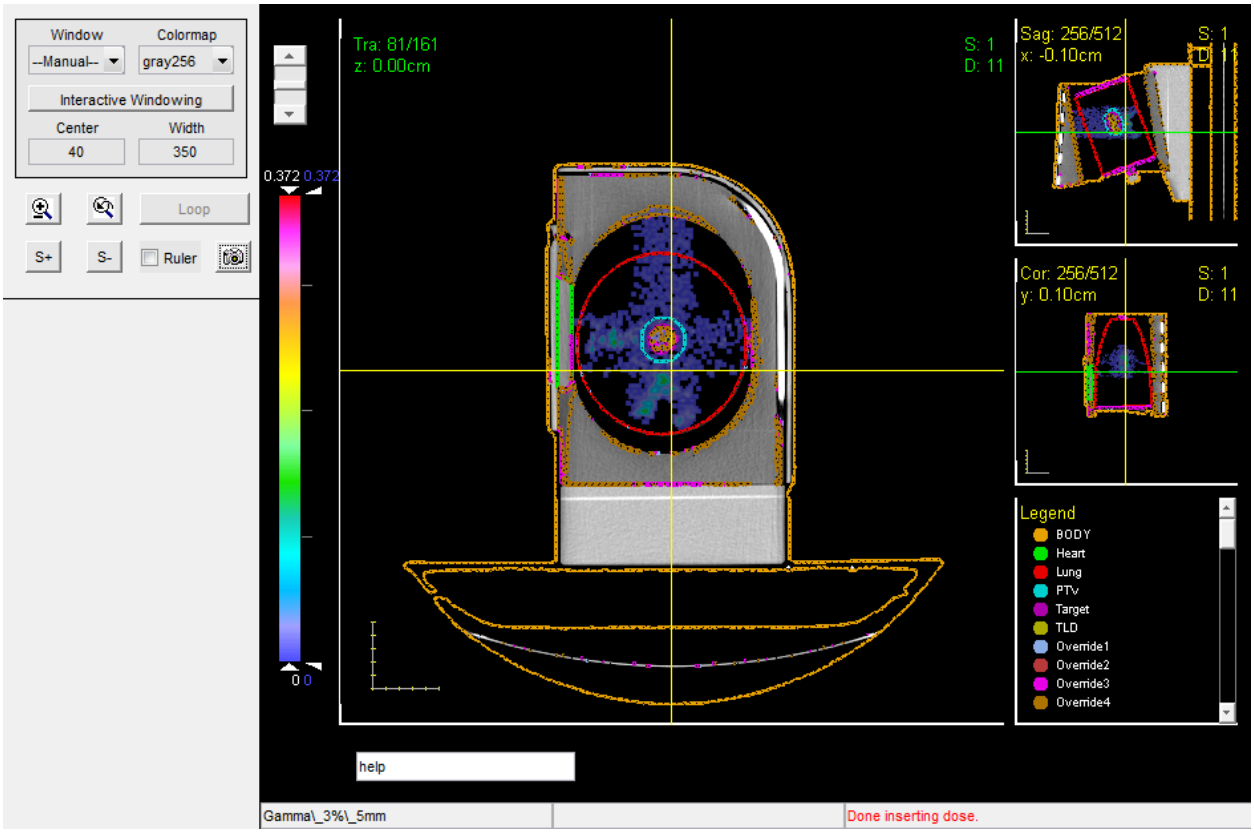

Figure 83. Gamma analysis at isocenter of plan corresponding to study reference curve compared with plan corresponding to 120 kV and 250 MeV with gamma criteria 3%/5mm

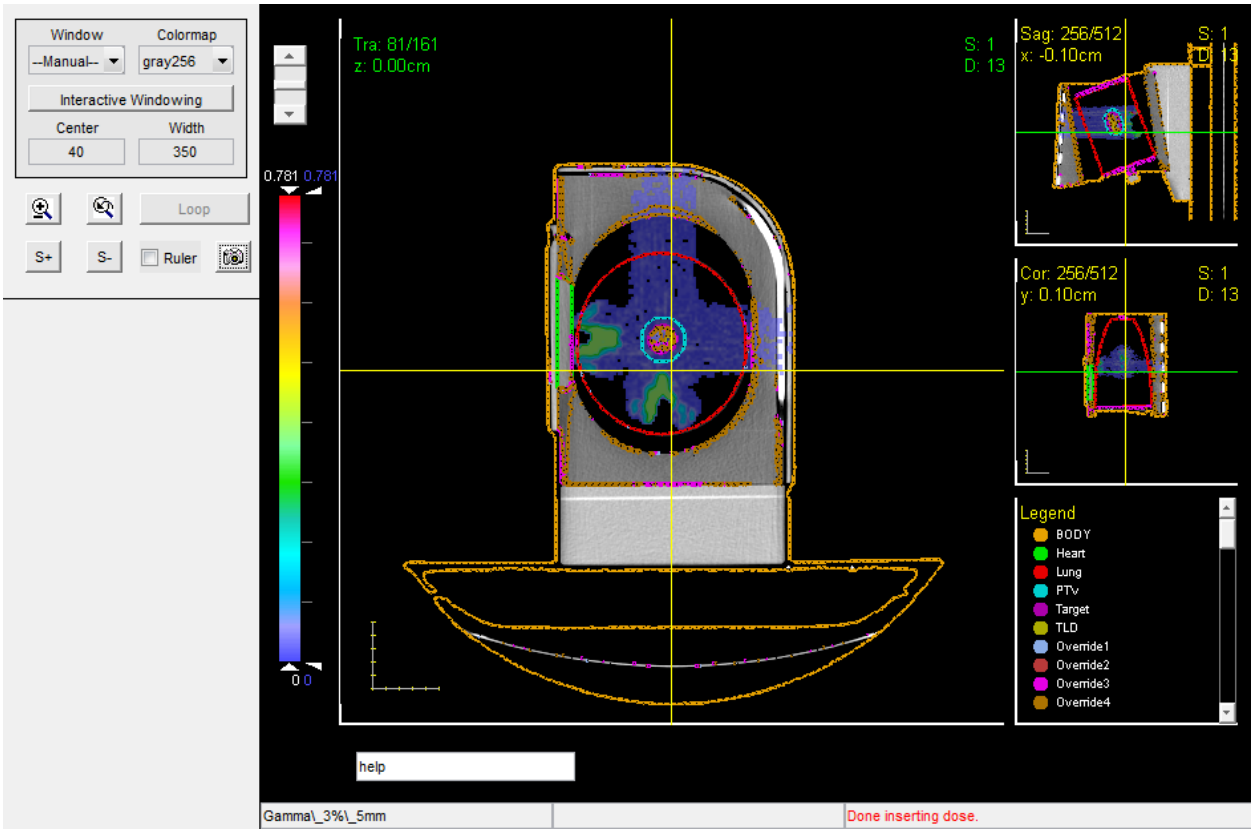

Figure 84. Gamma analysis at isocenter of plan corresponding to study reference curve compared with plan corresponding to 140 kV and 140 MeV with gamma criteria 3%/5mm

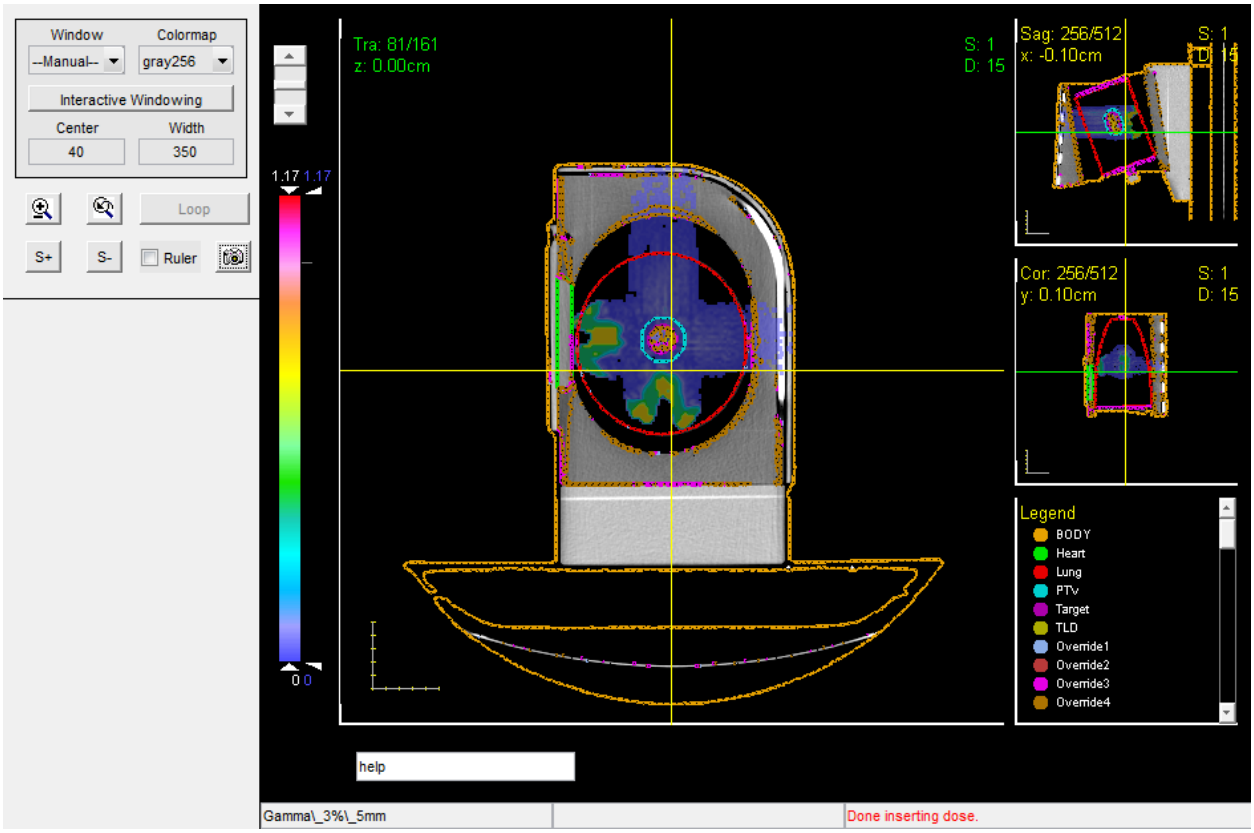

Figure 85. Gamma analysis at isocenter of plan corresponding to study reference curve compared with plan corresponding to 140 kV and 200 MeV with gamma criteria 3%/5mm

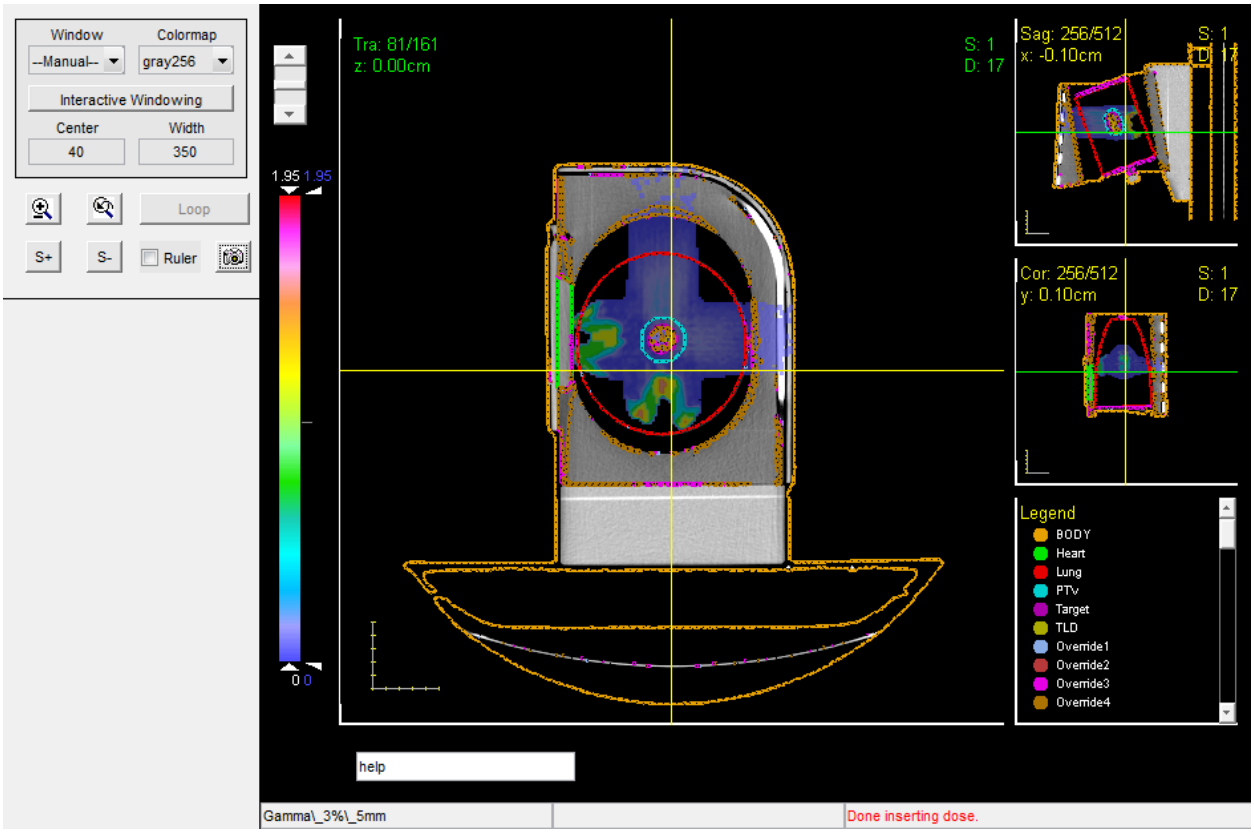

Figure 86. Gamma analysis at isocenter of plan corresponding to study reference curve compared with plan corresponding to 140 kV and 250 MeV with gamma criteria 3%/5mm

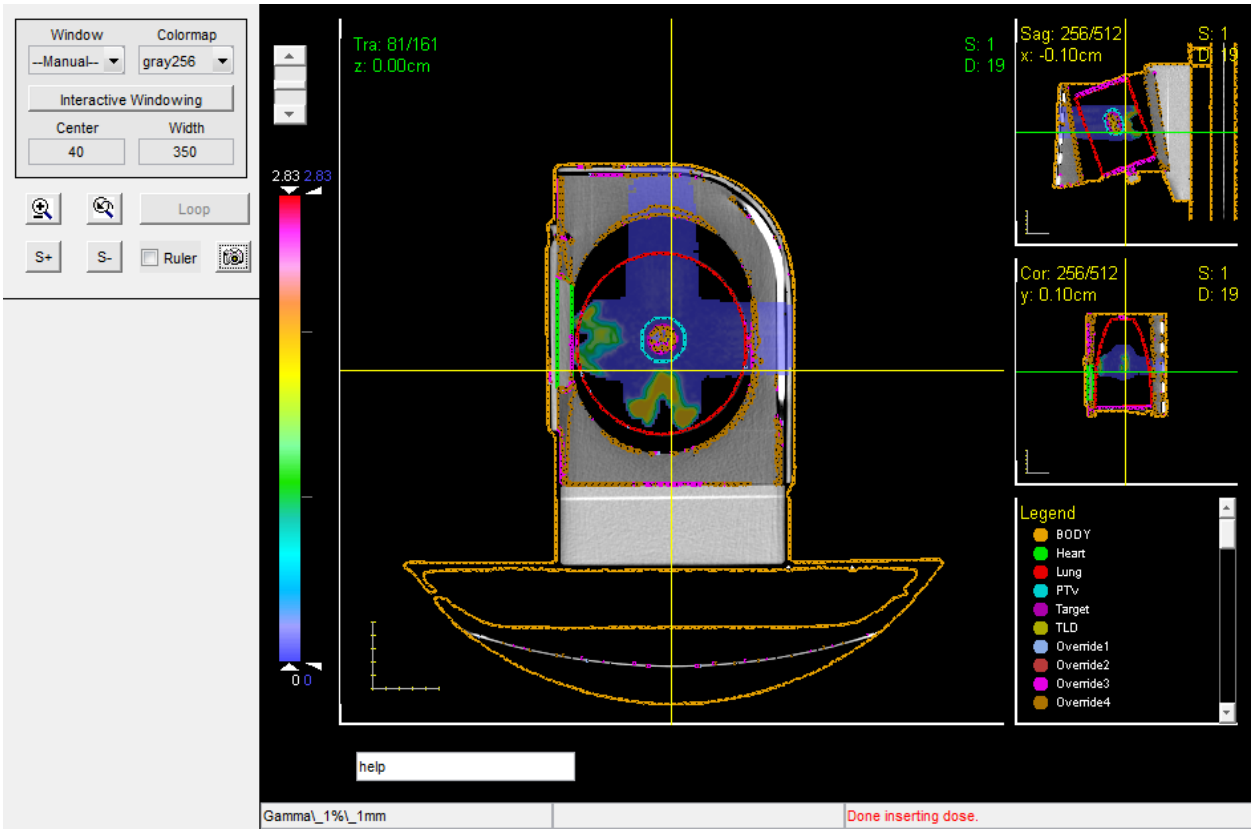

Figure 87. Gamma analysis at isocenter of plan corresponding to study reference curve compared with plan corresponding to 80 kV and 140 MeV with gamma criteria 1%/1mm

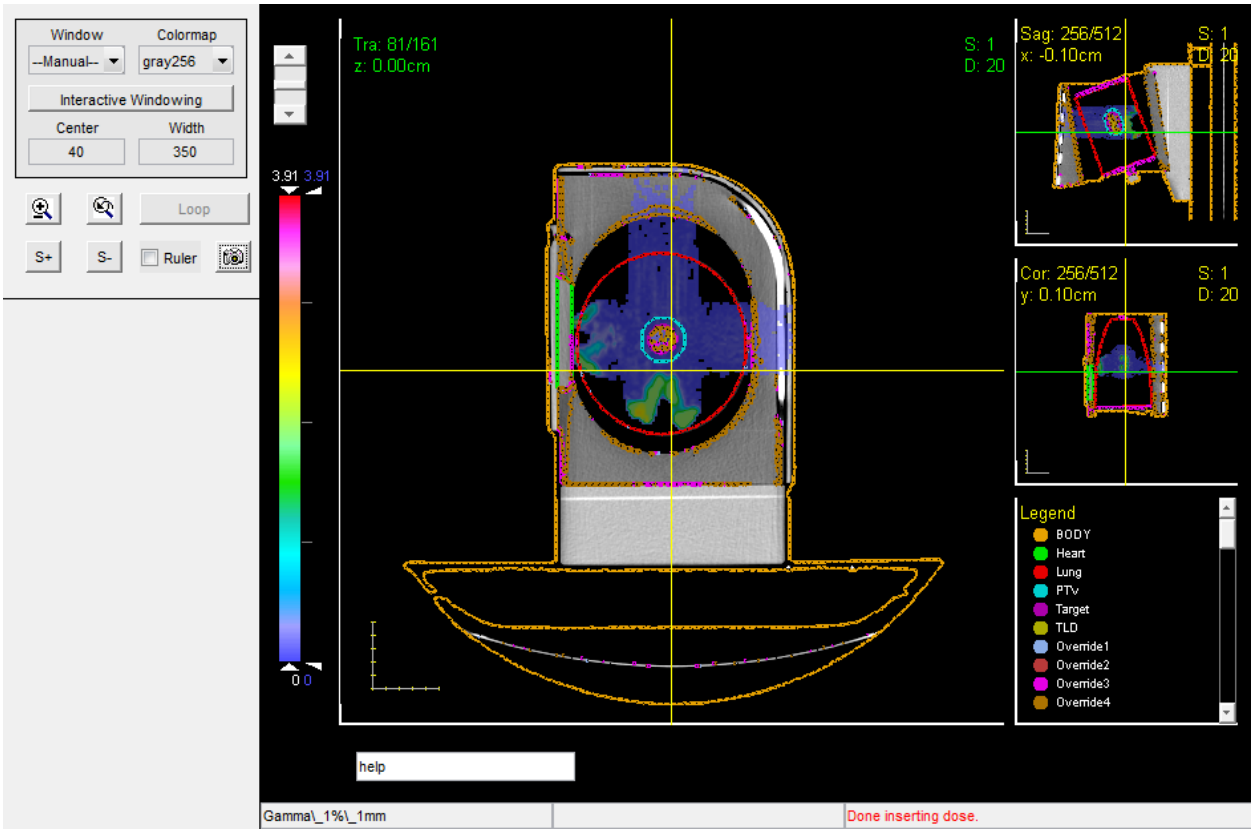

Figure 88. Gamma analysis at isocenter of plan corresponding to study reference curve compared with plan corresponding to 80 kV and 200 MeV with gamma criteria 1%/1mm

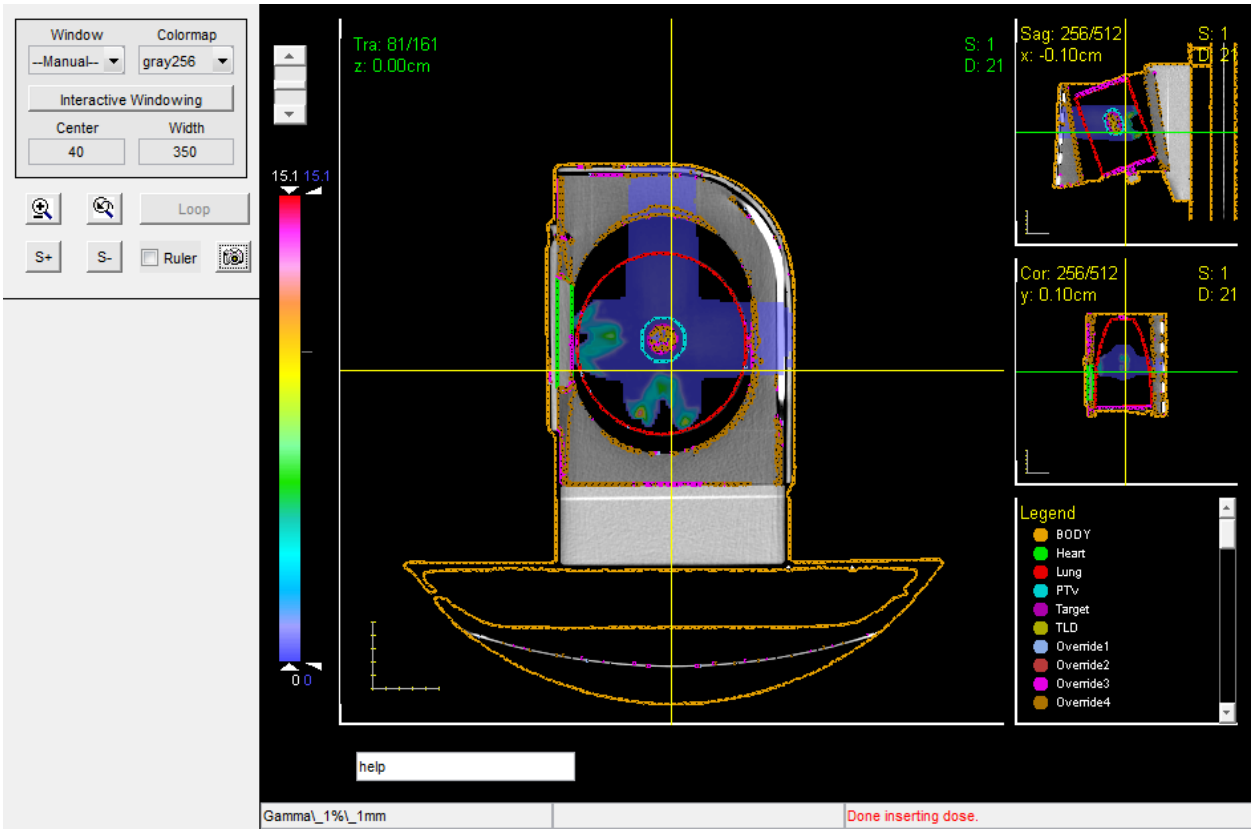

Figure 89. Gamma analysis at isocenter of plan corresponding to study reference curve compared with plan corresponding to 80 kV and 250 MeV with gamma criteria 1%/1mm

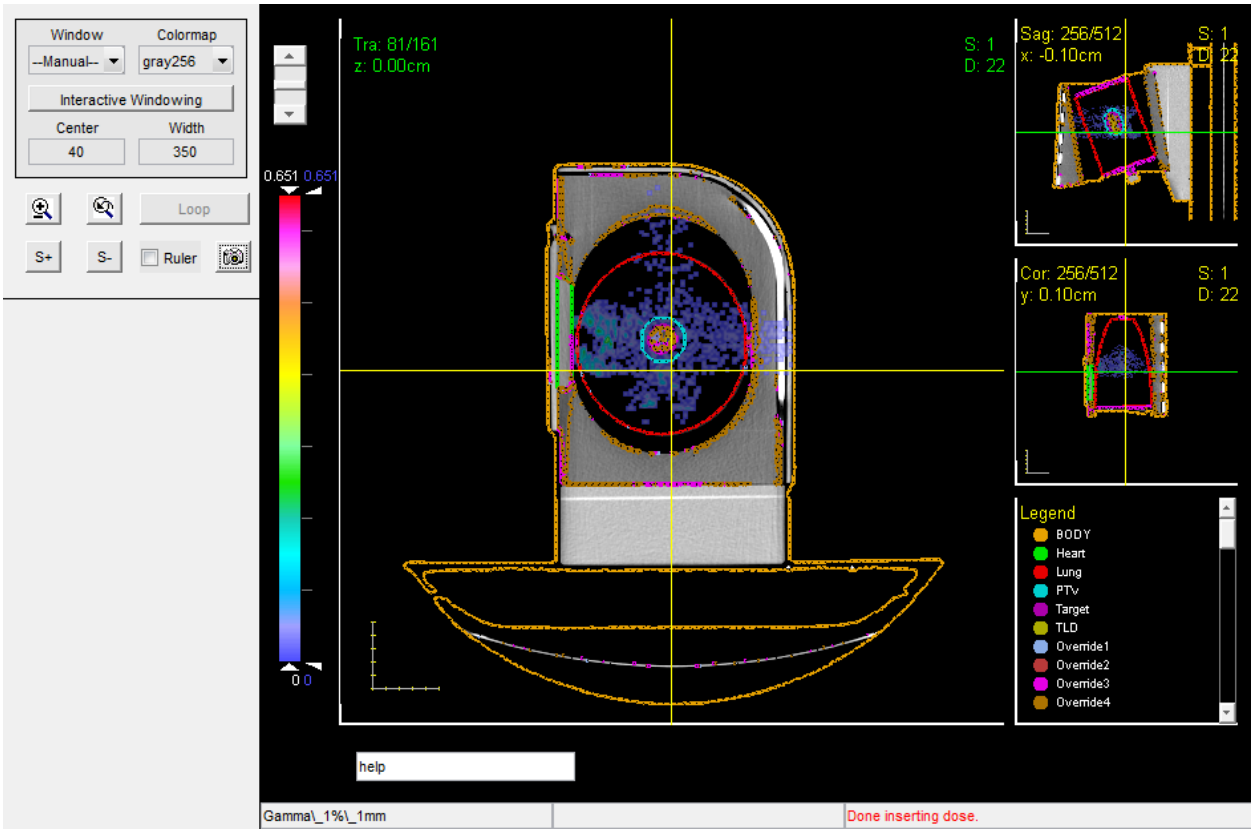

Figure 90. Gamma analysis at isocenter of plan corresponding to study reference curve compared with plan corresponding to 120 kV and 200 MeV with gamma criteria 1%/1mm

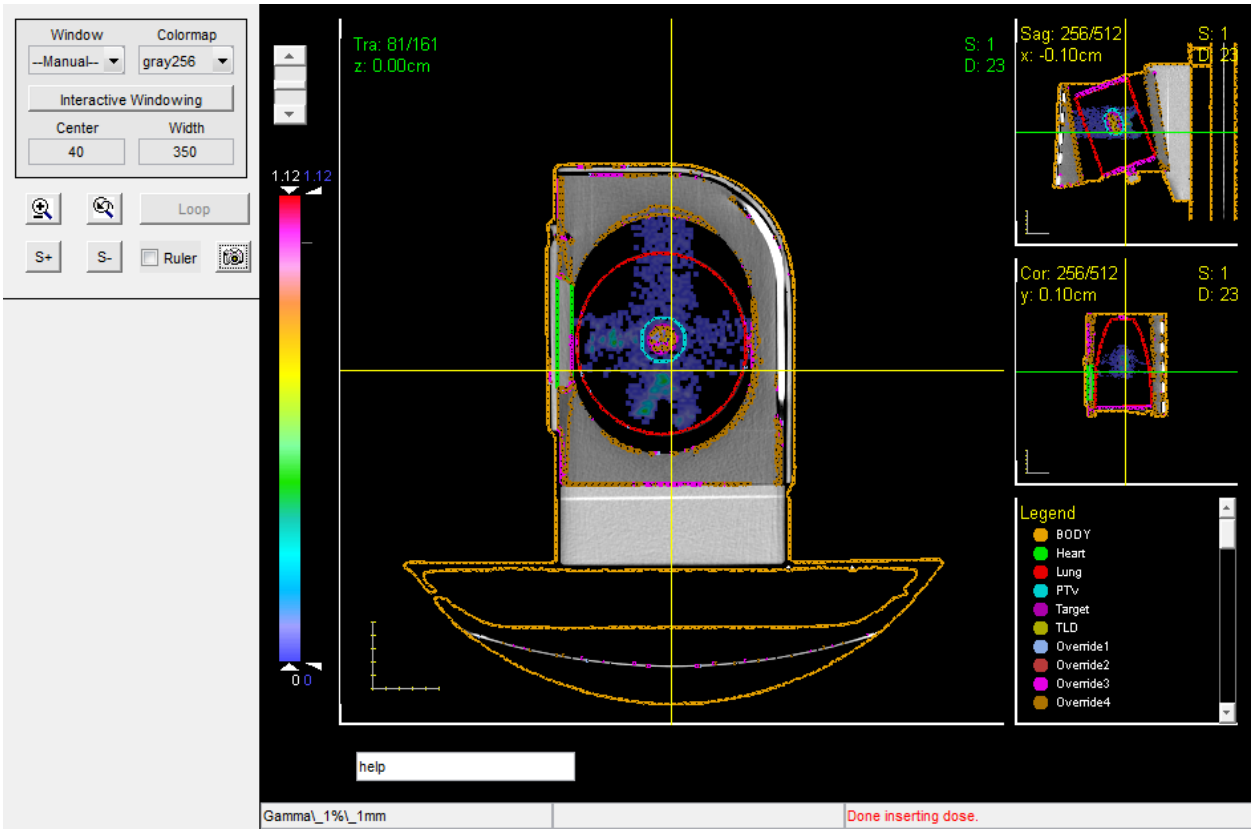

Figure 91. Gamma analysis at isocenter of plan corresponding to study reference curve compared with plan corresponding to 120 kV and 250 MeV with gamma criteria 1%/1mm

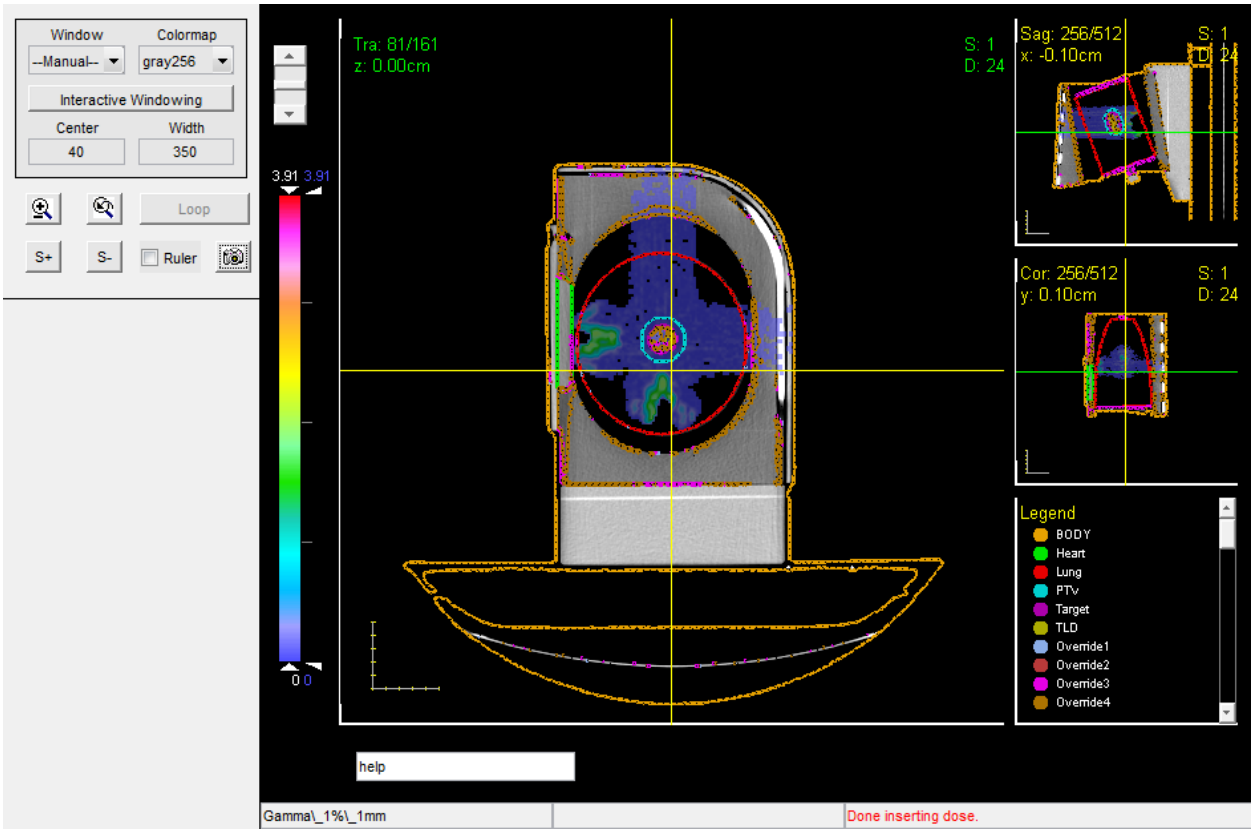

Figure 92. Gamma analysis at isocenter of plan corresponding to study reference curve compared with plan corresponding to 140 kV and 140 MeV with gamma criteria 1%/1mm

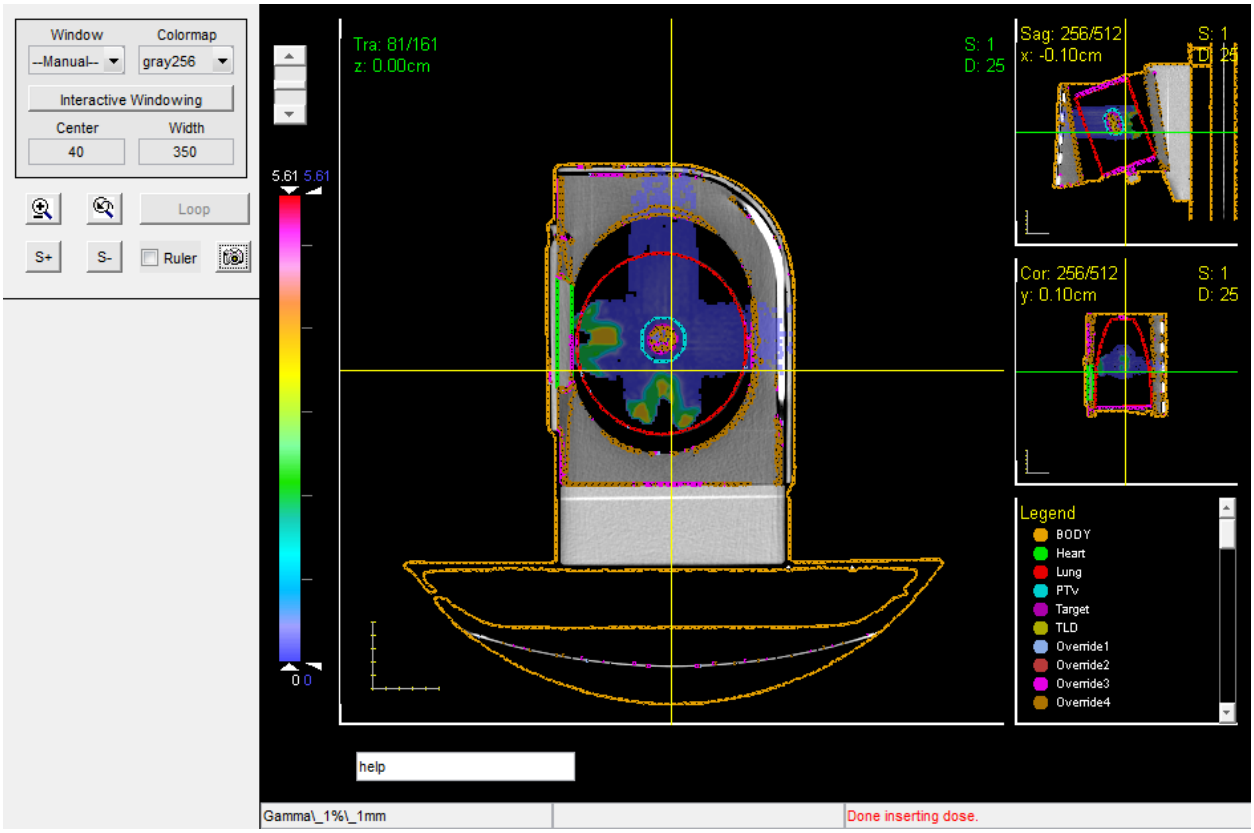

Figure 93. Gamma analysis at isocenter of plan corresponding to study reference curve compared with plan corresponding to 140 kV and 200 MeV with gamma criteria 1%/1mm

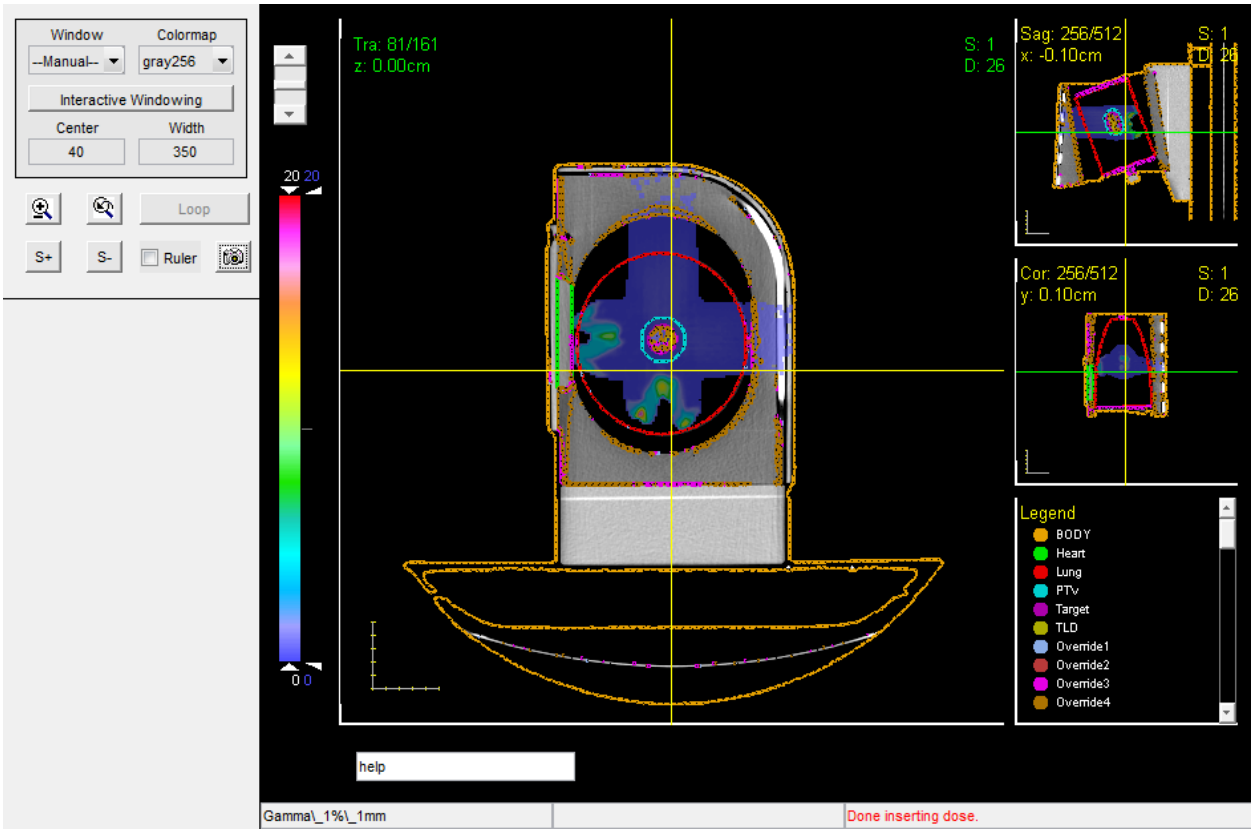

Figure 94. Gamma analysis at isocenter of plan corresponding to study reference curve compared with plan corresponding to 140 kV and 250 MeV with gamma criteria 1%/1mm

5.6 2D Gamma Analysis

5.6.1 Axial planes

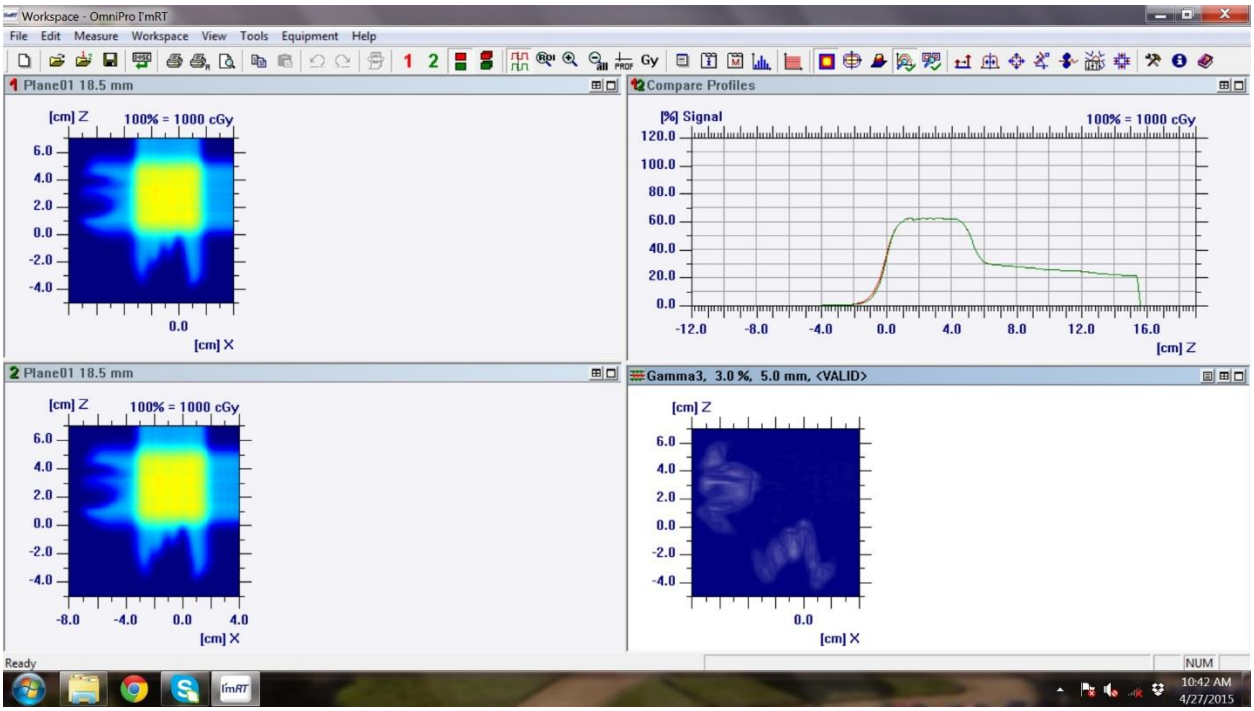

Figure 95. 2D gamma analysis of axial slice at isocenter comparing the study reference plan to the plan corresponding to 80 kV and 140 MeV with gamma criteria of 3%/5mm

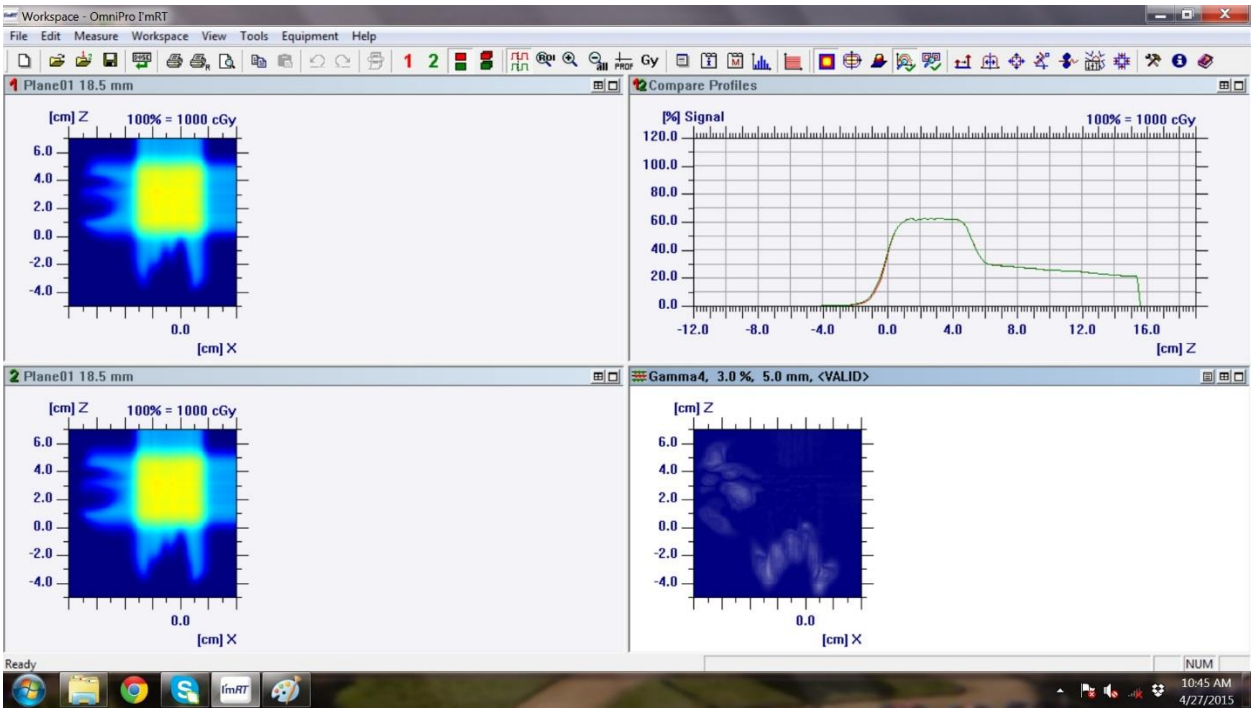

Figure 96. 2D gamma analysis of axial slice at isocenter comparing the study reference plan to the plan corresponding to 80 kV and 200 MeV with gamma criteria of 3%/5mm

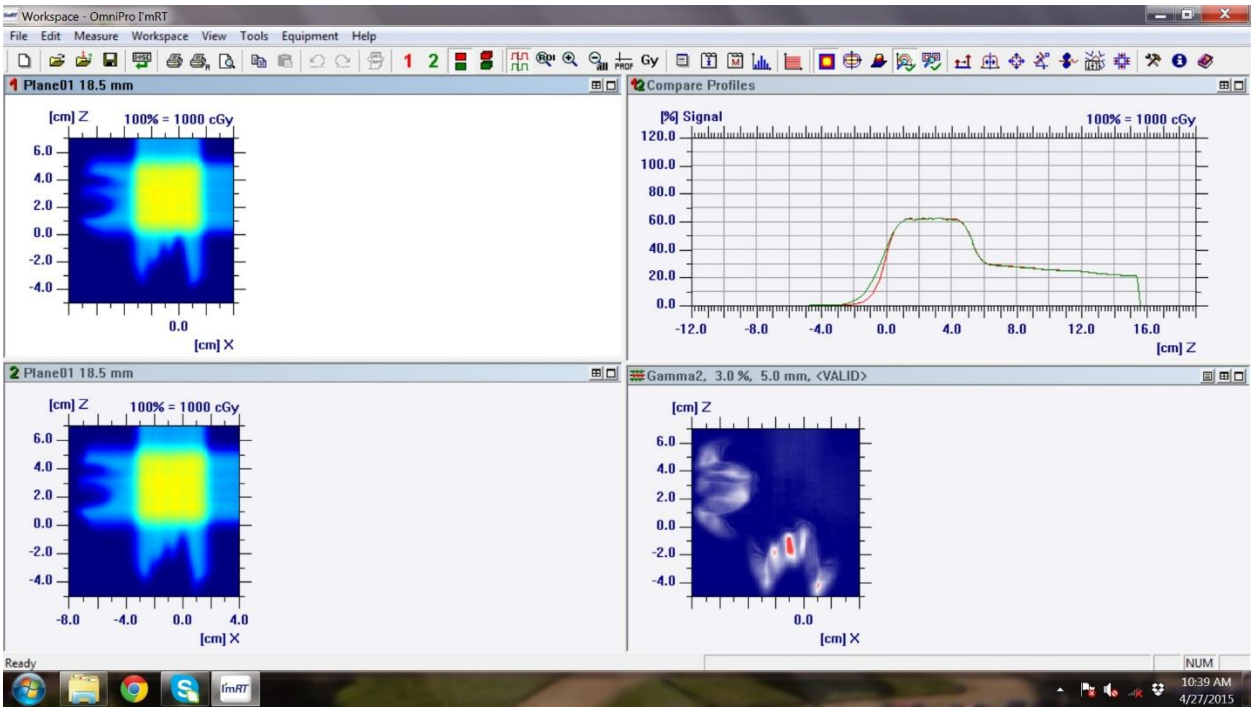

Figure 97. 2D gamma analysis of axial slice at isocenter comparing the study reference plan to the plan corresponding to 80 kV and 250 MeV with gamma criteria of 3%/5mm

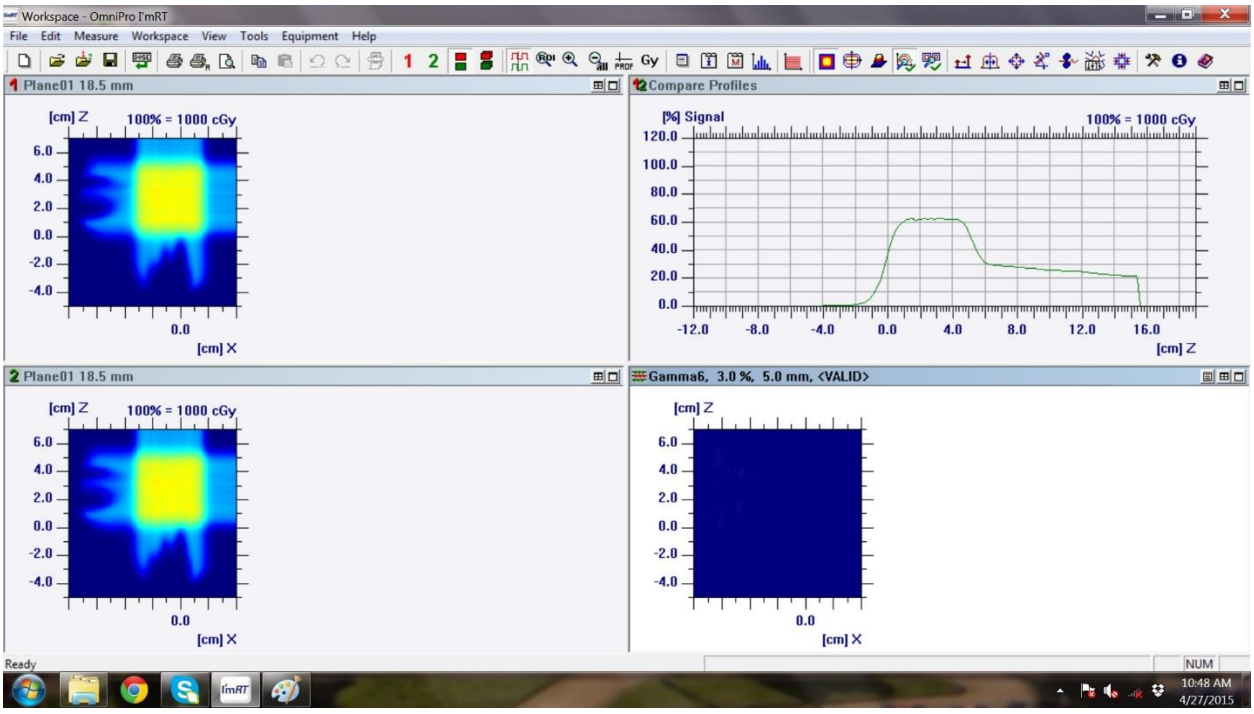

Figure 98. 2D gamma analysis of axial slice at isocenter comparing the study reference plan to the plan corresponding to 120 kV and 200 MeV with gamma criteria of 3%/5mm

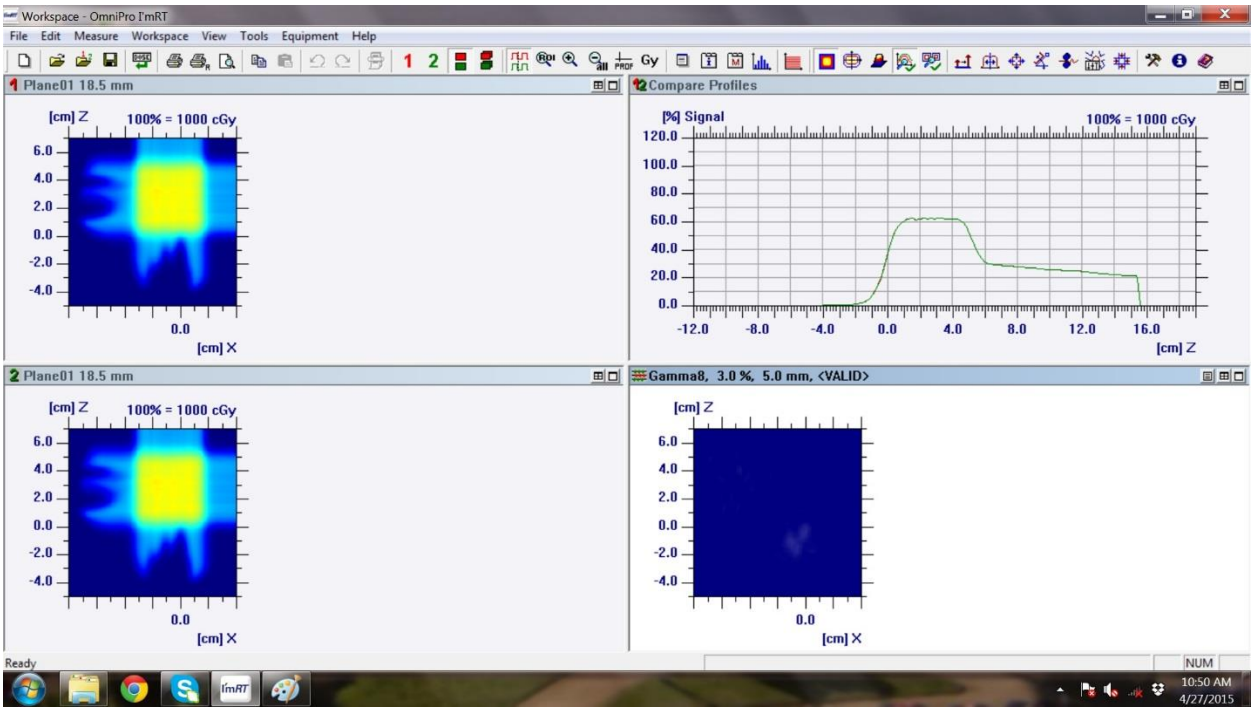

Figure 99. 2D gamma analysis of axial slice at isocenter comparing the study reference plan to the plan corresponding to 120 kV and 250 MeV with gamma criteria of 3%/5mm

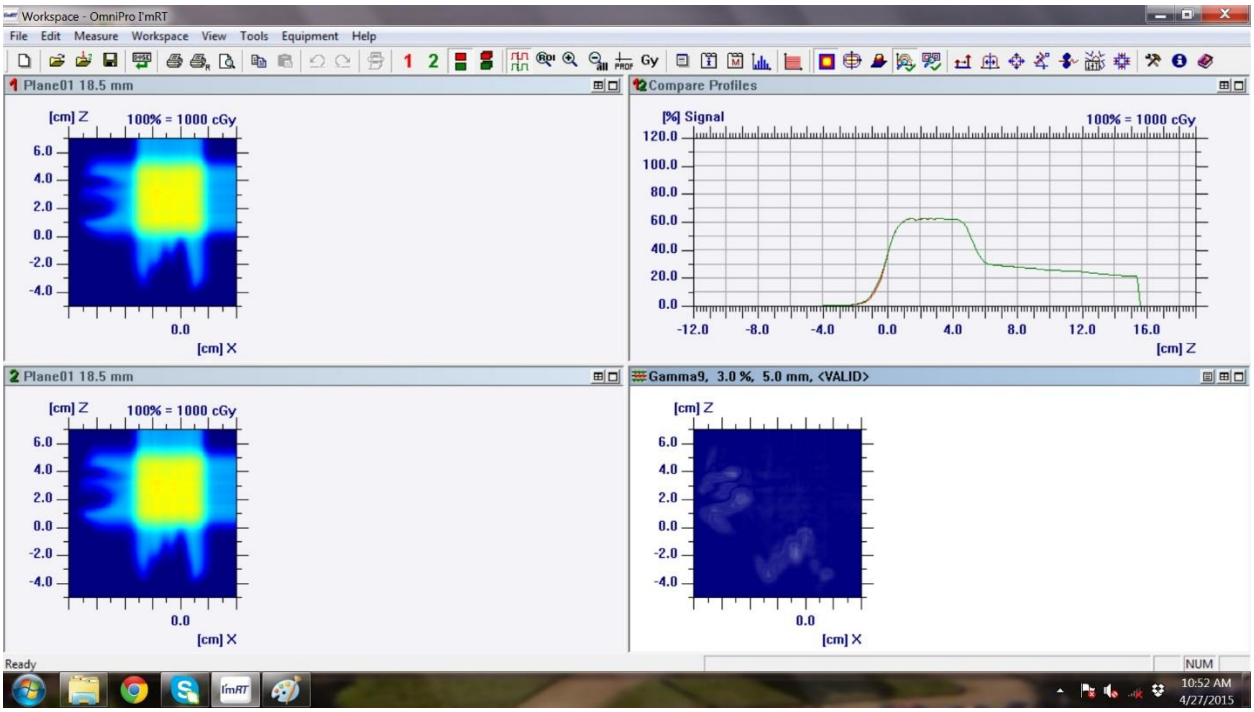

Figure 100. 2D gamma analysis of axial slice at isocenter comparing the study reference plan to the plan corresponding to 140 kV and 140 MeV with gamma criteria of 3%/5mm

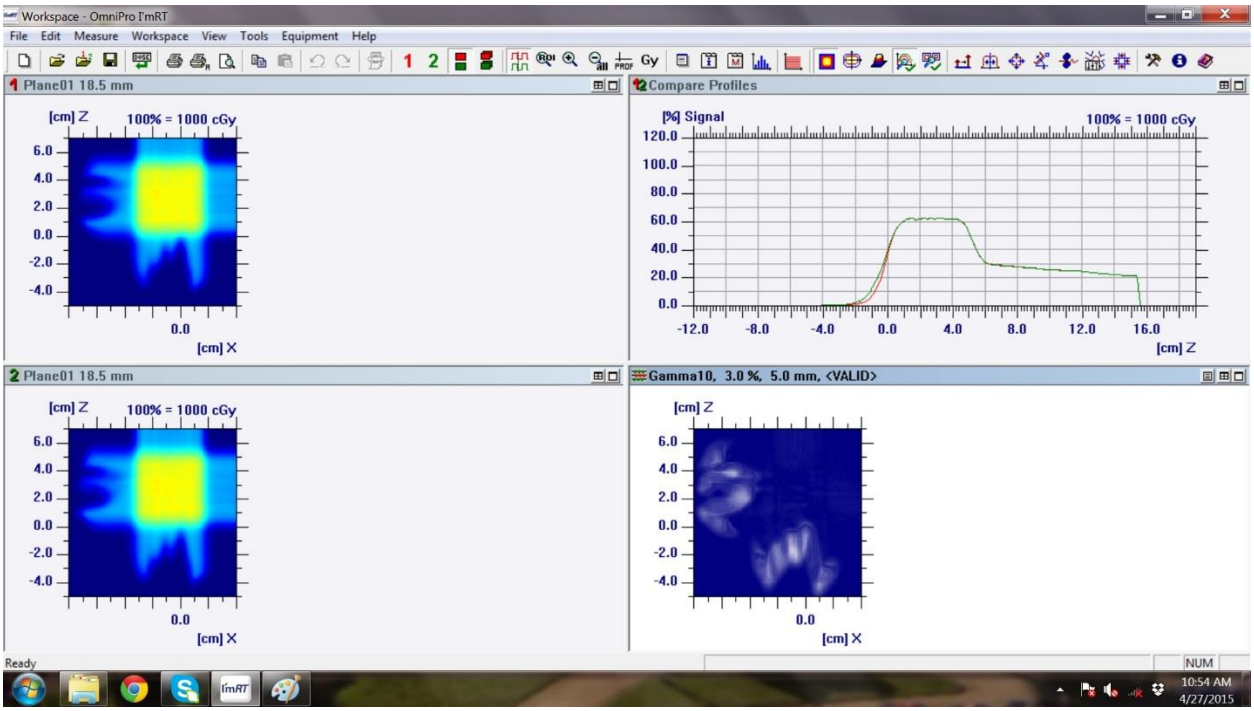

Figure 101. 2D gamma analysis of axial slice at isocenter comparing the study reference plan to the plan corresponding to 140 kV and 200 MeV with gamma criteria of 3%/5mm

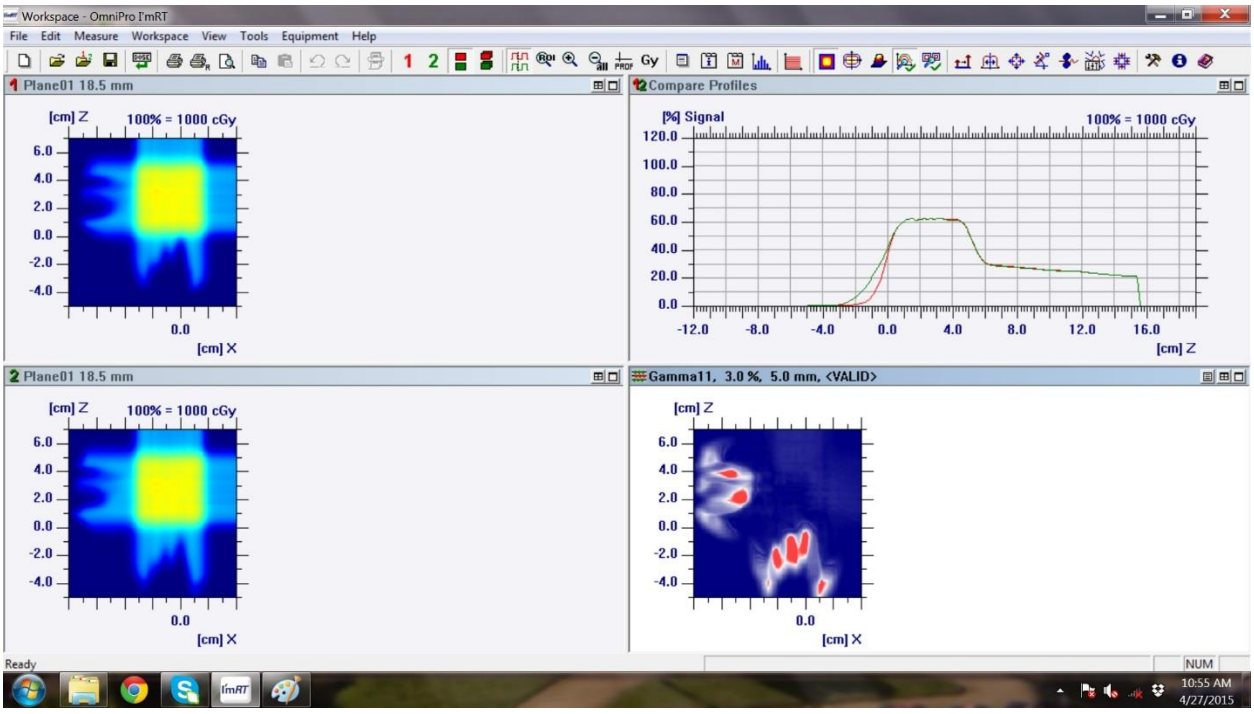

Figure 102. 2D gamma analysis of axial slice at isocenter comparing the study reference plan to the plan corresponding to 140 kV and 250 MeV with gamma criteria of 3%/5mm

5.6.2 Coronal planes

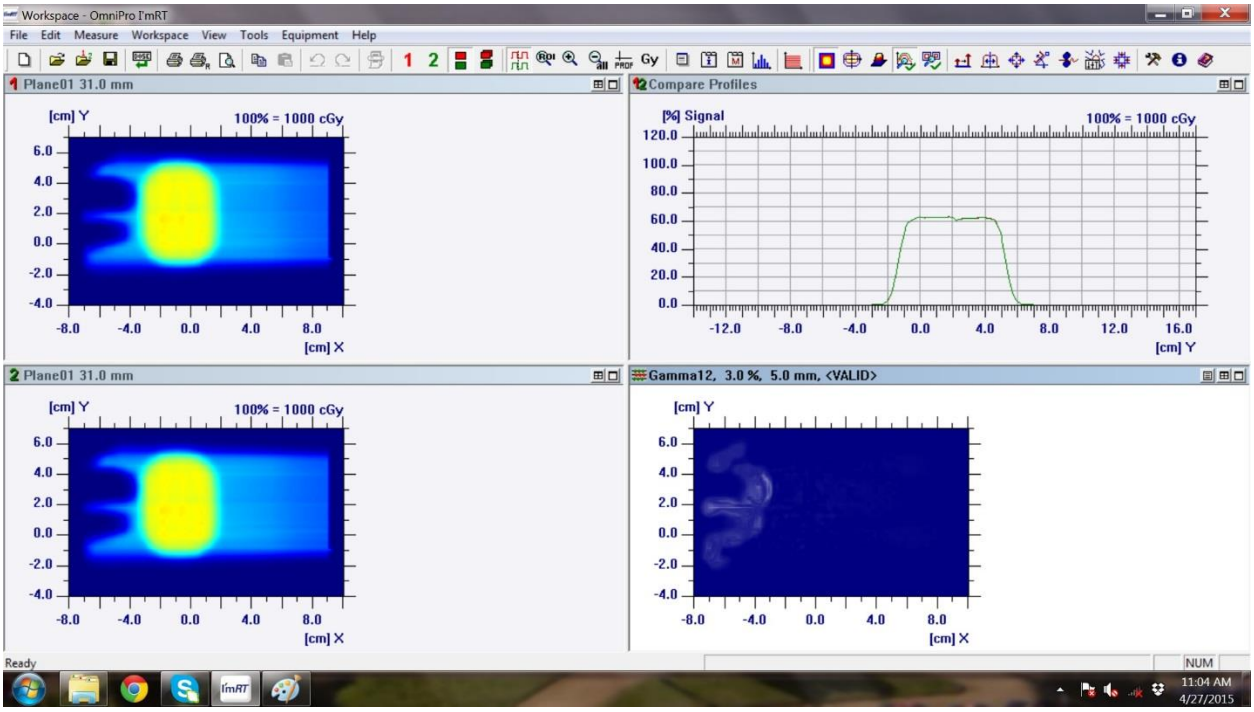

Figure 103. 2D gamma analysis of coronal slice at isocenter comparing the study reference plan to the plan corresponding to 80 kV and 140 MeV with gamma criteria of 3%/5mm

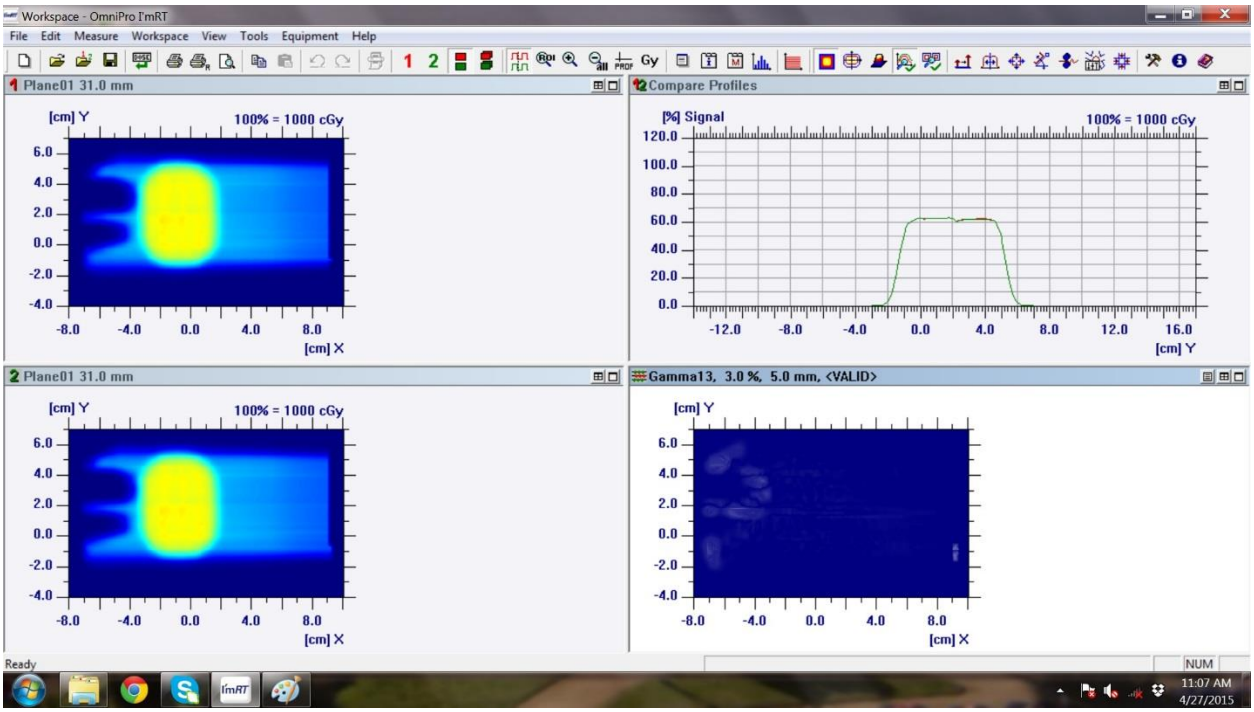

Figure 104. 2D gamma analysis of coronal slice at isocenter comparing the study reference plan to the plan corresponding to 80 kV and 200 MeV with gamma criteria of 3%/5mm

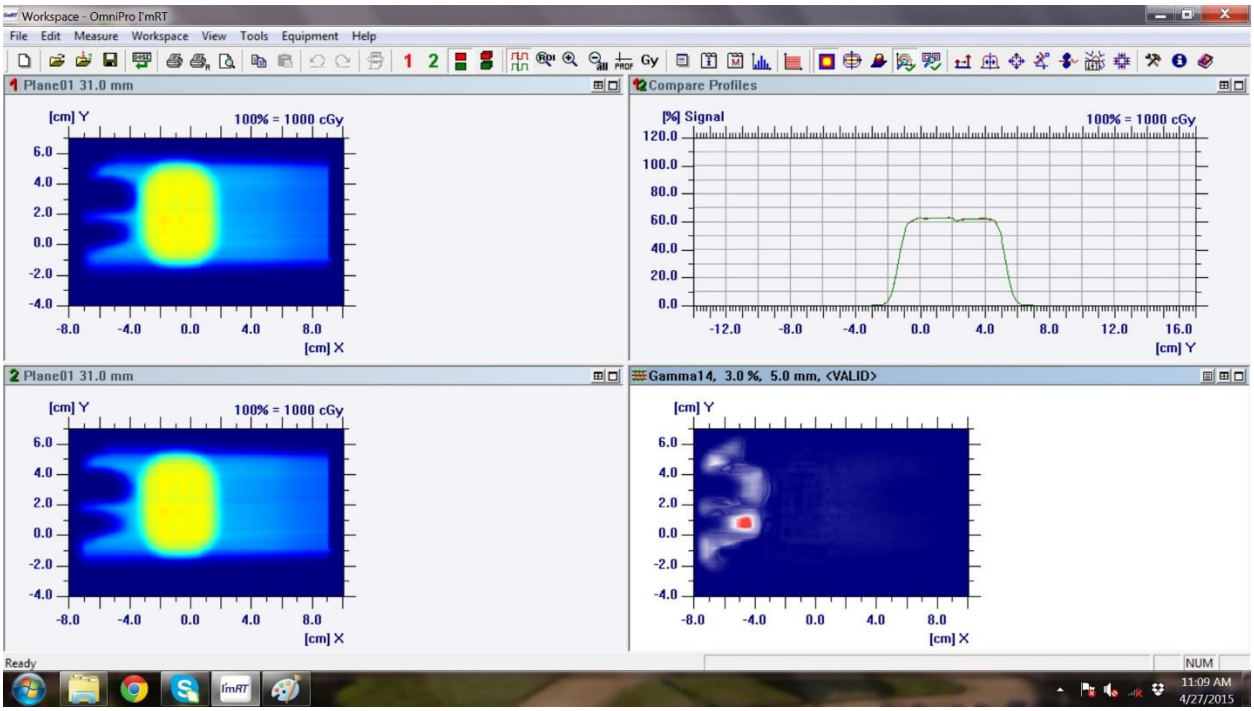

Figure 105. 2D gamma analysis of coronal slice at isocenter comparing the study reference plan to the plan corresponding to 80 kV and 250 MeV with gamma criteria of 3%/5mm

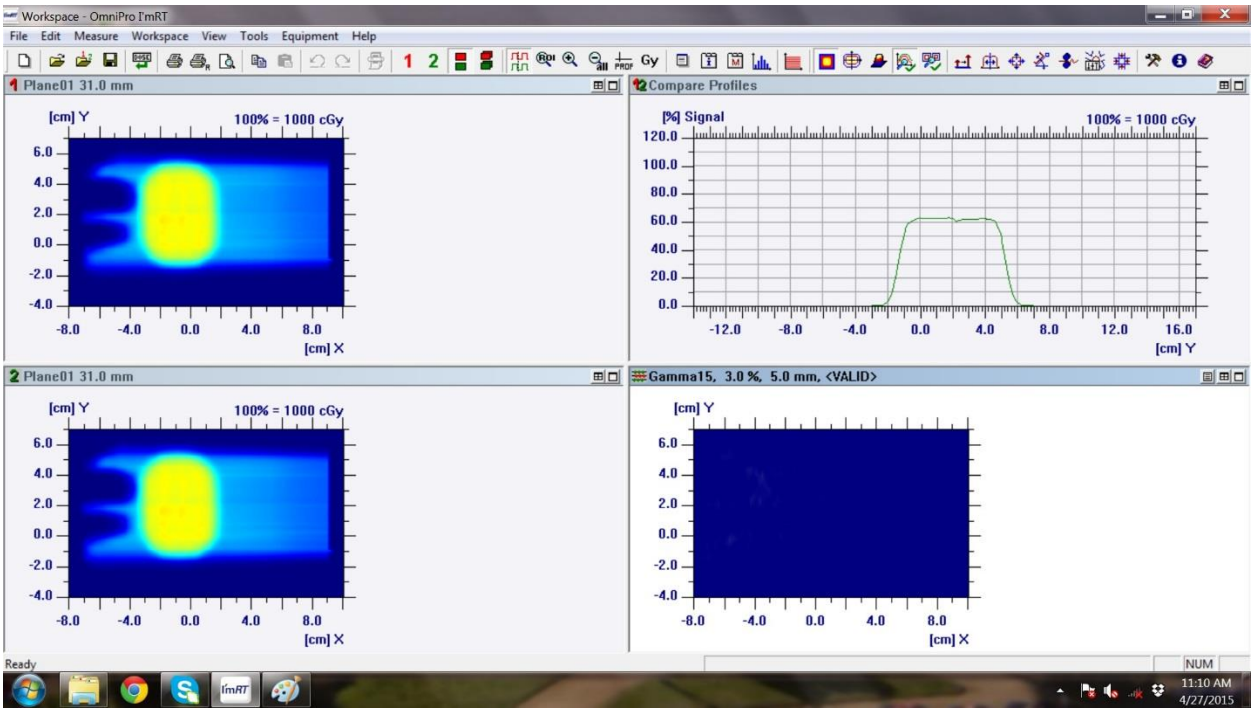

Figure 106. 2D gamma analysis of coronal slice at isocenter comparing the study reference plan to the plan corresponding to 120 kV and 200 MeV with gamma criteria of 3%/5mm

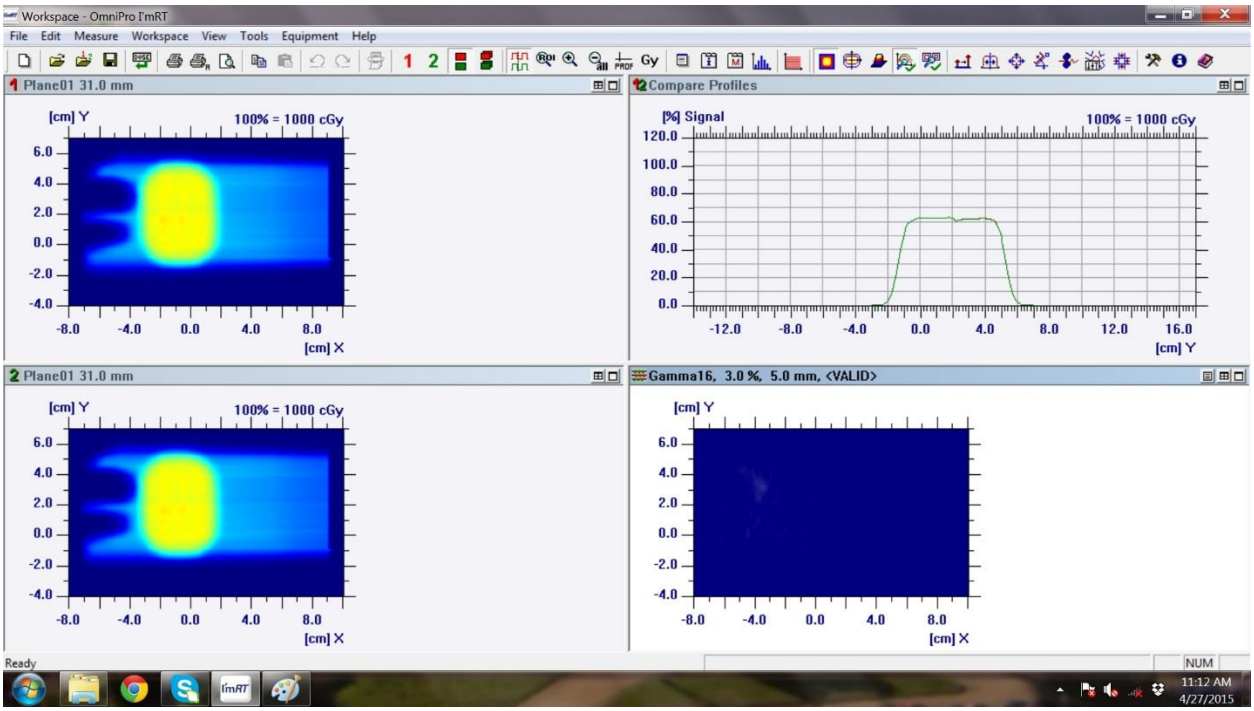

Figure 107. 2D gamma analysis of coronal slice at isocenter comparing the study reference plan to the plan corresponding to 120 kV and 250 MeV with gamma criteria of 3%/5mm

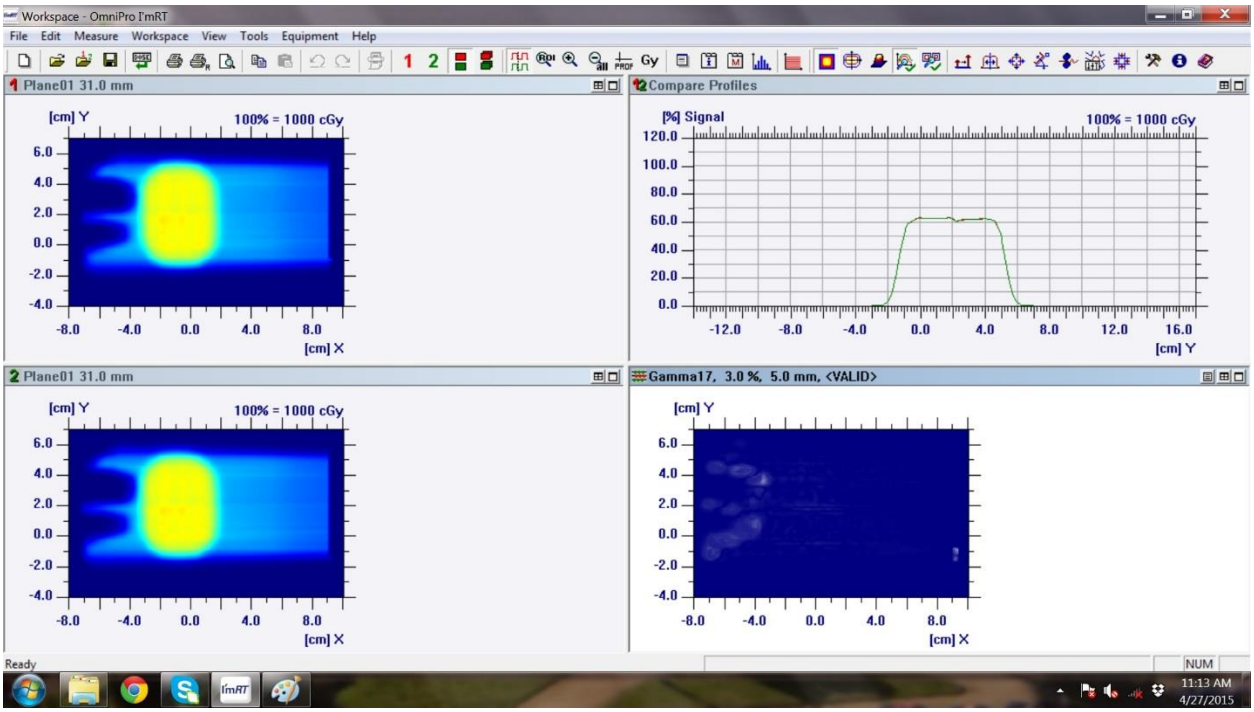

Figure 108. 2D gamma analysis of coronal slice at isocenter comparing the study reference plan to the plan corresponding to 140 kV and 140 MeV with gamma criteria of 3%/5mm

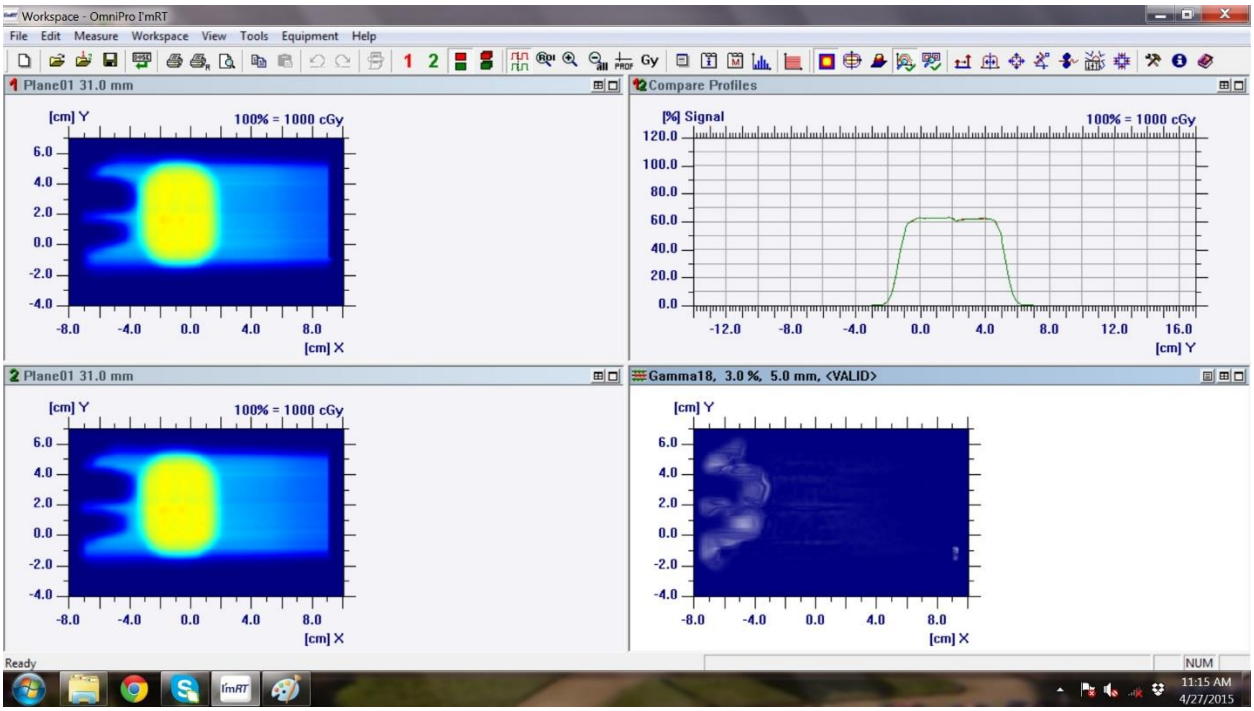

Figure 109. 2D gamma analysis of coronal slice at isocenter comparing the study reference plan to the plan corresponding to 140 kV and 200 MeV with gamma criteria of 3%/5mm

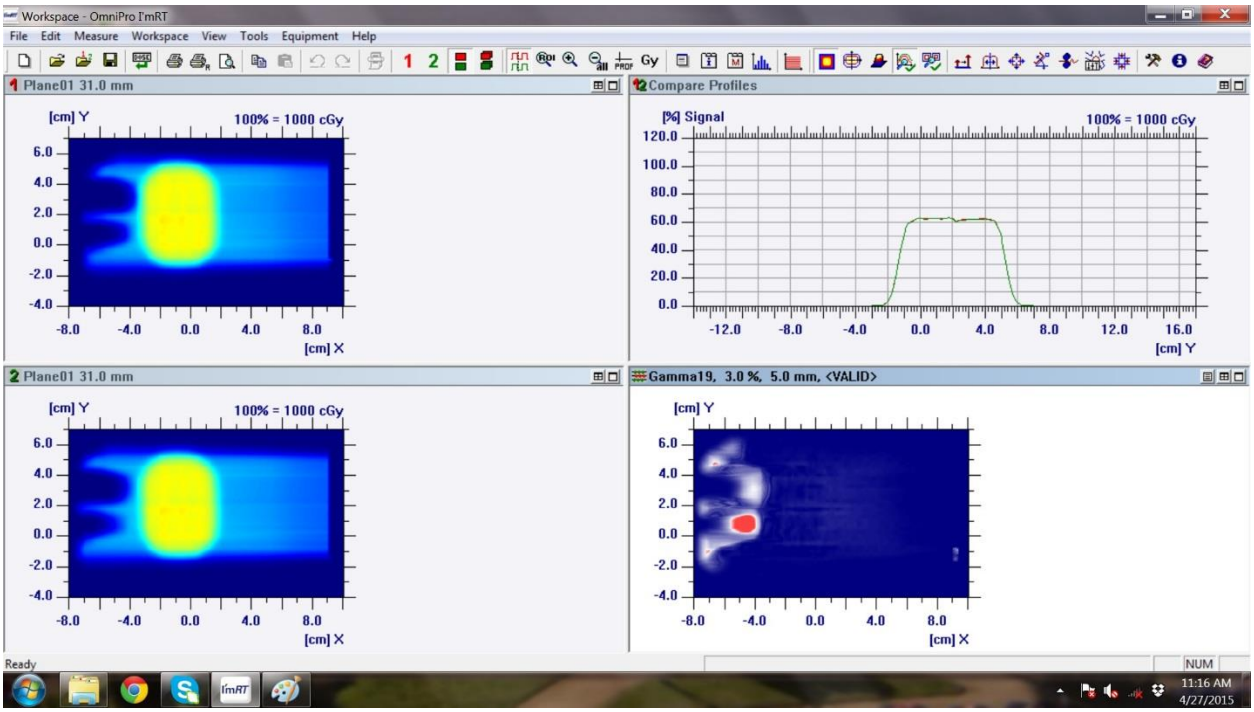

Figure 110. 2D gamma analysis of coronal slice at isocenter comparing the study reference plan to the plan corresponding to 140 kV and 250 MeV with gamma criteria of 3%/5mm

5.6.3 Sagittal planes

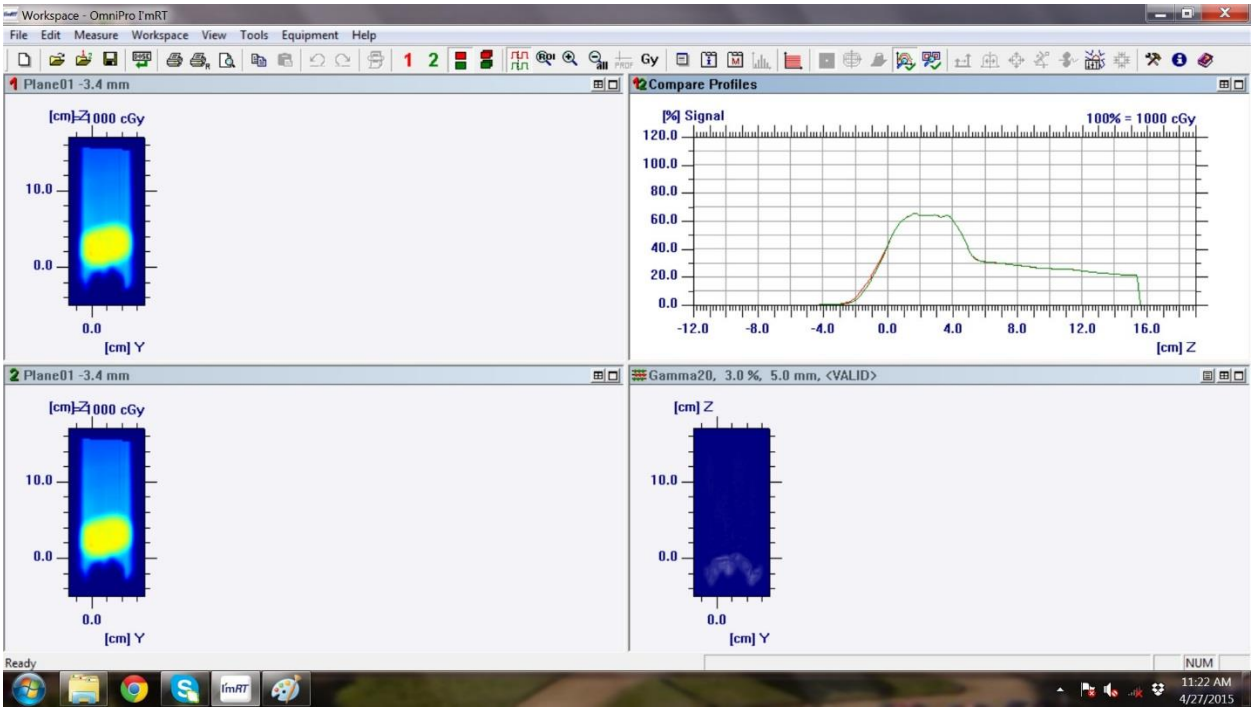

Figure 111. 2D gamma analysis of sagittal slice at isocenter comparing the study reference plan to the plan corresponding to 80 kV and 140 MeV with gamma criteria of 3%/5mm

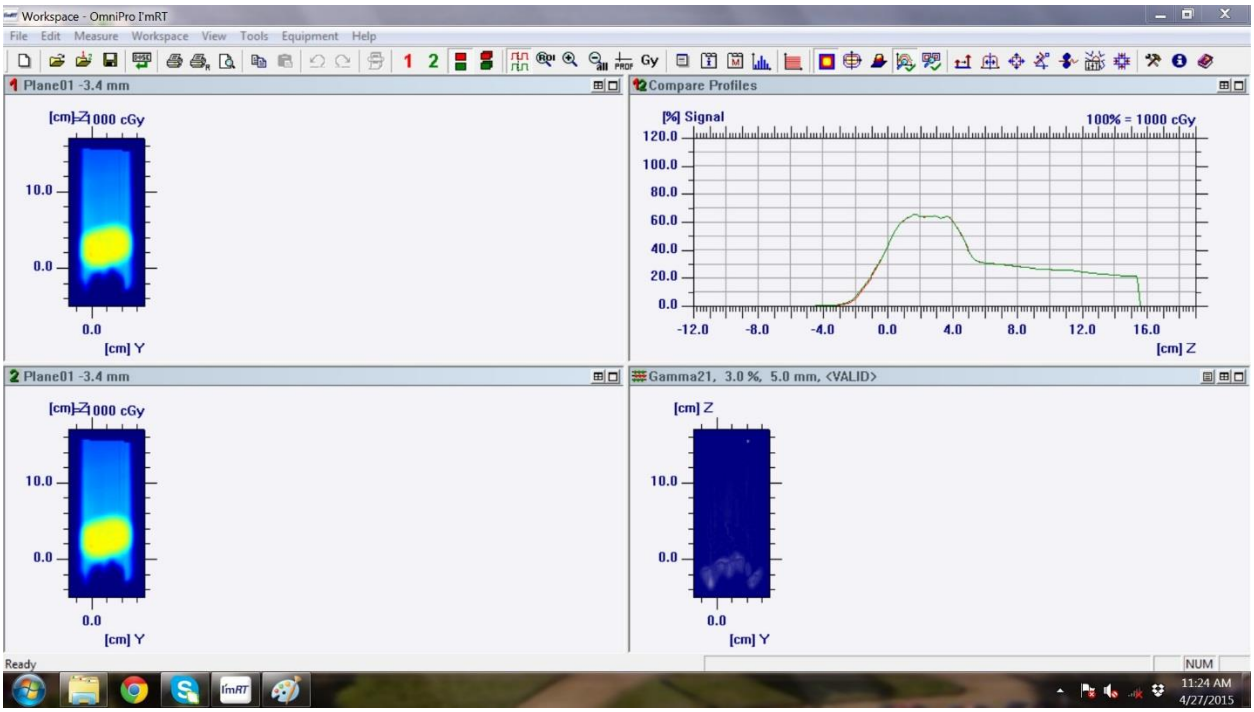

Figure 112. 2D gamma analysis of sagittal slice at isocenter comparing the study reference plan to the plan corresponding to 80 kV and 200 MeV with gamma criteria of 3%/5mm

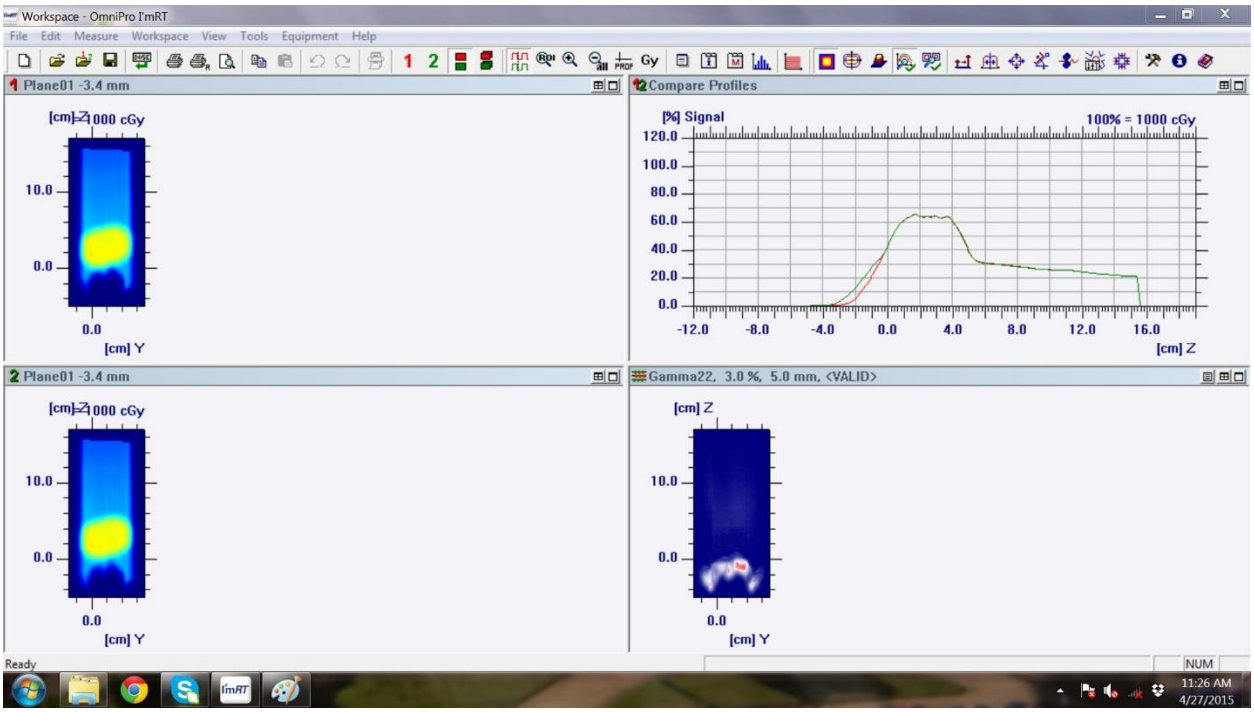

Figure 113. 2D gamma analysis of sagittal slice at isocenter comparing the study reference plan to the plan corresponding to 80 kV and 250 MeV with gamma criteria of 3%/5mm

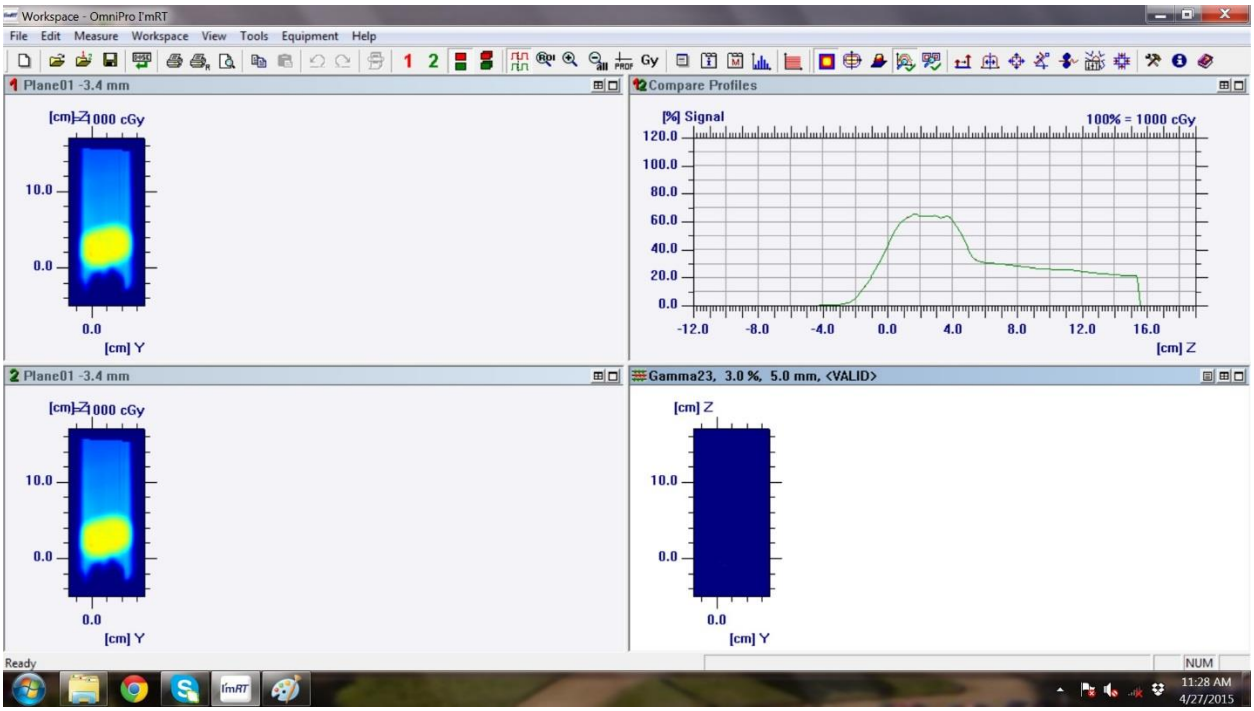

Figure 114. 2D gamma analysis of sagittal slice at isocenter comparing the study reference plan to the plan corresponding to 120 kV and 200 MeV with gamma criteria of 3%/5mm

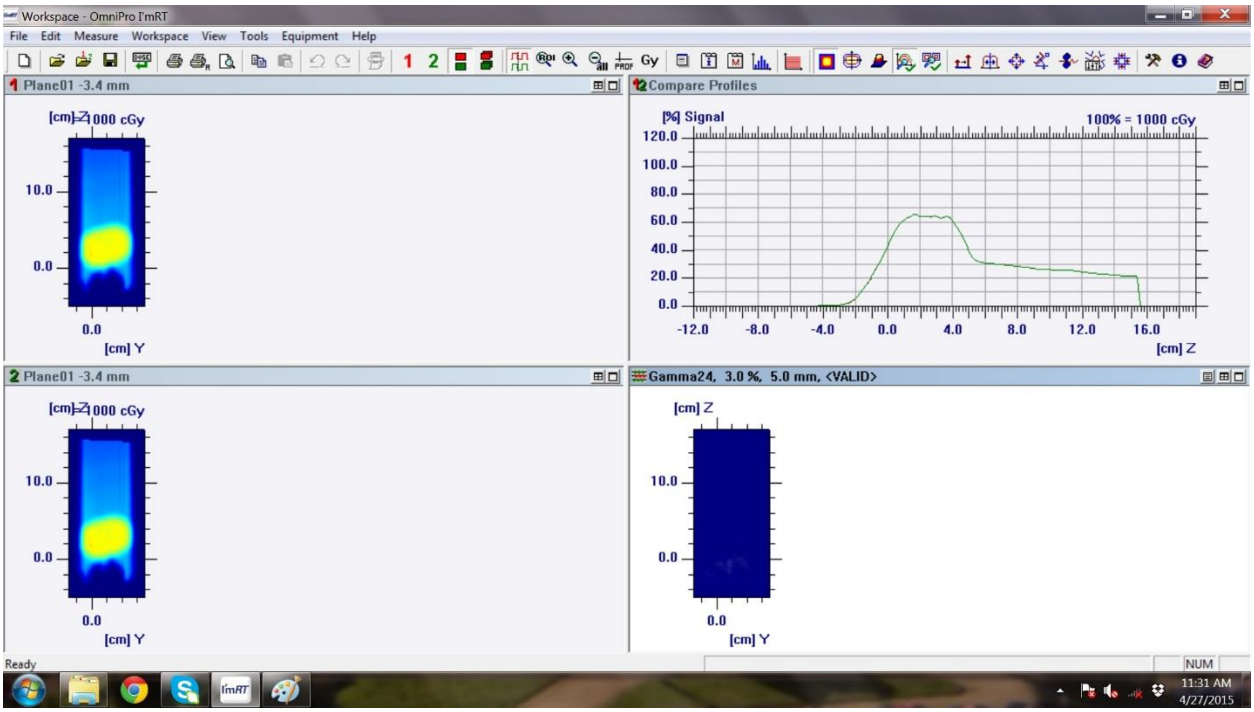

Figure 115. 2D gamma analysis of sagittal slice at isocenter comparing the study reference plan to the plan corresponding to 120 kV and 250 MeV with gamma criteria of 3%/5mm

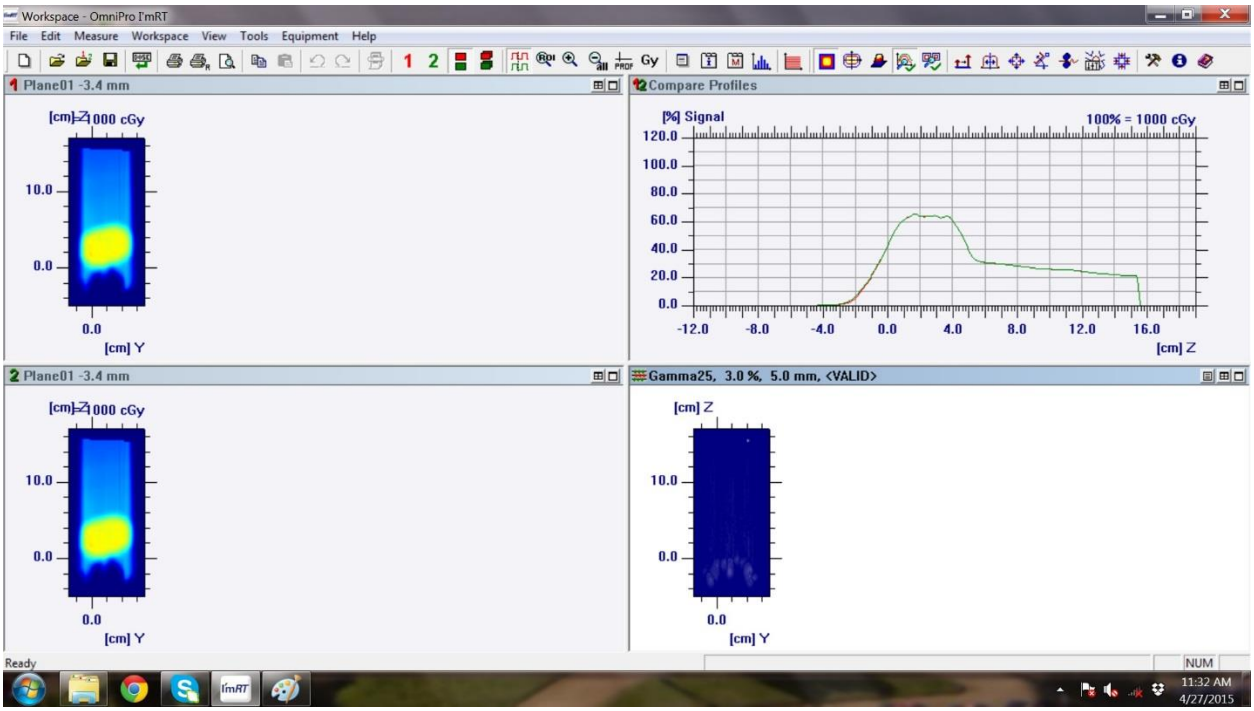

Figure 116. 2D gamma analysis of sagittal slice at isocenter comparing the study reference plan to the plan corresponding to 140 kV and 140 MeV with gamma criteria of 3%/5mm

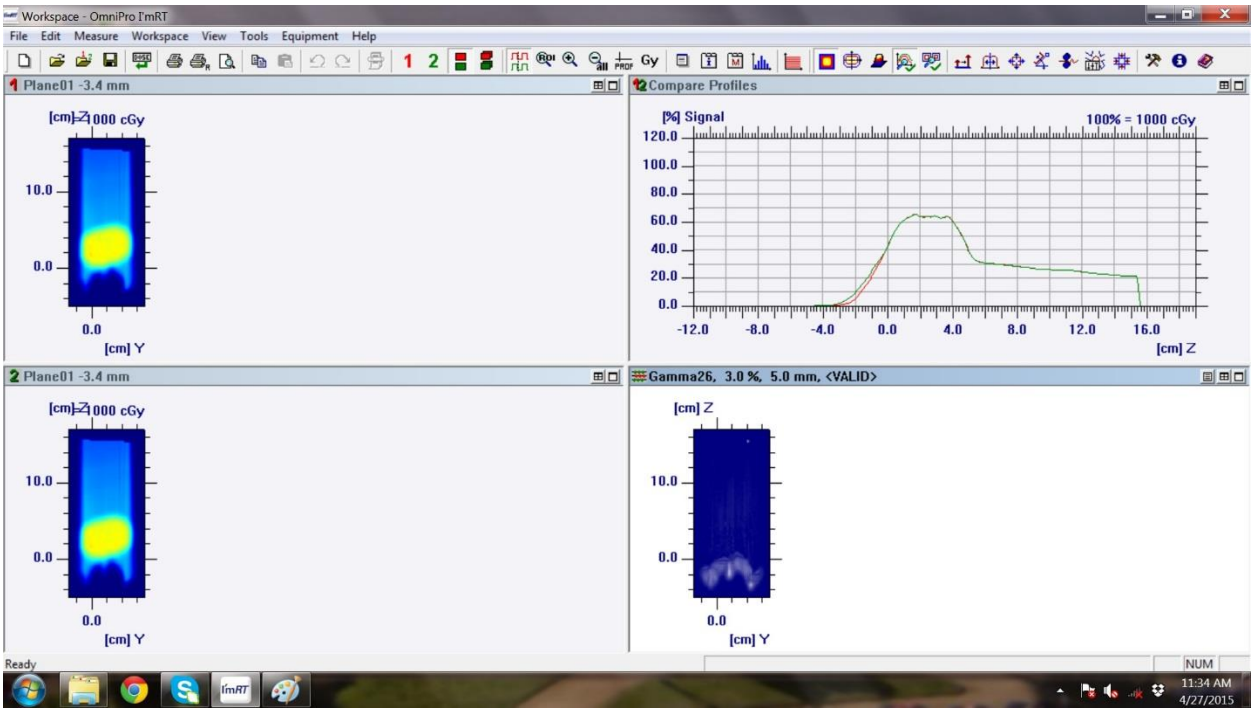

Figure 117. 2D gamma analysis of sagittal slice at isocenter comparing the study reference plan to the plan corresponding to 140 kV and 200 MeV with gamma criteria of 3%/5mm

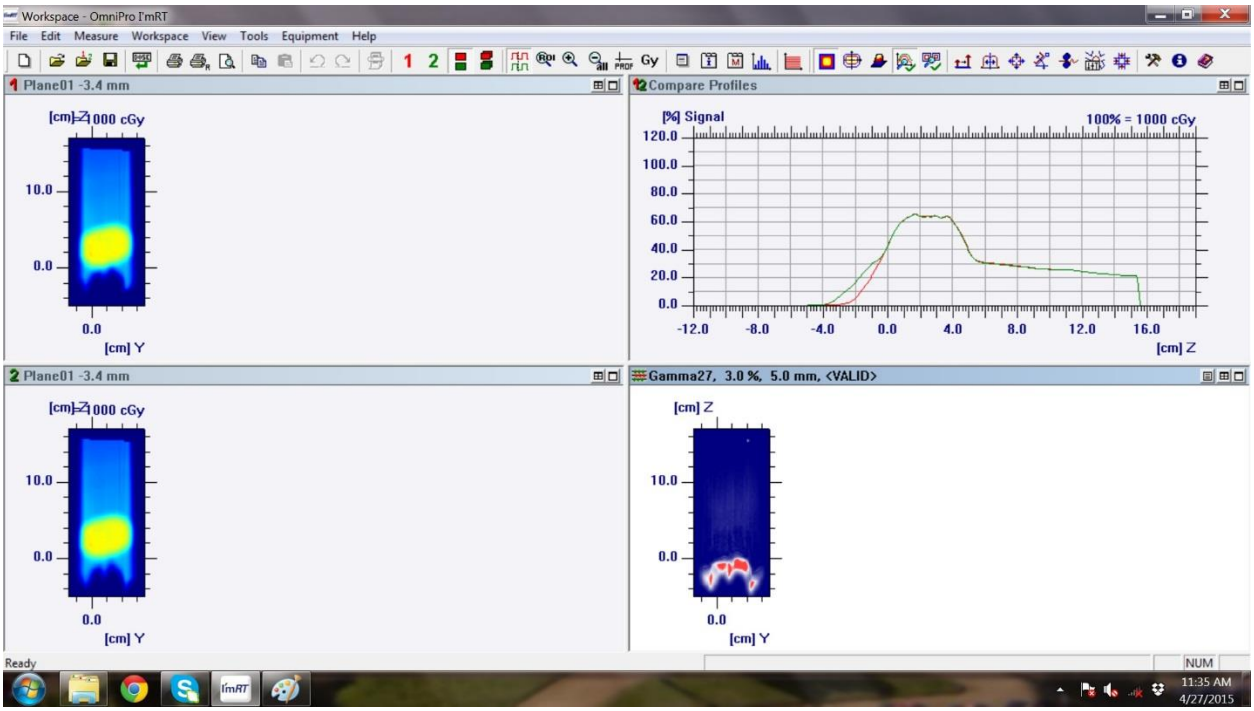

Figure 118. 2D gamma analysis of sagittal slice at isocenter comparing the study reference plan to the plan corresponding to 140 kV and 250 MeV with gamma criteria of 3%/5mm

Chapter 6

References

[1] "Particle Therapy Co-Operative Group," *Particle therapy facilities in operation*. [Online]. Available: http://www.ptcog.ch/index.php/facilities-in-operation.

[2] "Particle Therapy Co-Operative Group," *Particle therapy facilities under construction*. [Online]. Available: http://www.ptcog.ch/index.php/facilities-under-construction.

[3] "Particle Therapy Co-Operative Group," *Particle therapy facilities in a planning stage*. [Online]. Available: http://www.ptcog.ch/index.php/facilities-in-planning-stage.

[4] "Cancer Therapy Evaluation Program," *An Overview of NCI's National Clinical Trials Network*. [Online]. Available: http://ctep.cancer.gov/initiativesPrograms/nctn.htm.

[5] "IROC Houston Quality Assurance Center," *Phantom Services Group*. [Online]. Available: http://rpc.mdanderson.org/RPC/home.htm.

[6] R. L. Grant, P. A. Summers, J. L. Neihart, A. P. Blatnica, N. Sahoo, M. T. Gillin, D. S. Followill, and G. S. Ibbott, "Relative stopping power measurements to aid in the design of anthropomorphic phantoms for proton radiotherapy," *J Appl Clin Med Phys*, vol. 15, no. 2, p. 4523, 2014.

[7] M. F. Moyers, M. Sardesai, S. Sun, and D. W. Miller, "Ion stopping powers and CT numbers," *Med Dosim*, vol. 35, no. 3, pp. 179–194, 2010.

[8] "NCI's Clinical Trials Programs and Initiatives." [Online]. Available: www.cancer.gov.

[9] W. Bogdanich, "As Technology Surges, Radiation Safeguards Lag," *The New York Times*, 2010.

[10] W. B. and K. Rebelo, "The Check the Medical Equipment, but Who is Checking Up on Them?," *The New York Times*, 2010.

[11] E. Rutherford, "Atomic Projectiles and Their Collisions with Light Atoms," *Science (80-.).*, vol. 50, no. 1299, pp. 467–473, 1919.

[12] R. R. Wilson, "Radiological use of fast protons," *Radiology*, vol. 47, no. 5, pp. 487–491, 1946.

[13] "History of Proton Beam Therapy," *Synthesis*, vol. 9. UC Davis Cancer Center, UC Davis Cancer Center, 2006.

[14] “About the James M. Slater, MD Proton Treatment and Research Center.” [Online]. Available: www.protons.com.

[15] G. Coutrakon, J. Hubbard, J. Johanning, G. Maudsley, T. Slaton, and P. Morton, “A performance study of the Loma Linda proton medical accelerator.,” *Med. Phys.*, vol. 21, no. 11, pp. 1691–1701, 1994.

[16] A. Smith, M. Gillin, M. Bues, X. R. Zhu, K. Suzuki, R. Mohan, S. Woo, A. Lee, R. Komaki, J. Cox, K. Hiramoto, H. Akiyama, T. Ishida, T. Sasaki, and K. Matsuda, “The M. D. Anderson proton therapy system,” *Med Phys*, vol. 36, no. 9, pp. 4068–4083, 2009.

[17] H. Paganetti, *Proton Therapy Physics*. CRC Press, 2011.

[18] C. M. C. Ma and T. Lomax, *Proton and Carbon Ion Therapy*. Taylor & Francis, 2012.

[19] W. P. Levin, H. Kooy, J. S. Loeffler, and T. F. DeLaney, “Proton beam therapy.,” *Br. J. Cancer*, vol. 93, no. 8, pp. 849–854, 2005.

[20] N. Sahoo, X. R. Zhu, B. Arjomandy, G. Ciangaru, M. Lii, R. Amos, R. Wu, and M. T. Gillin, “A procedure for calculation of monitor units for passively scattered proton radiotherapy beams,” *Med Phys*, vol. 35, no. 11, pp. 5088–5097, 2008.

[21] U. Schneider, E. Pedroni, and A. Lomax, “The calibration of CT Hounsfield units for radiotherapy treatment planning,” *Phys Med Biol*, vol. 41, no. 1, pp. 111–124, 1996.

[22] X. R. Zhu, “CT Number Calibration for Proton Therapy.” 2006.

[23] B. Schaffner and E. Pedroni, “The precision of proton range calculations in proton radiotherapy treatment planning: experimental verification of the relation between CT-HU and proton stopping power,” *Phys Med Biol*, vol. 43, no. 6, pp. 1579–1592, 1998.

[24] X. Ding, “Commissioning of Treatment Beam.”

[25] D. A. Low, W. B. Harms, S. Mutic, and J. A. Purdy, “A technique for the quantitative evaluation of dose distributions,” *Med Phys*, vol. 25, no. 5, pp. 656–661, 1998.

[26] D. A. Low and J. F. Dempsey, “Evaluation of the gamma dose distribution comparison method,” *Med Phys*, vol. 30, no. 9, pp. 2455–2464, 2003.

[27] A. Blatnica and P. D. Geoffrey Ibbott, “Modification and Implementation of the RPC Heterogeneous Thorax Phantom for Verification of Proton Therapy Treatment Procedures,” University of Texas Graduate School of Biomedical Sciences at Houston, 2011.

[28] J. Neihart, “Development and implementation of a dynamic heterogeneous proton equivalent anthropomorphic thorax phantom for the assessment of scanned proton beam therapy,” University of Texas Graduation School of Biomedical Sciences at Houston, University of Texas Graduation School of Biomedical Sciences at Houston, 2013.

[29] M. Yang, “Dual Energy Computed Tomography for Proton Therapy Treatment Planning,” The University of Texas Health Science Center at Houston Graduate School of Biomedical Sciences, The University of Texas Health Science Center at Houston Graduate School of Biomedical Sciences, 2011.

[30] R. Raupach and S. Healthcare, “Dual Energy Imaging with Dual Source CT Systems,” in *AAPM*.

[31] I. B. A. Dosimetry, Ed., “Zebra with OmniPro-Incline: High Precision Particle Therapy Dosimetry,” *www.iba-dosimetry.com*. .

[32] K. B. Pulliam, J. Y. Huang, R. M. Howell, D. Followill, R. Bosca, J. O’Daniel, and S. F. Kry, “Comparison of 2D and 3D gamma analyses,” *Med Phys*, vol. 41, no. 2, p. 21710, 2014.

[33] P. Sriram, “A Study on Evaluation of kV-CBCT-image-based Treatment Planning using Anthropomorphic Phantom,” *J. Med. Biol. Eng.*, 2010.

[34] M. F. Moyers, “Comparison of x ray computed tomography number to proton relative linear stopping power conversion functions using a standard phantoma),” *Med. Phys.*, vol. 41, no. 6, p. 061705, 2014.

[35] R. J. Cropp, P. Seslija, D. Tso, and Y. Thakur, “Scanner and kVp dependence of measured CT numbers in the ACR CT phantom.,” *J. Appl. Clin. Med. Phys.*, vol. 14, no. 6, p. 4417, 2013.

[36] R. Zhang, P. J. Taddei, M. M. Fitzek, and W. D. Newhauser, “Water equivalent thickness values of materials used in beams of protons, helium, carbon and iron ions,” *Phys Med Biol*, vol. 55, no. 9, pp. 2481–2493, 2010.

[37] P. Balter, “Recommended dose-volume constraints for normal tissues in standard fractionation.” 2010.

[38] L. B. Marks, “Radiation Dose-Volume Effects in the Lung,” *Int. J. Radiat. Oncol.*, vol. 76, no. 3, pp. S70–S76, 2010.

Vita

Mattie Margaret McInnis was born in Houston, TX on January 4, 1990 to Noel and Julie McInnis. After graduating from James E. Taylor High School in Katy, TX she attended Texas A&M University in College Station, TX. In May 2013 she graduated from Texas A&M with a Bachelor of Science in Radiological Health Engineering with minors in physics and math. In the fall of 2013 she started at the University of Texas Graduate School Of Biomedical Sciences at Houston pursuing a Master of Science degree in Medical Physics. Mattie is currently in a therapeutic medical physics residency in Charlotte, NC with Landauer Medical Physics.